FRACTIONAL CRYSTALLIZATION IN CONVECTING MAGMA CHAMBERS

by

DANIEL MARTIN

A thesis submitted for the degree of

Doctor of Philosophy

of the Australian National University

Research School of Earth Sciences

October 1988

Except where otherwise mentioned in the text or in the acknowledgements, the research described in this thesis is my own.

Daniel Martin

Daniel Martin

ACKNOWLEDGEMENTS

I would first like to thank my supervisor, Ian Campbell, for his encouragement and support. Throughout my studentship, Ian was always available to discuss my work. His advice and guidance over the last three years constitute a major contribution to this thesis, which I gratefully acknowledge. He also helped during the preparations of our joint papers on which chapters four and five and parts of chapter three are based.

Stewart Turner was a source of much sound advice. Under his leadership the G.F.D. group is a cheerful, cooperative place in which to work. I am grateful to him for the opportunity to come and work here.

I am indebted to Ross Griffiths, whose patient explanations of fluid-dynamical principles were invaluable. Ross was particularly helpful during the preparation of the paper on which chapter four and parts of chapter three are based.

The assistance of Roger Nokes is also gratefully acknowledged. Roger wrote the data acquisition routine employed in the experiments described in chapter five, and contributed to chapter six through many discussions. He also helped with the analysis of the photographs in the experiments reported in chapters three and six.

The experiments described in this thesis would have been impossible without the technical support of Derek Corrigan, Ross Wylde-Browne, Tony Beasley and Pat Travers. I would especially like to thank Derek for all his help.

ABSTRACT

The research described in this thesis is aimed at understanding the fluid-dynamical processes that lead to fractional crystallization in magma chambers. The nature of thermal convection in magma chambers is first discussed. It is expected that thermal convection will normally be characterized by extremely large Rayleigh numbers, even at the slowest possible cooling rates. The style of convection in the majority of magma chambers is therefore expected to be unsteady, or 'turbulent'. However, the predicted values of the temperature drop across the thermal boundary-layer at the top of the fluid are very small, ranging between 0.02 and 1°C for conductively-cooled basaltic magma chambers

The *in situ* solidification model for fractional crystallization is assessed for the case of a high aspect ratio magma chamber cooling through the roof and crystallizing olivine at a horizontal floor. Since crystallization occurs in response to heat loss the compositional and thermal buoyancy fluxes are directly related. In this case the compositional Rayleigh number is about 10^6 times greater than the thermal Rayleigh number. The parameters describing the boundary-layers at the floor of a magma chamber are calculated. The latent heat thermal boundary-layer in a conductively cooled basaltic chamber is of the order of 1m thick, with very low thermal gradients, whereas the compositional boundary-layer is about 1cm thick with large compositional gradients. The variation in the degree of supercooling in front of the crystal-liquid interface is therefore dominated by compositional effects. The habit and composition of the growing crystals may also be controlled by the nature of the compositional boundary-layer. Elongate crystals are suggested to form when the thickness of the compositional boundary-layer is small compared with the crystal-size. In contrast, equant crystals may form when the boundary-layer is thicker than the crystals. Instability of the boundary-layer in the latter case can give rise to zoning within crystals. Diffusion of trace elements through the boundary-layer can also explain an inverse correlation, observed in layered intrusions, between Ni concentration in olivine and the proportion of Ni-bearing phases in the crystallizing assemblage.

Crystallization against sloping floors is also discussed. Convection from sloping boundaries under the conditions that are likely to prevail in magma chambers is expected to be very similar to convection from a horizontal surface. In particular, the thickness of the compositional boundary-layer and drop in composition across it are not appreciably different and there is only a weak dependence of these quantities on the angle of inclination of the sloping boundary. Compositional convection from an inclined floor in magma chambers is appropriately modelled by thermal convection from an inclined heat exchanger because in both cases the surfaces are comparatively smooth. Laboratory investigations show that in geologically realistic configurations the convection is characterized by a large-scale overturning on the scale of the entire tank, and significant stratification is therefore not developed. It is concluded that in magma chambers crystallization at a sloping floor is likely to homogenize, rather than stratify, the overlying

magma. Such a conclusion is supported by the eruption of large volumes of homogeneous magma such as the Columbia River Basalts. Models describing the crystallization of layered intrusions which involve the interaction of crystallization against an inclined floor with compositionally stratified magma require an external cause for the stratification.

The crystal-settling model for fractional crystallization in magma chambers is next considered. Predicted convective velocities in magma chambers are commonly orders of magnitude larger than settling velocities, v_S, for typical crystals calculated from Stokes' Law. However, settling is still possible because convective velocities are height-dependent and must decrease to zero at the boundaries of the fluid. Particles immediately adjacent to the bottom boundary settle out with their full Stokes' settling velocities. At the same time convection is vigorous enough to ensure that the distribution of particles in the fluid is uniform. It follows that the number of particles in suspension decays with time according to an exponential law, and the decay constant is simply the ratio of v_S to h, the depth of the fluid. Experiments confirm this relationship, at least for low particle concentrations, providing $s<0.5$ and there is no re-entrainment of particles from the floor of the tank. Using this relationship, residence times have been calculated for typical crystals in convecting magma chambers. For basaltic magmas the predicted residence times are small compared with the many thousands of years that a chamber takes to solidify if cooling is by conduction through the country rock. Crystal settling may therefore be an efficient differentiation mechanism. The data of Hiemstra (1986) on the variation of P.G.E. content with height in the UG-2 chromitite of the Bushveld Complex can be interpreted in terms of this model. During crystal settling, a steady-state may be achieved at which the rate of supply of crystals into the convecting magma due to crystallization balances the rate at which crystals settle out from the magma. This hypothesis can explain both the lack of hydraulic equivalence in cumulate rocks and the commonly observed discrepancy between the relative proportions of phenocrysts in basaltic lavas and the calculated proportions of the different minerals in the fractionating assemblage. A comparison of the calculated steady-state crystal content of convecting magma chambers with the observed phenocryst content of basaltic lavas suggests that magma chambers may often cool more rapidly than would be expected for conduction through the country rock alone.

Finally, laboratory experiments involving cooling and crystallizing aqueous solutions of varying viscosities are described. These solutions display a range of crystallization mechanisms between the two end-members of *in situ* crystallization and crystal settling. The nucleation of crystals within the crystallizing fluid, and hence crystal settling, is shown to be promoted by fast cooling rates and, to a lesser extent, by high viscosities. It is suggested that slowly cooled magma chambers may crystallize purely by the *in situ* mechanism, whilst more rapidly cooled magma chambers may solidify by a combination of *in situ* crystallization and crystal settling.

ERRATA

Page	Line	
3	1-3	Insert "of" between "range" and "depth".
3	4	Change "may" to "can".
5	2	Change "rises up" to "rises".
5	3	Change "if" to "of".
5	14	Insert "; Yoder, 1973" between "1966" and ")."
7	14-15	Insert "is" between "dykes" and "likely".
9	13	Change "from" to "form".
15	10	Delete "such observables as".
19	19	Replace "$g\alpha\Delta Td_T$" with "$g\alpha\Delta T\kappa_T$".
24	13	Replace "Based on his calculations Shaw suggested" with "Shaw's calculations showed".
34	3&5	Change "different from" to different to".
34	-5	Change "due to" to "owing to".
41	3	Replace "κ_T" with "κ_S" in the last equation.
47	12	Insert "As noted by Tiller et al. (1953) and Burton et al. (1953)" between "boundary-layer." and "Trace elements".
54	7	Replace "expansion coefficient" with "diffusivity"
73	4	Insert "(McBirney *et al.*, 1985)" between "magma" and ", whereas".
76		Insert " " on the top line of equation (A5.4).
77	6-7	After "*in situ*" insert "on the floor and walls of the chamber".
82	11-12	Change "multiplying" to "dividing" and "dividing" to "multiplying".
98		Change "(28)" in the figure caption to "(6.13)".
116		Replace "It is suggested.....to orthocumulate." with "It is suggested that the range in cumulate textures from ad- to orthocumulate may reflect, at least in part, the relative importance of *in situ* crystallization and crystal settling. A similar suggestion may have been made by Morse (1986b)."
124		Add "Burton, J.A., Prim, R.C. & Schlichter, W.P., 1953. The distribution of solute in crystals grown from the melt. *J. Chem. Phys.* **21**, 1987-91." to references.
131		Add "Tiller, W.A., Jackson, K.A., Rutter, J.W. & Chalmers, B., 1953. The redistribution of solute atoms during the solidification of metals. *Acta Metall.* **1**, 428-37." to references.
132		Add "Yoder, H.S. Jr., 1973. Contemporaneous basaltic and rhyolitic magmas. *Am. Miner.* **58**, 153-71." to bottom of list.

CONTENTS

CHAPTER ONE

INTRODUCTION

Towards the end of the nineteenth century, petrologists began to realize that different igneous rocks within a given area frequently possess close compositional relationships to one another. The notion developed that such rocks might be derived from a single, common parent magma by a process that became known as differentiation. In 1928, N.L. Bowen, in his influential "Evolution of the Igneous Rocks", argued extensively that the major differentiation mechanism, the "evolutionary principle" of igneous petrology, was fractional crystallization.

When a magma crystallizes, the crystals that form normally have a different chemical composition to that of the magma. Removal of crystals during crystallization thus alters the bulk composition of the magma. This process is fractional crystallization. As Bowen demonstrated, and as has been extensively confirmed later, the chemical relationships observed between igneous rocks in many areas is consistent with the predicted effects of fractional crystallization.

Since the days of Bowen, with the development of trace-element and isotope geochemistry, petrologists have recognized that processes in addition to fractional crystallization are required in many cases. Nevertheless, fractional crystallization is still a central concept in igneous petrology. However, despite the fact that the effects of fractional crystallization are well known and widely encountered, the mechanism by which fractional crystallization operates remains poorly understood. It is this problem which is the major theme of this thesis. In the following chapters I shall attempt to consider, from a fluid-dynamical point of view, the two major models that have been proposed whereby crystals and magma may become separated during crystallization. These competing hypotheses have become known as "crystal settling" and "convective fractionation".

The work presented in this thesis belongs to the new field of geological fluid mechanics. Research in this multidisciplinary field has involved the application of fluid-dynamical experiments and calculations to problems in earth sciences. In chapter two I

briefly review the advances made by geological fluid mechanics in the last ten years in understanding petrological processes. This chapter also serves to place in context the specific geological problem with which this thesis is concerned.

In chapter three I review the fluid mechanics of convection, present some new data on fluid velocities in turbulent convection and apply this knowledge to thermal convection in magma chambers. Chapters four and five consider the convective-fractionation model for fractional crystallization. In these chapters I attempt to quantify the details of compositional convection from horizontal and sloping floors in magma chambers, paying special attention to the properties of the chemical boundary-layer. In addition, in chapter five, the influence of compositional convection from sloping floors on the homogeneity of the magma chamber is investigated.

In chapter six I address the crystal-settling hypothesis using experiments and simple theoretical considerations that take convection of the magma into account. A modified theory of crystal settling in turbulently convecting magmas is proposed and applied to geological situations, including the formation of platinum-group element deposits in layered intrusions. The consequences of a "steady-state" model of crystal settling are discussed with particular reference to the properties of phenocrysts in lavas.

In chapter seven I describe some experiments in which aqueous solutions of potassium nitrate are cooled from above. These experiments are designed to simulate cooling magma chambers and illustrate the range of possibilities for crystallization in magma chambers. In this chapter the circumstances under which crystal settling is likely to occur, and those under which convective fractionation is more probable, are discussed.

Finally the conclusions of this work are summarized in chapter eight.

Various parts of this study have been published or are currently under review. Parts of chapters three and four appeared in Martin *et al.* (1987), chapter five is based on Martin and Campbell (1988) and the work described in chapter six has written up in Martin and Nokes (1988, 1989).

CHAPTER TWO

IGNEOUS DIFFERENTIATION AND FLUID MECHANICS

Magma is generated by the melting of pre-existing rocks within the Earth. The formation of magma by partial melting is a complex process, frequently involving the simultaneous generation and extraction of melt from a range depths. Partial melting of the same rock under different conditions may generate a variety of compositions. Therefore, a relationship between rock compositions within a given area may not reflect differentiation from a single parent magma, but may instead be due to the generation of a range of parent magmas by the partial melting process. A full discussion of partial melting is beyond the scope of this chapter. It is, however, a topic which, like the differentiation mechanisms discussed below, has benefited greatly from recent fluid-dynamical investigations (*e.g.* McKenzie, 1984; Scott and Stevenson, 1986).

Magma, once generated, may be subjected to one or more of a variety of differentiation processes, and a range of daughter compositions may result. Most textbooks of igneous petrology contain a list of differentiation processes, which usually includes the following.

- Diffusion
- Magma-mixing
- Assimilation of country rock
- Liquid immiscibility
- Fractional crystallization.

Diffusion on its own can be disregarded as an important differentiation process in most situations, since it is too slow a process be significant at geologically important lengthscales. As for the remaining mechanisms, petrologists have sought to infer their operation by examining relationships between rocks. Thus the demonstration that two magmas have a chemical relationship that is consistent with the removal or addition of olivine signifies that fractional crystallization has operated; or isotopic characteristics may indicate magma-mixing, for example. In addition, experimental petrologists have for many years been concerned with determining phase relationships in igneous systems and

using these it has been possible to understand the chemical effects of the above processes. However, it is only recently that researchers have begun to pay much attention to the physics of the proposed differentiation processes.

In the rest of this chapter I briefly review the fluid-dynamical advances made in the last few years in understanding igneous differentiation.

Magma-mixing

There exists substantial evidence in favour of the mixing of two or more different magmas as an important petrogenetic process (*e.g.* Eichelberger, 1978; Dungan and Rhodes, 1978; Sakuyama, 1981). Magma-mixing may take place within a magma chamber, or in dykes during eruption.

In 1980, Huppert and Sparks published the first of a series of important papers on the replenishment of magma chambers and magma-mixing. Evidence from layered intrusions suggests that chambers containing evolved magma are frequently replenished by pulses of more primitive magma. Huppert and Sparks (1980) realized, however, that replenishment may not lead immediately to magma-mixing. Because hotter, primitive magma is often more dense than colder, more evolved magma, the replenishing magma may simply pond at the floor of the chamber. Such a ponded layer of dense magma is envisaged to lose heat rapidly to the overlying cooler more evolved magma. As the primitive magma cools, it undergoes fractional crystallization which progressively reduces its density. Eventually the density of the lower layer may become equal to that of the upper layer, at which time complete overturning and magma-mixing may occur. This model has also been simulated in the laboratory (Huppert and Turner, 1981). A magma chamber in this model acts as a "density filter", an idea that has been used to explain the scarcity of picritic magmas at the Earth's surface. Subsequent papers have investigated effects of compositional stratification in the chamber and varying rates of input and magma viscosity (*e.g.* Huppert *et al.*, 1982, 1983). Turner *et al.* (1983) demonstrated how the release of volatiles during overturning and mixing in such a model can lead to eruption of the chamber.

Campbell and Turner (1989) considered the effect of increasing the input rate of the replenishing magma so that a turbulent fountain is formed which rises up to a few hundred metres into the chamber. In this model there may be substantial mixing of the replenishing and host magma during replenishment. Mixing is not uniform throughout the chamber, however, and hybrid magma forms a stratified zone at the base of the chamber which breaks up into double-diffusive layers. The subsequent evolution of the chamber is broadly similar to the original model of Huppert and Sparks. Campbell and Turner (1986b) apply the fountain model to the formation of platinum-group element and chromite deposits in layered intrusions. Turbulent fountains do not always lead to substantial mixing, however. Campbell and Turner (1986a) showed that if the host magma is significantly more viscous than the replenishing magma, mixing in fountains may be effectively suppressed. This observation is in accord with field evidence which shows that felsic and mafic magmas may co-exist with little sign of mixing (Walker and Skelhorn, 1966).

Huppert *et al.* (1986a) considered the case where the replenishing fluid is less dense than the host magma. If the input is slow enough to be laminar, little mixing occurs and the replenishing magma ponds at the top of the chamber. If the appropriate Reynolds numbers are large enough for the input to be turbulent, however, substantial mixing may result.

Magma-mixing may also occur during eruption. Blake and Ivey (1986) showed that during eruption from a compositionally layered magma chamber, magma from more than one layer may be erupted simultaneously. This observation led Blake and Campbell (1986) to conduct an experimental study of the flow of two miscible liquids of different viscosities passing concentrically through a vertical pipe. A similar study was briefly reported by Koyaguchi (1985). Blake and Campbell concluded that, when the outer fluid is more viscous (the geologically relevant case), the amount of mixing between the fluids depends on a Reynolds number based on the properties if the inner, less viscous fluid. They apply their model to the formation of composite dykes and mixed pumice sequences. Koyaguchi (1987) suggests that some magma conduits may behave more like

squeezed tubes than rigid pipes, in which case significant mixing can occur even at low Reynolds number.

Assimilation

When hot magma comes into contact with country rock, the potential exists for the magma to melt and assimilate the rock. Bowen (1928) argued against assimilation as a major petrogenetic process on the grounds that the heat capacities of magmas are small compared with the latent heat of solution of rocks. It is now recognized, however, that the heat required for assimilation can be offset by the latent heat released by simultaneous crystallization. Assimilation is currently a popular differentiation mechanism, primarily as a result of isotope-geochemical studies (*e.g.* Moorbath and Thompson, 1980; Taylor, 1980; DePaolo, 1981). Fluid-dynamical investigations of assimilation both in magma chambers and during flow through dykes have been published in the last few years.

In mafic magma chambers, the melting of relatively felsic country rock at the chamber boundaries gives rise to buoyant magma which has a tendency to rise through the chamber. This process was modelled experimentally by McBirney *et al.* (1985) and Campbell and Turner (1987). If the contaminating melt is produced at a horizontal or sloping floor, it will mix with the resident magma. On the other hand, if it is produced at a vertical wall or at the roof, complete mixing will not be achieved. In this situation the buoyant contaminating magma flows upwards clinging to the boundary, ultimately collecting and ponding beneath the chamber roof. Campbell and Turner (1987) showed that if melting occurs at a horizontal roof there is little mixing between resident magma and the contaminating magma. However, if the contaminant is produced at a steeply sloping roof, mixing may be very extensive. A prediction of this model of assimilation is that there should be a layer of ponded felsic melt at the roof of a magma chamber, evidence for which can be found both in layered intrusions (*e.g.* Irvine and Smith, 1967) and in pyroclastic eruptions (*e.g.* Hildreth, 1981).

Campbell and Turner (1987) discussed the dynamics of assimilation in magma chambers in the context of the geochemical model of assimilation and fractional crystallization (A.F.C.). A.F.C. refers to a magma which is undergoing both

assimilation and fractional crystallization, with the heat required to melt the country rock coming mostly from the latent heat released by crystallization. The geochemical equations developed to model this situation assume that the magma remains completely mixed during assimilation (DePaolo, 1981). Campbell and Turner pointed out that, although the heat required to enable assimilation may indeed come from crystallization, the contaminating magma may not mix completely with the host magma so that the chemical link between assimilation and fractional crystallization may be only weak. When melting is occurring at the roof of a chamber true A.F.C., in the sense envisaged by DePaolo (1981), is improbable.

Huppert and Sparks (1988a,b) have recently published a theoretical analysis of the melting process at a horizontal roof. Their calculations show that large volumes of melt can be generated by melting above basaltic magma chambers.

The fluid dynamics of assimilation during flow through dykes has been described by Huppert and Sparks (1985). These authors suggest that flow in dykes likely to be often within the turbulent régime, especially for low-viscosity, Mg-rich magmas. The properties of such turbulent flow can be related to the melting and assimilation of country rock *via* an empirical heat transfer coefficient. Calculations show that wholesale ingestion of country rock by magma flowing through dykes may be very significant: a komatiitic magma may contain up to 30wt.% of contaminant. Contrary to the A.F.C. process, the most primitive (hottest and least viscous) magmas are likely to be the most contaminated. Such a style of contamination, Huppert and Sparks note, has been observed in basalts from the Deccan Traps and the Isle of Skye. Campbell (1985) suggests in addition that contamination during flow through dykes is responsible for many of the differences between continental and oceanic tholeiites.

Liquid immiscibility

There is strong evidence that certain silicate melts may split on cooling into two immiscible liquids (Roedder, 1979). A differentiation mechanism based on this property of some silicate melts was first proposed in the late nineteenth century and it has remained a possibility, albeit one rarely resorted to in recent years.

Liquid immiscibility has not yet been addressed in any particular fluid-dynamical study, probably because of its dubious significance as a petrogenetic process. Immiscible droplets will in general have a different density to the host magma which will cause them to rise or sink through the magma and collect at the roof or floor of the magma body. The essence of this differentiation mechanism should therefore be similar to the crystal-settling mechanism discussed below and in chapter six.

Fractional crystallization

As suggested in the introductory chapter, fractional crystallization is perhaps historically the most important differentiation mechanism. Fractional crystallization requires a means of separating crystals and residual melt during crystallization. Possible mechanisms that have previously been proposed include:

(i) Crystal settling

Under the crystal-settling model, crystals form within the main body of the magma and settle out due to the action of gravity. Such a model gained in popularity following the work of Bowen (1915) who demonstrated its efficacy in stagnant silicate melts in the laboratory. However, the original hypothesis of crystal settling assumed a stationary magma, whereas, as will be shown in chapter three, thermal convection is almost inevitable in magma chambers. Various attempts to include convection in models of crystal settling have been made (*e.g.* Wager and Deer, 1939) but these have been largely qualitative in nature. It was not until Bartlett (1969) that any quantitative attempt to consider the effect of convection on crystal settling was made.

More recently, Sparks *et al.* (1984) have questioned whether crystal settling can normally be possible since turbulent convective velocities in magma chamber usually greatly exceed typical crystal-settling velocities. Marsh and Maxey (1985) and Weinstein *et al.* (1988) also attempted to study crystal-settling. However, these authors started out with the assumption that thermal convection in magma chambers is ordered and cellular. As shown later, this is unlikely to be the case. In chapter six an experimental investigation of particle settling in turbulent convection is described, and a new model of crystal settling in magma chambers is proposed.

In the last few years several problems have emerged with the crystal-settling model. Campbell (1978) and McBirney and Noyes (1979) argue that field relationships in the Jimberlana and Skaergaard intrusions are inconsistent with the crystal-settling model. There has also been considerable debate as to whether plagioclase crystals, which clearly accumulate on the floor in layered intrusions, can be more dense than some basaltic magmas (Campbell *et al.*, 1977). McBirney and Noyes (1979) also discuss the possibility that magmas possess a yield strength which inhibits crystal settling. However at liquidus temperatures they suggest that magma is a Newtonian fluid with no yield strength.

(ii) Convective fractionation

An alternative to the crystal-settling model is the idea of convective fractionation. Campbell (1978) and McBirney and Noyes (1979) both proposed that crystals do not from in suspension in the main body of the magma, but instead grow *in situ* on the floor and walls of the chamber. As recognized by these authors, *in situ* crystallization alone cannot produce fractional crystallization. A mechanism is required to mix the fluid rejected by the growing crystals back into the main body of the magma and supply undepleted magma to the growing crystals. Diffusion, as noted above, is too slow to produce significant differentiation on the likely available timescales. Turner (1980) proposed that, because the residual fluid is often expected to be less dense than the main body of the magma, the redistribution can be accomplished by compositional convection. This mechanism of *in situ* crystallization coupled with compositional convection, has become known as "convective fractionation" (Rice, 1981; Sparks *et al.*, 1984). In chapters four and five I attempt to gain a quantitative understanding of the details of compositional convection in magma chambers.

The convective-fractionation model has been the focus of several experimental studies, particularly involving crystallization against vertical boundaries (Turner, 1980; McBirney, 1980; Turner and Gustafson, 1981; McBirney *et al.*, 1985). In this configuration, buoyant residual fluid rises up adjacent to the wall and forms a stratified region of light fluid at the top of the tank. This process has been analyzed theoretically by Nilson *et al.* (1985) who showed that in geological situations, evolved fluid can

accumulate in significant amounts at the top of magma chambers. Sidewall crystallization thus provides an alternative explanation for compositional zonation in magma chambers. Recent papers by Huppert *et al.* (1986b, 1987) describe experiments involving crystallization against sloping floors and these authors suggest that this too can lead to compositional stratification. The experiments reported in chapter five, in which fluid is heated through a sloping floor, point to a different conclusion.

(iii) Filter pressing

Given an accumulation of crystals and interstitial liquid, the liquid may be expelled from the mush as a result of a compaction process. This process provides a third possible mechanism for fractional crystallization. The efficiency of compaction as a fractional-crystallization process depends on the speed and effectiveness of the compaction process. Sparks *et al.* (1985) apply the results of McKenzie (1984) to the compaction of cumulates in layered intrusions and conclude that significant compaction can occur on timescales of a few hundred to several thousand years. They further conclude that compaction may be able to expel nearly all of the melt and reduce the porosity of the mush down to less than 1 vol.%. Tait *et al.* (1984) suggest that expulsion of liquid from the crystal mush may be assisted by compositional convection during further interstitial growth (a model which is an extension of the convective-fractionation hypothesis described above).

Filter pressing is a postcumulus process. If it occurs it happens after the formation of a mush of crystals and liquid. Either crystal settling or *in situ* crystallization is required to produce the cumulate mush. Filter pressing is therefore a secondary differentiation mechanism. The chemical effect of filter pressing depends on the difference between the initial porosity of the mush and the final porosity preserved in the solidified rock. Many cumulates in layered intrusions retain a high porosity (*i.e.* they are orthocumulates) suggesting that solidification has occurred before a filter-pressing process has been able to operate to any great extent. On the other hand, many cumulates have close to zero porosity (*i.e.* they are adcumulates), although Campbell (1987) has argued that these low porosities may be primary features. However, if a mush is formed during the crystallization of a large, slowly-cooled layered intrusion filter pressing would seem to be a distinct possibility.

(iii) Flow differentiation

The flow-differentiation model relies on the concentration of crystals towards the centre of a conduit during laminar flow of a crystal-bearing magma. This effect is a consequence of the increase in velocity gradient towards the margins of the conduit (Komar, 1972). It is not clear, however, how magma can be tapped from the sides of dykes to produce differentiation on a large scale. Another problem with this differentiation mechanism is that flow in conduits is required to be laminar. Huppert and Sparks (1985) have shown that for mafic magmas turbulent flow will often occur. Turbulence can be expected to keep the distribution of crystals uniform across the flow. It therefore seems highly improbable that flow differentiation can be important during flows through sills up to 600m thick as has been envisaged by Bhattacharji (1967).

Nevertheless, although it seems unlikely to be a major large-scale differentiation process, flow differentiation may be the explanation for the observed gradients in crystal content in some narrow dykes. For example, Gibb (1968) describes picritic dykes generally between 1 and 10m wide from Skye in which the crystals are concentrated in the middle of the dyke. Gibb considers that the solidified dykes provide an instantaneous picture of the molten state and attributes the observed crystal distribution to flow differentiation. He does discuss an alternative origin, that the dykes are formed by the intrusion of crystal-rich magma into the middle of a pre-existing crystal-poor dyke, but rejects this on the grounds that the observed increase in phenocryst content, although rapid, is gradational. One alternative interpretation that still seems worthy of consideration, however, is that the solidified dyke does not provide a simple snapshot of the fluid state. For example, solidification of the dyke inwards from its margins could have occurred while the magma was still flowing in the dyke, with the flowing, cooling magma becoming progressively more crystal-rich with time.

CONCLUSION

Many aspects of igneous differentiation have been clarified in the last few years as a result of fluid-mechanical investigations. The phenomena of magma-mixing and country-rock assimilation in particular are now much better understood. However, it is

fractional crystallization that has historically been the most frequently invoked differentiation process and there still remains considerable debate as to how it is achieved. In this thesis I shall focus on the physics behind the two most popular models: crystal settling and convective fractionation. Of these two models it is convective fractionation that has benefited most from fluid-dynamical investigations. However much of this work has been qualitative in nature: analogue experiments with aqueous solutions have been used to delineate the possible situations in magma chambers. Here I attempt a quantitative evaluation of some aspects of convective fractionation, particularly the problem of crystallization against sloping and horizontal floors in magma chambers. I also discuss the crystal-settling model. Despite the recent interest in the fluid-mechanics of geological processes there has so far been no experimental study of the phenomenon of particle settling in turbulent convection. Such a study is described in chapter six where a simple theory of crystal settling is developed and applied to magma chambers.

CHAPTER THREE

THERMAL CONVECTION

The term 'free convection' refers to the motion produced by the action of the gravitational field on density variations in a fluid. Convection is a common geophysical phenomenon and it is also frequently encountered in engineering situations. It has therefore been extensively studied. In the first half of this chapter I review the fundamental fluid mechanics of single-component convection with emphasis on those aspects that pertain to magma chamber dynamics. In the second half of the chapter I attempt to apply this knowledge to thermal convection in magma chambers.

This chapter is specifically concerned with thermal convection, that is to say with convection resulting from density variations due to temperature differences in a fluid. However, the same principles apply to compositional convection (which is discussed in chapters four and five).

THERMAL CONVECTION IN GENERAL

In the following discussion of thermal convection I have drawn on the reviews of Turner (1973) and Palm (1975).

The governing equations

Consider a horizontal layer of incompressible fluid of dynamic viscosity, η, contained between two parallel plates of separation, h, between which a temperature difference, ΔT, is maintained. The fluid motion is governed by the following equations which express the conservation of mass, momentum and heat respectively:

$$\nabla.\mathbf{u} = 0 \tag{3.1}$$

$$\rho_0\left(\frac{\partial \mathbf{u}}{\partial t} + \mathbf{u}.\nabla\mathbf{u}\right) = -\nabla P + \eta\nabla^2\mathbf{u} + \mathbf{g}\rho \tag{3.2}$$

$$\frac{\partial T}{\partial t} + \mathbf{u}.\nabla T = \kappa_T\nabla^2 T \tag{3.3}$$

where $\mathbf{u}$ is the velocity of the fluid, P is the pressure in the fluid, $\mathbf{g}$ is the acceleration due to gravity (positive downwards), t is time, ρ is the density of the fluid and κ_T is the thermal diffusivity of the fluid. Equation (3.2) is the Navier-Stokes equation using the

Boussinesq approximation (whereby all density variations due to temperature differences are ignored except in the buoyancy term). An expansion coefficient, α, may be defined by

$$\rho = \rho_0(1-\alpha(T-T_0)) \tag{3.4}$$

where ρ_0 is the density of the fluid at T_0, a standard temperature. The dependence of density on temperature is thus assumed to be linear. Temperature, T, is conveniently written

$$T = T_0 - \frac{\Delta T}{h} z + \theta \tag{3.5}$$

where z is the vertical co-ordinate (positive upwards). $\frac{\Delta T}{h} z$ is the temperature distribution that would be produced by conduction alone and θ is the deviation from this linear distribution. Similarly, pressure P is composed of the hydrostatic pressure, p_s, and the deviation, p, of the pressure from the hydrostatic pressure. p_s is given by

$$\frac{\partial p_s}{\partial z} = -g\rho_0\left(1 + \frac{\alpha \Delta T}{h} z\right) \tag{3.6}$$

in which only the pressures corresponding to the first two terms of (3.5) have been included. Substituting (3.5) and (3.6) into (3.2) and (3.3) gives

$$\rho_0\left(\frac{\partial \mathbf{u}}{\partial t} + \mathbf{u}.\nabla \mathbf{u}\right) = -\nabla p + g\rho_0\left(1+\frac{\alpha\Delta T}{h} z\right)\mathbf{k} + \eta\nabla^2\mathbf{u} + g\rho_0\left(1-\alpha\left(\theta-\frac{\Delta T}{h} z\right)\right)$$

$$= -\nabla p + g\alpha\theta\rho_0\mathbf{k} + \eta\nabla^2\mathbf{u} \tag{3.7}$$

and

$$\frac{\partial \theta}{\partial t} + \mathbf{u}.\nabla\theta - \frac{\Delta T}{h}\mathbf{u}.\mathbf{k} = \kappa_T\nabla^2\theta$$

$$\Rightarrow \quad \frac{\partial \theta}{\partial t} + \mathbf{u}.\nabla\theta = \kappa_T\nabla^2\theta + w\frac{\Delta T}{h} \tag{3.8}$$

where $\mathbf{k}$ is a unit vertical vector (positive upwards) and w is the vertical fluid speed. Equations (3.1), (3.7) and (3.8) may be non-dimensionalized by putting

$$(x,y,z) = h(x',y',z') \qquad t = h^2t'/\kappa_T$$

$$\theta = \kappa\nu\theta'/\alpha g h^3 \qquad p=\kappa_T^2\rho_0 p'/h^2$$

where ν is the kinematic viscosity of the fluid. Thus, dropping the primes from the dimensionless variables, (3.1), (3.7) and (3.8) become

$$\nabla.\mathbf{u} = 0 \tag{3.9}$$

$$\frac{\partial \mathbf{u}}{\partial t} + \mathbf{u}.\nabla\mathbf{u} = -\nabla p + \theta k Pr + Pr\nabla^2\mathbf{u} \tag{3.10}$$

$$\frac{\partial \theta}{\partial t} + \mathbf{u}.\nabla\theta = \nabla^2\theta + wRa \qquad (3.11).$$

Ra and Pr are the non-dimensional groups:

$$Ra = \frac{g\alpha\Delta Th^3}{\nu\kappa_T} \qquad \text{(Rayleigh number)} \qquad (3.12)$$

and

$$Pr = \frac{\nu}{\kappa_T} \qquad \text{(Prandtl number)} \qquad (3.13).$$

The Rayleigh number and the Prandtl number are the only independent non-dimensional groups.

Equations (3.9) to (3.11) must be considered simultaneously. Because these equations are non-linear, experimental studies of convection have been especially useful. These laboratory studies have investigated the influence of Ra and Pr on such observables as the structure of convection, the heat transfer properties of convection and the magnitude of convective velocities.

The influence of the Rayleigh number and the Prandtl number on the structure of convection

A layer of fluid may, under certain circumstances, be in stable equilibrium even if its density increases upwards. A layer of fluid heated from below will be stable provided the Rayleigh number is below a critical value, R_c, of order 10^3. When this critical Ra is exceeded the style of convection is initially ordered, steady and cellular. As Ra increases, however, the style of convection undergoes a series of transitions and becomes progressively more disordered. Eventually cellular flow disappears completely and is replaced by a random array of transient plumes, or 'thermals' which are generated at the heated and cooled surfaces. These plumes drive an unsteady and chaotic flow in the interior of the fluid that may be termed 'turbulent'[1]. If the Rayleigh number is increased still further it is found that the plumes combine to drive an overall circulation in the interior of the fluid, the lengthscale of which is of the order of the depth of the fluid or

[1]In this thesis I adopt Tritton's (1985a) usage of the word 'turbulent': a turbulent flow is one "that should be described statistically because a sequence of instabilities has led to a low level of predictability". Used in this way turbulence is by no means confined to high-Reynolds-number flows (such as convection in relatively low-Pr basaltic magma chambers) but may also be used to describe unsteady low-Reynolds-number flows (such as convection in high-Pr granitic chambers).

greater (Deardorff and Willis, 1967; Fitzgerald, 1976; Krishnamurthi and Howard, 1981).

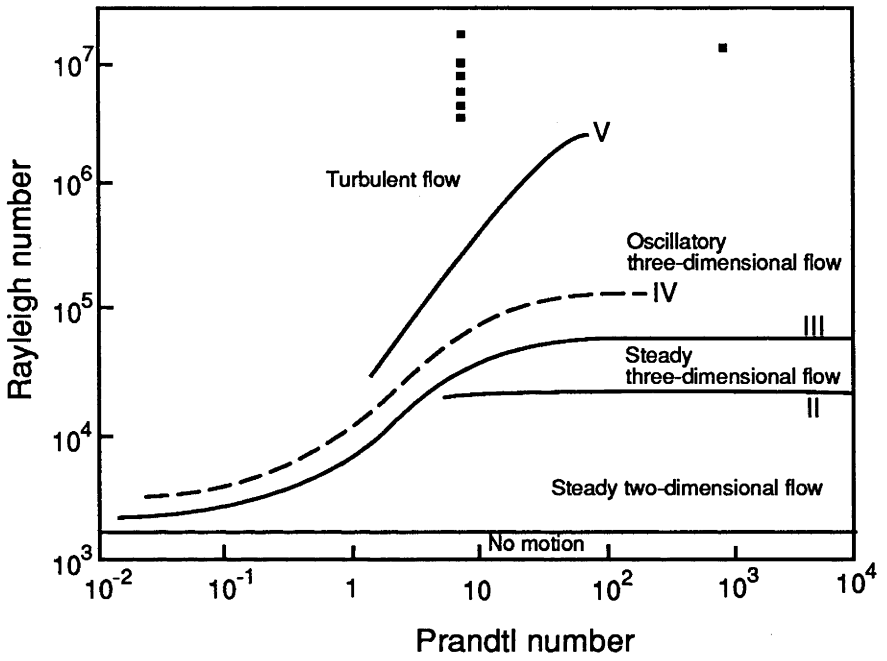

Figure 3.1. Flow-régime diagram for convection. The dotted line labelled IV corresponds to a heat-flux transition that occurs within the régime of oscillatory three-dimensional flow. The solid boxes represent the points where turbulent flow with a large-scale overall circulation has been observed. (From Krishnamurthi and Howard, 1981).

The values of critical Rayleigh numbers at the various transitions depend on the Prandtl number of the fluid (see figure 3.1). As far as magma chambers are concerned, it is the critical Ra at the transition to turbulence that is the most important. For water turbulent convection is observed for Ra > $O(10^5)$ and, although the transition to turbulent flow does depend on Pr, this dependence is expected to be weak for sufficiently large Pr. Laboratory experiments and numerical simulations confirm this expectation. Tritton *et al.* (1980) and Tritton (1985b) found that their fluid underwent turbulent convection at Ra = 3×10^6 with Pr = 8×10^4; and Jarvis (1984) discovered in a numerical experiment that even for an infinite-Pr fluid, convection is turbulent for Ra>10^9.

Howard (1963) proposed a simple model of turbulent convection centred on the idea of thermals. His model has received support from laboratory and numerical experiments and atmospheric temperature measurements (*e.g.* Townsend, 1959; Elder, 1968). As described above, observations show that high-Ra convection is initiated through an instability which originates near the boundaries. First there is a conductive

phase during which a layer of buoyant fluid is built up in a boundary-layer adjacent to the heated plate. This is followed by a short interval during which the boundary-layer fluid erupts to form a thermal, restoring the original conditions at the plate. Suppose the fluid initially has a constant temperature T=0. At time t=0 the upper and lower boundaries are at temperatures -1/2 ΔT and 1/2 ΔT respectively. As the fluid adjacent to the boundaries heats up, error function temperature profiles are produced:

$$T = \frac{1}{2}\Delta T \, \mathrm{erf}\left(\frac{z}{2\sqrt{\kappa_T t}}\right) \qquad (3.14).$$

Howard suggested that the thickness of the boundary-layer, $d_T = \sqrt{\pi \kappa_T t}$, grows until a Rayleigh number Ra_δ, given by

$$Ra_\delta = \frac{g\alpha\Delta T d_T^3}{\nu\kappa_T} \qquad (3.15),$$

reaches a critical value of order 10^3. At this time, t_*, the buoyant fluid in the boundary-layer breaks away to form a plume, after which the process is repeated. Howard's model enables boundary-layer thicknesses to be determined and, as described in the following section, also leads to predictions about heat transfer by convection.

Heat transfer by convection

The influence of convection on the heat transfer properties of the fluid is of considerable interest to engineers and has therefore been thoroughly studied. A dimensionless heat-transfer coefficient, or Nusselt number (Nu), may be defined by

$$Nu = \frac{qh}{\kappa_T \rho c_p \Delta T} \qquad (3.16)$$

where q is the heat flux through the fluid. Nu is the ratio of the actual heat flux through the fluid to that which would be expected for the same temperature difference, ΔT, if the fluid were not convecting.

The Nusselt number is a function of the Rayleigh number and the Prandtl number. Experiments show that the dependence of Nu upon Ra changes at critical Rayleigh numbers which correspond to the critical Rayleigh numbers at transitions in the structure of the flow (Krishnamurthi, 1970). At very high Ra, however, the heat flux should only depend on conditions near the boundaries and is therefore expected to be independent of the depth of the fluid layer. Hence Nu should be given by

$$Nu = CRa^{1/3} \tag{3.17}$$

where C is a constant.

Howard's (1963) model of turbulent convection predicts a Rayleigh number dependence given by

$$Nu = \frac{h}{d_T} = \left(\frac{Ra}{Ra_\delta}\right)^{1/3} \tag{3.18}.$$

If $Ra_\delta \sim 10^3$ is fed into equation (3.18), the constant C is predicted to be of the order of 0.1. Experimental measurements of Nu at very high Ra support the one-third power dependence (Katsoras *et al.* (1977)). The value of the constant, C, given by the data of Katsoras *et al.* (1977) is 0.062, in good agreement with the prediction of Howard's model. My own experiments (see below and table 3.1) give $C \approx 0.08$.

Up to this point I have considered a layer of fluid heated from below and cooled from above, *i.e.* a turbulently convecting fluid with two boundary-layers. Magma chambers are not heated from below and there is only one thermal boundary-layer (neglecting for the moment the release of latent heat by any crystallization at the base of the fluid). In practise this makes little difference, since at high Ra the boundary-layers should not affect each other. There are, however, differences in detail. Heat must be transferred by conduction across only one boundary-layer in the magmatic situation, and the temperature difference used in the definition of Ra is one half the temperature difference used to determine Ra for the two-boundary-layer-case. When there is only one boundary-layer Katsoras *et al.* (1977) showed that the constant C in equation (3.18) is about 0.156. My own experiments give $C \approx 0.16$. For the purposes of the calculations in the rest of this thesis it is sufficient to assume C=0.2.

The magnitude of convective velocities

Unfortunately, engineers are not so curious about convective velocities as they are about convective heat transfer. To date very few experimental measurements of convective velocities have been carried out. At high Rayleigh number the only published laboratory data that I am aware of are those of Malkus (1954) and Garon and Goldstein (1973).

Equations for convective velocities have been derived by Kraichnan (1962) who presents a theoretical description of turbulent convection in a horizontal layer of fluid in which convection is driven both from above and below. Kraichnan used a mixing-length type of analysis, assuming that the effective mixing length at height z is of order z. Thus the local coefficients of eddy conductivity and eddy viscosity are given by $w_{rms}(z).z$, where w_{rms} is the r.m.s. vertical component of convective velocity. In the case where Pr>1 the fluid can be divided into three regions:

I. $z < d_T$

II. $d_T < z < z_v$

III. $z_v < z < \frac{1}{2}h$

where z is the vertical distance from the lower boundary, z_v is the thickness of a viscous boundary-layer and d_T is the thickness of a thermal boundary-layer. In region I, molecular viscosity and molecular conductivity dominate; in region II, eddy conductivity and molecular viscosity are dominant; in region III, it is eddy viscosity and eddy conductivity that are most important. Kraichnan obtains approximate expressions for the r.m.s. vertical component of convective velocity, w_{rms}. In region II

$$w_{rms} \approx 3.0\kappa_T d_T^{-1}(z/d_T), \tag{3.19}$$

whilst in region III

$$w_{rms} \approx 1.0(g\alpha\Delta T d_T)^{1/3}(z/d_T)^{1/3}, \tag{3.20}$$

where the numerical constants in these equations are crude estimates only, being based upon idealized models of the flow. Depending on the values of Ra and Pr, it is possible for region II to occupy all of the fluid outside the thermal boundary-layer (with region III absent) so that either of these equations may be appropriate for the mid-depth r.m.s. velocity. Whether region III is present or not depends on the value of z_v, which according to Kraichnan is given by

$$z_v \approx 3.2Pr^{1/2}d_T \tag{3.21}.$$

If $z_v > \frac{h}{2}$ then equation (3.19) should be used for mid-depth convective velocity, W, otherwise equation (3.20) holds. In order to apply these equations and determine which is appropriate, expressions for the boundary-layer thicknesses are required. In magma

chambers, thermal convection is driven only by cooling from above and in this configuration the thermal boundary-layer thickness is given by

$$d_T \approx \frac{h}{Nu} \tag{3.22}$$

which can be compared with the equation for heating from below and cooling from above:

$$d_T \approx \frac{h}{2Nu} \tag{3.23}.$$

The factor of two difference arises because in the former case there is only one boundary-layer, whereas in the latter case there are two boundary-layers.

Putting $\frac{z}{h}=\frac{1}{2}$ in equation (3.19), and using equation (3.22) and the definition of Nu (equation (3.16)) gives

$$W \approx 1.3\left(\frac{g\alpha q h^2}{\nu \rho c_p}\right)^{\frac{1}{2}}, \tag{3.24a}$$

which can also be expressed as

$$W \approx 0.06\,\frac{\kappa_T}{h} Ra^{2/3} \tag{3.24b}$$

using (3.22) and the definitions of Nu and Ra (equations (3.16) and (3.12)). Equation (3.20) together with equation (3.22) and the definition of Nu yields

$$W \approx 1.0\left(\frac{g\alpha q h}{2\rho c_p}\right)^{\frac{1}{3}} \tag{3.25a}$$

at $\frac{z}{h}=\frac{1}{2}$. Alternatively, using the definitions of Ra, Nu and Pr (equations (3.12), (3.16) and (3.13)) equation (3.25a) can be expressed as

$$W \approx 1.0\frac{\kappa_T}{h}\left(\frac{Ra.Nu.Pr}{2}\right)^{\frac{1}{3}}. \tag{3.25b}$$

Because the various factors of two cancel out in the algebra, equations (3.24) and (3.25) are also applicable to the configuration of heating from below and cooling from above.

The key parameter in deciding whether equation (3.24) or (3.25) is appropriate for the mid-depth velocity is the thickness of the viscous boundary-layer. Substituting for d_T in equation (3.21) gives

$$\frac{z_\nu}{h} \approx 3.2\,\frac{Pr^{1/2}}{Nu}. \tag{3.26}$$

Equation (3.24) is expected to apply when $\frac{z_\nu}{h} > \frac{1}{2}$, whereas equation (3.25) applies when $\frac{z_\nu}{h} < \frac{1}{2}$.

TABLE 3.1

Convection driven by cooling from above - experimental velocity determinations

(a) cooling from above only

Ra	Pr	Nu	$C = Nu.Ra^{-\frac{1}{3}}$	κ_T/h (m s^{-1})	w_{rms} (m s^{-1})
$1.8x10^8$	7	68	0.12	$7.05x10^{-7}$	$3.31x10^{-3}$
$5.1x10^8$	7	85	0.11	$7.05x10^{-7}$	$4.78x10^{-3}$
$1.2x10^9$	7	122	0.11	$7.05x10^{-7}$	$8.13x10^{-3}$
$7.2x10^6$	265	45	0.14	$7.05x10^{-7}$	$7.02x10^{-4}$
$2.2x10^7$	265	53	0.19	$7.05x10^{-7}$	$1.19x10^{-3}$
$6.6x10^7$	210	73	0.18	$7.05x10^{-7}$	$4.95x10^{-3}$
$2.9x10^7$	7	42	0.14	$1.25x10^{-6}$	$2.69x10^{-3}$
$8.0x10^7$	7	54	0.13	$1.25x10^{-6}$	$3.76x10^{-3}$
$1.8x10^8$	7	80	0.14	$1.25x10^{-6}$	$5.13x10^{-3}$
$6.5x10^6$	40	34	0.18	$1.28x10^{-6}$	$1.72x10^{-3}$
$1.7x10^7$	40	45	0.18	$1.28x10^{-6}$	$2.36x10^{-3}$
$4.2x10^7$	40	61	0.18	$1.28x10^{-6}$	$4.75x10^{-3}$
$1.4x10^6$	265	25	0.22	$1.23x10^{-6}$	$5.88x10^{-4}$
$4.6x10^6$	210	34	0.20	$1.23x10^{-6}$	$1.08x10^{-3}$
$1.1x10^7$	196	50	0.22	$1.23x10^{-6}$	$2.00x10^{-3}$
$2.1x10^7$	72	55	0.20	$7.05x10^{-7}$	$1.43x10^{-3}$
$6.4x10^7$	72	66	0.17	$7.05x10^{-7}$	$2.62x10^{-3}$
$1.9x10^8$	61	88	0.15	$7.05x10^{-7}$	$4.90x10^{-3}$
		$C_{average}$=0.16			

(b) cooling from above and heating from below

Ra	Pr	Nu	$C = Nu.Ra^{-\frac{1}{3}}$	κ_T/h (m s^{-1})	w_{rms} (m s^{-1})
$2.1x10^7$	851	20	0.07	$7.05x10^{-7}$	$1.36x10^{-3}$
$8.6x10^7$	199	26	0.06	$7.05x10^{-7}$	$1.80x10^{-3}$
$3.9x10^7$	199	18	0.05	$7.05x10^{-7}$	$1.92x10^{-3}$
$1.1x10^7$	1890	22	0.10	$7.05x10^{-7}$	$4.70x10^{-4}$
$5.1x10^6$	4070	11	0.07	$7.05x10^{-7}$	$8.0\ x10^{-5}$
		$C_{average}$=0.07			

There are very few published experimental measurements of mid-depth r.m.s. vertical convective velocities. For this reason an experimental investigation was conducted using the apparatus described in chapter six. Streak photographs of convection driven by cooling from above (and sometimes heating from below as well) were taken, and W was determined by measuring the length of streaks projected onto the vertical. In order to obtain an unbiased estimate of W the photograph was divided by vertical lines into 14 sections of equal area. For each section a mean streak length projected onto the vertical was determined at mid-depth (usually from ten individual streak measurements). The r.m.s. vertical convective velocity is then given by the r.m.s. length of these 14 mean values divided by the exposure time. The accuracy of these measurements is estimated to be about $\pm$ 20%. The results are presented in table 3.1 and illustrated in figure 3.2. Also plotted on figure 3.2 are the results of Malkus (1954) and Garon and Goldstein (1973), both of whose experiments involved heating and cooling, rather than just cooling.

In figure 3.2a the ratio of the experimentally determined velocity to that given by equation (3.25) is plotted against $\frac{z_v}{h}$. This graph shows that, as predicted by the theory of Kraichnan (1962), equation (3.25) gives reasonable velocities for $\frac{z_v}{h} < \frac{1}{2}$, but does not seem to work when $\frac{z_v}{h} > \frac{1}{2}$. In the régime of applicability of equation (3.25), *i.e.* $\frac{z_v}{h} < \frac{1}{2}$, the results suggest that a slightly different numerical constant should be used (0.7 rather than 1.0) and I have adopted this in the calculations below.

Unfortunately it was not possible to test equation (3.24) because of the low aspect ratio of the experimental apparatus. The experimental fluids are sufficiently viscous, when $\frac{z_v}{h} > \frac{1}{2}$, that the drag exerted by the sidewalls has an effect throughout the fluid, whereas equation (3.24) ignores the influence of the sidewalls. The restricted dimensions of the tank result in reduced convective velocities for high-Pr fluids. Another problem with using viscous fluids in this apparatus is that it is only possible to achieve rather low Rayleigh numbers. For the sake of completeness, in figure 3.2b the ratio of the experimentally determined velocity to that given by equation (3.24) is shown plotted against $\frac{z_v}{h}$. This plot confirms that, as expected, when $\frac{z_v}{h} > \frac{1}{2}$, convective velocities in our tank are less than would be predicted by equation (3.24).

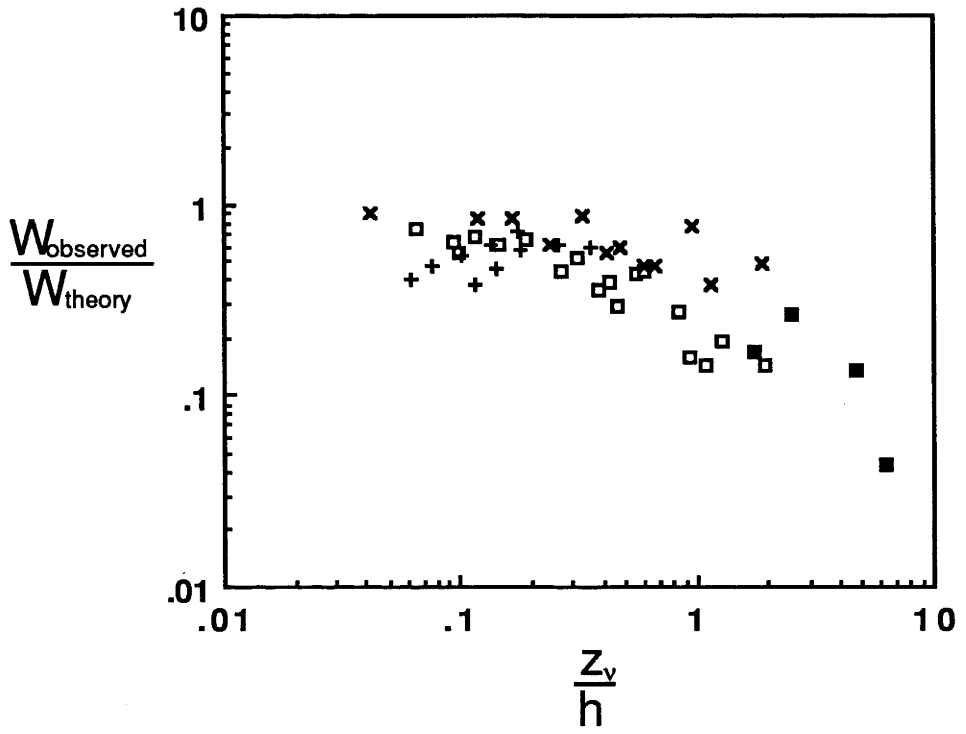

Figure 3.2a. Observed velocities divided by the velocities predicted using equation (3.25). Open squares: my results (cooling from above only); solid squares: my results (heating from below and cooling from above); crosses: Malkus' (1954) results; plus signs: the results of Garon and Goldstein (1973).

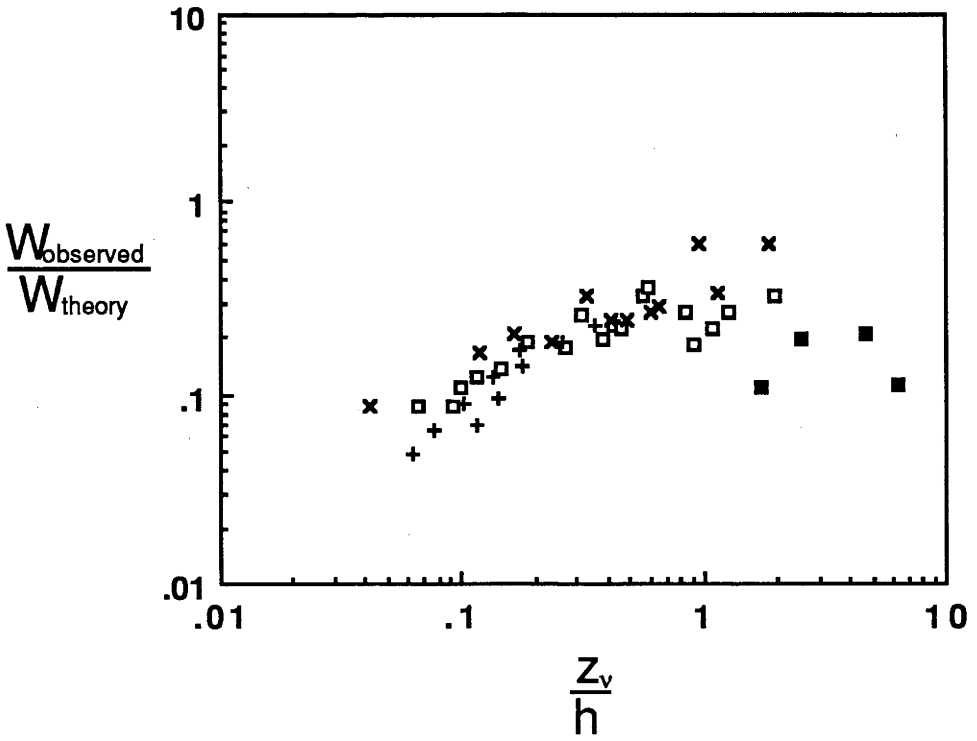

Figure 3.2b. Observed velocities divided by the velocities predicted using equation (3.24). Open squares: my results (cooling from above only); solid squares: my results (heating from below and cooling from above); crosses: Malkus' (1954) results; plus signs: the results of Garon and Goldstein (1973).

In summary, equation (3.25) has both theoretical and experimental support while equation (3.24) has theoretical support but has yet to be tested experimentally. Equation (3.24) has, however, received confirmation from numerical experiments (*e.g.* Herring, 1964). For the purposes of this work it is sufficient to obtain only an order-of-magnitude estimate of convective velocity . Therefore, whilst there is clearly room for more precise experimental work with more sophisticated (and expensive) equipment, it is felt that there is sufficient support for equations (3.24) and (3.25) to justify their use in this thesis.

THERMAL CONVECTION IN MAGMA CHAMBERS

The possibility of convection in magma chambers was recognized at least as early as Becker (1897). Until the 1960's, however, the discussion was predominantly based on geological field evidence and was qualitative in character. In 1965, a quantitative analysis of the problem of convection in a granitic magma body of the form of a vertical cylinder was published (Shaw, 1965). Based on his calculations Shaw suggested that thermal convection would be likely in any large granitic pluton. Shaw's work was followed by Bartlett (1969) who considered convection in all types of magma. He demonstrated that the normal heat fluxes from the earth are sufficient to cause convection in plutons larger than 15 metres high for magmatic viscosities up to 10^8 poise (10^7 Pa s).

Magmatic Rayleigh numbers

The following represents an extension of Bartlett's approach in which the Rayleigh numbers characterizing convection in magma chambers are estimated. Rather than choosing an arbitrary temperature difference, ΔT, (as was done, for example, by Rice, 1981) Rayleigh numbers will instead be calculated from estimates of the likely heat flux, q, from the chamber. The calculations refer specifically to a high aspect ratio magma chamber containing homogeneous magma. After this work was completed and published (Martin *et al.*, 1987), Carrigan (1987) applied a similar approach to the problem of convection in cooling lava lakes.

A Rayleigh number based on the heat flux from the chamber may be defined by

$$Ra_f = \frac{g\alpha q h^4}{\nu \kappa_T^2 \rho c_p} \tag{3.27}$$

where q is the heat flux through the roof of the chamber. This flux Rayleigh number is related to the conventional Rayleigh number by

$$Ra_f = Nu.Ra \tag{3.28},$$

where Nu is the Nusselt number as defined in (3.16).

Using the relationship between the Nusselt number and the Rayleigh number (equation (3.17)) equation (3.28) gives

$$Ra = \left(\frac{Ra_f}{C}\right)^{3/4} = \left(\frac{g\alpha q h^4}{\nu \kappa_T^2 \rho c_p C}\right)^{3/4} \tag{3.29}$$

Because of the use of equation (3.17), equation (3.29) is only valid for very large Ra_f.

TABLE 3.2

Values of parameters used in calculations

Symbol	Units	Value
c_p	$J\,kg^{-1}\,{}^oC^{-1}$	1.1×10^3
C	-	0.2
g	$m\,s^{-2}$	9.8
κ_T	$m^2\,s^{-1}$	8×10^{-7}
α	$^oC^{-1}$	5×10^{-5}
ρ	$kg\,m^{-3}$	3×10^3

In order to compute thermal Rayleigh numbers an estimate of the likely heat flux from the magma chamber is required. The slowest method of cooling a magma chamber is solely by conduction through country rock. It is unclear how much heat is lost through the floor of a magma chamber. However, the geothermal gradient, the fact that the depth of cover above the chamber is finite and the insulating effect of crystals accumulating at the floor of the chamber all ensure that the heat flux through the roof will be dominant (Irvine, 1970; Turner and Campbell, 1986). Consider a magma chamber buried

underneath 15km of country rock of thermal conductivity K = 3 W $^{o}C^{-1}$ m^{-1} (a typical value). If the temperature of the magma is 1000°C and the temperature of the surface of the earth is 0°C, the steady-state heat flux through the roof of the chamber will be

$$q = K\frac{dT}{dz} = 3 \times \frac{1000}{15000} = 0.2 \text{ Wm}^{-2}.$$

Unsteady conductive heat fluxes such as will occur during the first few thousand years after emplacement of a chamber can be orders of magnitude larger than this steady flux. In this thesis the minimum estimate for conductive-cooling rates is taken to be of the order of 10^{-1} Wm^{-2}, which can be compared with the estimated global average heat flux from continental crust of $6x10^{-2}$ Wm^{-2} given by Sclater *et al.* (1980).

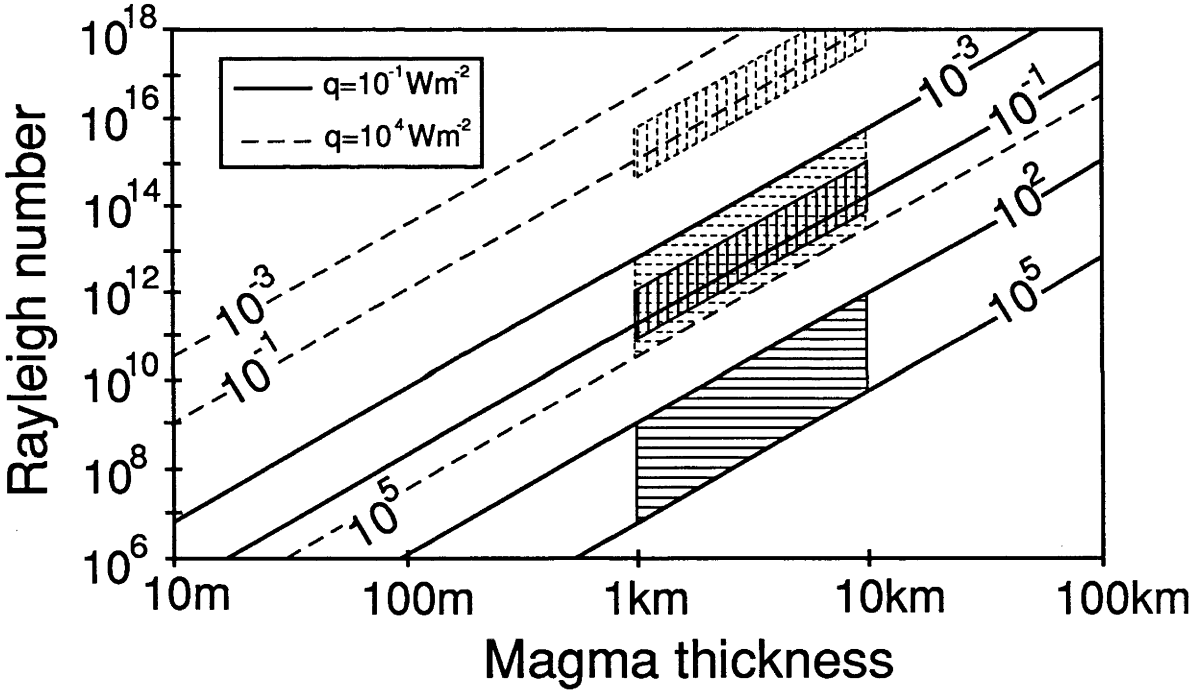

Figure 3.3. Conventional Rayleigh number (Ra) plotted against magma thickness (h) for the most rapidly cooled chambers (broken lines) and the most slowly cooled chambers (solid lines). Lines are plotted for different kinematic viscosities (in m^2 s^{-1}) and are labelled accordingly. Fields are plotted for mafic intrusions (*e.g.* Bushveld, Great Dyke, Stillwater, Jimberlana, vertically shaded boxes) and granitic intrusions (horizontally shaded boxes). The solid fields are for the slowest cooling rates, the dashed fields are for the highest cooling rates.

In other situations heat conduction through the country rock may not be the dominant mechanism for cooling the magma. Huppert and Sparks (1988a,b) have shown that if the magma in the chamber is hot enough to melt the surrounding country rock the heat fluxes from the chamber may be much higher. Similarly, if a magma body is heterogeneous due, for example, to emplacement of a picritic layer underneath a more

evolved magma (Huppert and Sparks, 1980) then the heat flux from the bottom layer may be as high as 10^4 Wm^{-2}. This is taken as the maximum possible cooling rate.

Typical magmatic Rayleigh numbers have been calculated using these cooling rates and other parameters as specified in table 3.2. Figure 3.3 illustrates the results. Rayleigh numbers in the most slowly cooled basaltic chambers range from 10^{11} to 10^{15}, for the most rapidly cooled chambers the range is 10^{15} to 10^{19}. For granitic chambers the ranges are from 10^7 to 10^{12} and 10^{10} to 10^{15} respectively. Prandtl numbers for basalts range from 10^4 to $5x10^5$, and for granitic magmas from 10^8 to 10^{11}. Cellular convection is therefore only possible in the most slowly cooled, most viscous granitic magma chambers. Thermal Rayleigh numbers are sufficiently large for all other types of chamber to ensure that convection is highly disordered and unsteady.

The thermal boundary-layer in magma chambers

In high-Ra convection the horizontally averaged temperature distribution is uniform outside the boundary-layers (assuming that the fluid is incompressible). In the magmatic situation the heat flux, q, through the roof must all pass through the upper thermal boundary-layer. This intermittently unstable boundary-layer may be approximated by a layer of constant thickness across which heat is transported solely by steady-state conduction, so that

$$d_T = \kappa_T \rho c_p \frac{\Delta T}{q} \qquad (3.30),$$

where d_T is the thickness of the thermal boundary-layer. Since convective stirring keeps the magma homogeneous outside the boundary-layers, the temperature drop across the thermal boundary-layer in (3.30) is equal to the overall temperature difference available to drive convection. It follows that the boundary-layer thickness scales as the inverse of the Nusselt number:

$$d_T = \frac{h}{Nu} = \left(\frac{\rho c_p \nu \kappa_T^2}{C^3 g \alpha q} \right)^{1/4} \qquad (3.31)$$

and

$$\Delta T = \frac{qh}{\kappa_T \rho c_p Nu}$$

$$= \left(\frac{\nu}{g\alpha\kappa_T^2}\right)^{1/4}\left(\frac{q}{\rho c_p C}\right)^{3/4} \qquad (3.32)$$

using (3.17) and (3.27).

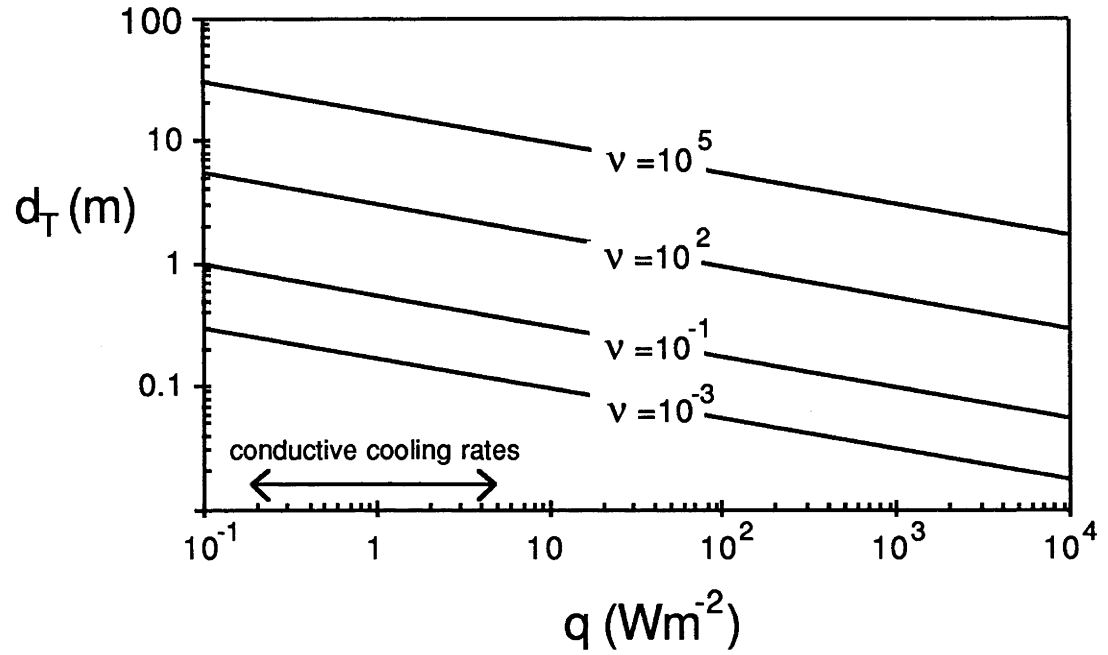

Figure 3.4a. The thickness of the thermal boundary as a function of cooling rate for different kinematic viscosities (in $m^2\ s^{-1}$). A rough estimate of the range of conductive-cooling rates is indicated.

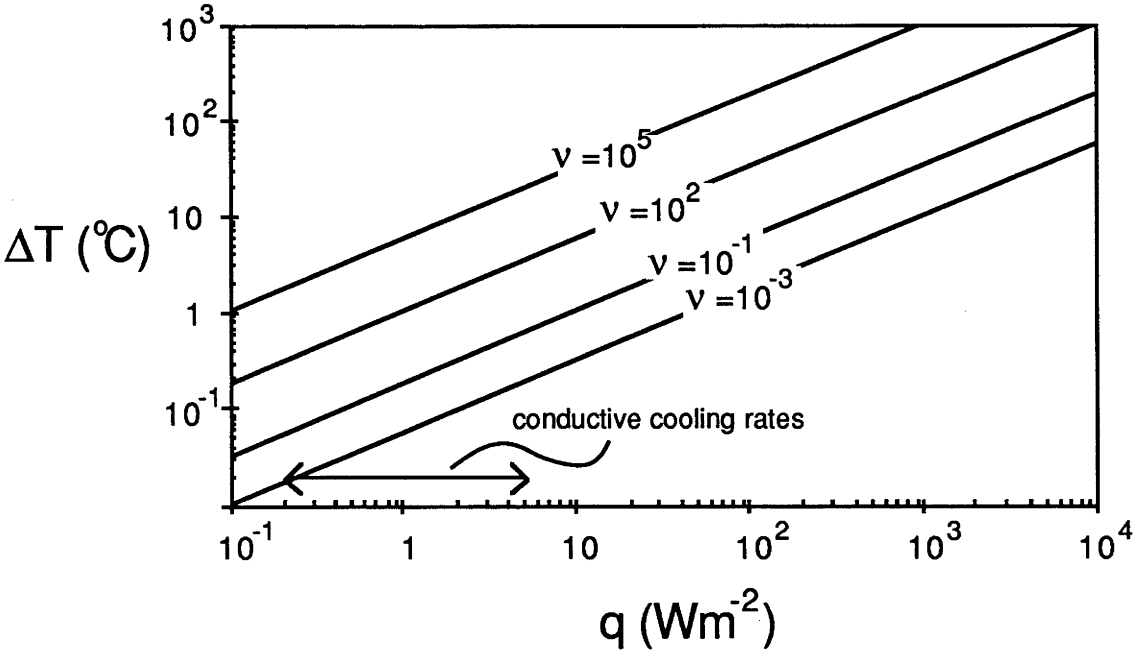

Figure 3.4b. The temperature drop across the thermal boundary as a function of cooling rate for different kinematic viscosities (in $m^2\ s^{-1}$). A rough estimate of the range of conductive-cooling rates is indicated.

Figure 3.4 illustrates predicted values of the thermal boundary-layer thickness and the temperature drop across the boundary-layer for magma properties as specified in table 3.2. The thermal boundary-layer thickness is generally between 20cm and 2m for conductively cooled mafic magmas and between 50cm and 20m for conductively cooled granitic magmas. For higher cooling rates the boundary-layer may be appreciably thinner. The corresponding temperature difference lies between 0.02°C and 1°C for conductively cooled basalts and 0.3 and 30°C for conductively cooled granites. ΔT increases with cooling rate.

A word of caution is necessary at this point. In these calculations I have neglected two effects: the temperature-dependence of magmatic viscosity and the possibility of crystallization in the thermal boundary-layer.

Temperature-dependence of magmatic viscosity. The likely change in the viscosity of the magma across the thermal boundary-layer can be estimated. At temperatures above the liquidus the temperature-dependence of magmatic viscosity obeys the Arrhenius equation:

$$\ln \nu = H_0 + \frac{E^*}{RT} \tag{3.33}$$

where H_0 is a constant, E^* is the activation energy, R is the gas constant (8.31 J $^oC^{-1}$ mol^{-1}) and T is the absolute temperature. For magmas E^* has a magnitude of approximately $2x10^5$ J mol^{-1} (Ryan and Blevins, 1987). The ratio of magmatic viscosity at temperature $T+\Delta T$ to that at temperature T is thus

$$\frac{\nu_{T+\Delta T}}{\nu_T} = \exp\left(\frac{-E^*\Delta T}{R(T(T+\Delta T))}\right) = \exp\left(\frac{-2.4x10^4\Delta T}{T(T+\Delta T)}\right)$$

putting $T=T+\Delta T=1000$ as an order-of-magnitude estimate gives

$$\frac{\eta_{T+\Delta T}}{\eta_T} = \exp(-2.4x10^{-2}\Delta T) \tag{3.34}$$

Substituting the values for ΔT calculated above gives fractional viscosity changes across the thermal boundary-layer of .9995 to .98 for basalts and .993 to .49 for granites. For most conductively cooled magmas, therefore, taking the temperature-dependence of viscosity into account will have little effect on the predicted properties of convection. In basaltic chambers the temperature-dependence of viscosity is only likely to be important at extremely rapid cooling rates (when $\Delta T>50$°C or so). The temperature-dependence of viscosity is likely to have a stronger effect on convection in granitic chambers, however.

If temperature-dependent viscosity is important, the effect will be to increase the stability of the boundary-layer. This will lead to higher values of d_T and ΔT than would occur for the isoviscous case.

The effects of crystallization in the thermal boundary-layer. The coldest part of a magma chamber is the thermal boundary-layer. It might therefore be expected that the magma temporarily resident in the boundary-layer will undergo at least some crystallization. This is the classic model of Grout (1918) and Wager and Deer (1939), which has recently been reassessed by Brandeis and Jaupart (1986) and Morse (1986a). There are two reasons, however, why crystallization need not occur in the boundary-layer. Firstly, although the thermal boundary-layer is the coldest part of the chamber it need not be the most supersaturated part. The effect of pressure on the liquidus causes supersaturation to increase by some 3°C per kilometre depth in the chamber (Jackson, 1961), in kilometre-sized conductively-cooled basaltic chambers this is often sufficient to outweigh the temperature drop across the boundary-layer and ensure that the magma at the bottom of the chamber is the most supersaturated. Secondly, the Wager and Deer model requires homogeneous nucleation to occur in the thermal boundary-layer in preference to heterogeneous nucleation against the walls and floor of the chamber (Campbell, 1978). This problem will be discussed more fully in chapter seven, and I will just note here that the possibility of homogeneous nucleation in the thermal boundary-layer is somewhat undermined by the small temperature drops predicted above. For fast cooling rates, however, crystallization in the thermal boundary-layer is a distinct possibility. Brandeis and Jaupart showed, in calculations that apply to magma chambers just after their emplacement, that for a temperature drop across the boundary-layer of some 600°C, some crystallization will occur provided the viscosity of the magma exceeds about 40 poise ($\sim 10^{-3}$ m^2 s^{-1}). Such crystallization will have at least two effects. The viscosity of the magma in the boundary-layer will be increased due to the presence of crystals (Shaw, 1965), and the density excess of the magma in the boundary-layer will be increased. It seems likely that this will lead to crystal-laden plumes, as envisaged by Wager and Deer (1939), the fate of which as they descend into the convecting magma chamber is uncertain.

Convective velocities in magma chambers

Convective velocities in magma chambers may be estimated by using equations (3.24) and (3.25). Plotted on figure 3.5 are the predicted magnitudes of the mid-depth vertical component of convective velocity, W, using parameters as specified in table 3.2. The horizontal line-segments are mid-depth velocities in the regime where equation (3.25) applies, whilst the sloping line-segments are in the field of applicability of equation (3.24). In general it is the equation yielding the lowest estimate of W that is appropriate.

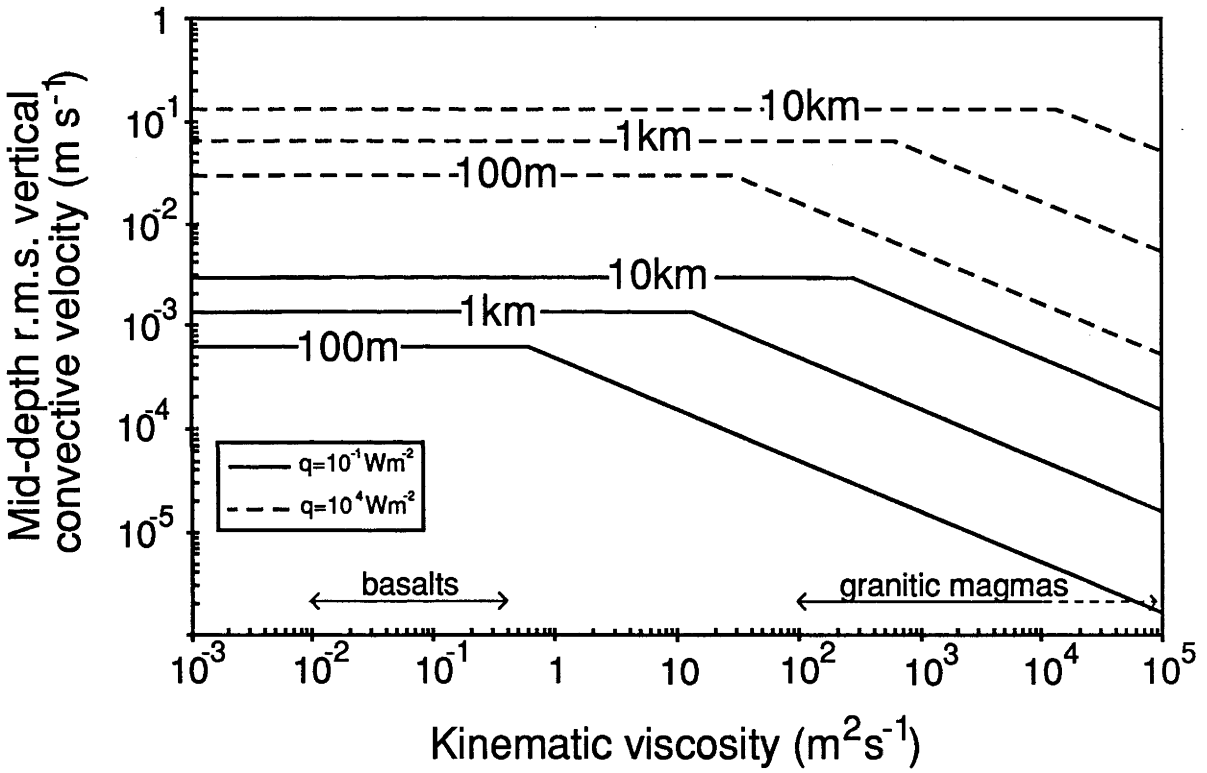

Figure 3.5. Mid-depth r.m.s. vertical component of convective velocity in magma chambers plotted against kinematic viscosity. The solid lines are predictions for slowly cooled magma chambers and the broken lines are predictions for rapidly cooled magma chambers. The lines are labelled with the depth of the chamber.

Mid-depth convective velocities range between 5×10^{-4} to 10^{-1} m s^{-1} for basaltic chambers (50m to 10km per day) and between 10^{-6} and 10^{-1} m s^{-1} for granitic chambers (10cm to 10km per day).

Using a Reynolds number as defined by

$$\mathrm{Re} = \frac{Wh}{\nu} \qquad (3.35)$$

the range of Reynolds numbers for basalts is 10^{-1} to 10^{5} and for granites from 10^{-9} to 10.

Convection granitic chambers can therefore be described as a low Reynolds number flow. On the other hand, convection in basaltic magma chambers may be low Re or high Re. The magnitude of this Reynolds number, however, has little bearing on the turbulence of convective motions, using the word 'turbulence' in the manner recommended by Tritton (1985a).

Effects of the Earth's rotation

Griffiths (1987) has calculated that the rotation of the Earth should have a strong influence on the structure of convection in basaltic chambers greater than 100m deep at high and intermediate latitudes on the Earth. To describe rotating convection a third dimensionless parameter, in addition to Ra and Pr, is required. This is the Taylor number (Ta) which is defined by

$$Ta = \frac{4\Omega^2 h^4}{\nu^2} \qquad (3.36),$$

where Ω is angular velocity of the fluid layer about a vertical axis. Griffiths predicted that, for basaltic chambers, Ta ranges from 10^7 to 10^{14}. At such large Taylor numbers Coriolis forces have a strong effect on the fluid as it converges in the boundary-layer to form a plume, causing it to spin faster than (and in the same direction as) the system as a whole. Rotation thus causes the turbulent convective motions to form into intense vortices the axes of which are nearly vertical. These vortices are expected to be tall and thin, to be very unsteady and to have rapid vertical motion in their cores. Effects of the Earth's rotation are not expected to alter the mean properties of the thermal boundary-layer, however, nor the properties of the compositional boundary-layer, which are calculated in the following chapter.

CONCLUSION

It is expected that thermal convection in most magma chambers will be characterized by extremely large Rayleigh numbers, even at the slowest possible cooling rates. The style of convection in the majority of magma chambers is therefore expected to be unsteady or 'turbulent'. Convective velocities in basaltic chambers are of the order of

metres to kilometres per day, in granitic chambers the range is from centimetres to kilometres per day.

The predicted values of the temperature drop across the thermal boundary-layer are very small. In the majority of magma chambers temperature-dependent viscosity can be neglected. Crystallization in the thermal boundary-layer remains a possibility but is considered unlikely at low cooling rates.

CHAPTER FOUR

CONVECTIVE FRACTIONATION: CRYSTALLIZATION ON HORIZONTAL FLOORS

In this chapter I shall begin to examine the *in situ* solidification model for fractional crystallization. When a magma crystallizes, the crystals that form usually have a different composition to that of the magma. The magma next to the crystal/liquid interface is therefore depleted in some components and enriched in others. In general this residual magma will have a different density to that of the far-field magma. If it is relatively buoyant, compositional convection will occur during *in situ* crystallization on the floor of the chamber. If, on the other hand, it is more dense than the ambient magma, the residual fluid will simply pond at the bottom of the chamber.

The *in situ* solidification model for fractional crystallization relies on compositional convection to redistribute residual liquid away from the growing crystals. Without compositional convection fractional crystallization is impossible since the redistribution of chemical components must then rely on compositional diffusion alone, which is an inherently slow process and will be unable to keep pace with the cooling of the magma.

The purpose of this chapter is to estimate the parameters which describe this convective-fractionation model. The specific example considered is that of a mafic magma crystallizing olivine against a horizontal floor in a high-aspect-ratio magma chamber. This particular example should be directly relevant to the Bushveld, Stillwater, Muskox, Great Dyke, Jimberlana and Rhum intrusions, amongst others. Olivine crystallization was chosen because the necessary thermodynamic data are available to model olivine fractionation with confidence. Some preliminary calculations are also presented for orthopyroxene, but the results are less reliable due to the poorer quality of the available data. Nevertheless the broad conclusions of this work are believed to apply to any magma undergoing *in situ* crystallization when a light residual fluid is produced. Any possible complications that might be associated with the formation of a "mushy zone" of mixed crystals and liquid are ignored.

The approach taken below is identical to that applied in the previous chapter to the problem of thermal convection. The intention is therefore to proceed by calculating flux Rayleigh numbers and then to deduce the properties of the boundary-layers in compositional convection.

Compositional Rayleigh numbers

Convection driven purely by compositionally induced buoyancy is analogous to thermal convection and may be described in terms of a compositional Rayleigh number Rs, which is defined as

$$Rs = \frac{g\beta\Delta S h^3}{\nu\kappa_S} \tag{4.1}$$

where κ_S is the diffusivity of the solute in the magma, β is a compositional "expansion" coefficient such that liquid density obeys $\rho = \rho_0(1+\beta\Delta S)$ and ΔS is some (at this stage unknown) concentration difference between top and bottom boundaries. The corresponding flux Rayleigh number is given by

$$Rs_f = \frac{g\beta f h^4}{\nu\kappa_S^2\rho} \tag{4.2}$$

where f is the mass flux out of the liquid due to crystallization of the heavier "solute", S. The quantity $g\beta f$ is the buoyancy flux, corresponding to the mass flux, f.

It is required to link the mass flux, f, to the heat flux through the chamber roof, q. The rate at which the magma cools, $\frac{dT}{dt}$, is determined by two factors: the rate of heat loss, q, out of the chamber and the rate of release of latent heat of crystallization. The conservation of heat gives

$$q = \rho h c_p \frac{dT}{dt} + Lf \tag{4.3}$$

where L is the latent heat of crystallization. Note that in equation (4.3) I have neglected the slow change of h as crystallization proceeds. If a constant degree of supersaturation is assumed then the rate of change of magma temperature is also related to the mass flux associated with crystallization through the slope of the liquidus in the T-S plane:

$$\frac{dT}{dt} = \frac{f}{\rho h}\left(\frac{\partial T}{\partial S}\right)_{liq} \tag{4.4}$$

where the liquidus slope, $\left(\frac{\partial T}{\partial S}\right)_{liq}$, is expressed in °C per weight fraction. From (4.3) and (4.4) the mass flux onto the surface of the crystal pile is given by

$$f = \frac{q}{\left(L + c_p\left(\frac{\partial T}{\partial S}\right)_{liq}\right)} \qquad (4.5).$$

From (4.2) and (3.27) the ratio of compositional flux Rayleigh number to thermal flux Rayleigh number is

$$\frac{Rs_f}{Ra_f} = \left(\frac{\kappa_T}{\kappa_S}\right)^2 \frac{c_p \beta f}{\alpha q} \qquad (4.6)$$

which, using (4.5), becomes

$$\frac{Rs_f}{Ra_f} = \left(\frac{\kappa_T}{\kappa_S}\right)^2 \frac{c_p \beta}{\alpha\left(L + c_p\left(\frac{\partial T}{\partial S}\right)_{liq}\right)} \qquad (4.7).$$

The ratio of the two Rayleigh numbers is fixed for a given fluid.

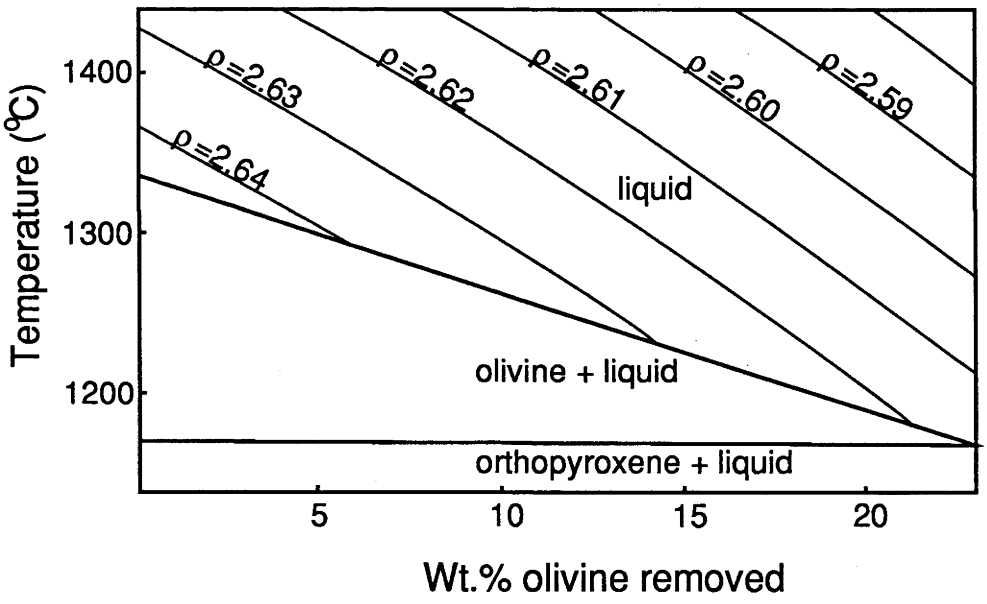

Figure 4.1. Calculated phase diagram for the parental liquid of the Great Dyke (Wilson, 1982) undergoing olivine fractionation, contoured for density (in g cm^{-3}).

In order to compute compositional Rayleigh numbers the quantities β and $\left(\frac{\partial T}{\partial S}\right)_{liq}$ need to be estimated. For mafic magmas the temperature at olivine saturation for a given mole fraction of MgO in the magma is known from the experiments of Roedder (1975), Arndt (1977) and Campbell and Nolan (unpublished). Computer modelling of fractional crystallization then enables the liquidus temperature to be calculated as a function of weight per cent olivine removed. A series of simulations of fractional crystallization was

conducted using a simple BASIC program incorporating the Roedder and Emslie (1970) relationship between Fe/Mg ratios in olivine and liquid. The compositional expansion coefficient was estimated at the same time by calculating liquid densities using the method of Bottinga and Weill (1970) with partial molar volume data taken form Nelson and Carmichael (1979) and Mo *et al.* (1982). Viscosities were also calculated using the method of Shaw (1972).

A similar approach can be used to gain an indication of the effect on convection of orthopyroxene crystallization. In this case it is assumed that the liquidus slope when orthopyroxene is crystallizing is about 1/9 that when olivine is crystallizing (estimated from the phase diagram for the MgO-SiO_2 system given by Bowen and Anderson, 1914).

Typical values calculated for the various parameters are presented in table 4.1. Figure 4.1 is a phase diagram produced by the computer modelling, including superimposed liquid-density contours.

The equivalent equations to (3.17) and (3.27) also hold for the compositional Rayleigh number:

$$Nu_s = C.Rs^b \tag{4.8}$$

and

$$Rs_f = Nu_s.Rs \tag{4.9}$$

where $C \approx 0.2$ and $b=1/3$ as above. Nu_s is the compositional Nusselt number defined by

$$Nu_s = \frac{hf}{\kappa_S \rho \Delta S} \tag{4.10},$$

where ΔS is the compositional drop across the chamber in weight fraction of dissolved olivine. The ratio of the conventional Rayleigh numbers is therefore given by

$$\frac{Rs}{Ra} = \left(\frac{Rs_f}{Ra_f}\right)^{3/4} \tag{4.11}.$$

Typical values for Rs/Ra while olivine or orthopyroxene is crystallizing have been calculated using parameters given in table 4.2. Rs/Ra is generally of the order of 10^6, as shown in table 4.1, while the ratio of flux Rayleigh numbers is of the order of 10^7. Figure 4.2 shows how the ratio varies as a function of the density coefficient, β, for various values of the liquidus slope.

TABLE 4.1

Calculated parameters for various fluids

	Bushveld U[a] magma	Great Dyke[b] parent	MORB[c] picrite	Great Dyke[d] evolved	Na_2CO_3[e] aq. soln.
Phase on liquidus	olivine	olivine	olivine	ortho-pyroxene	$Na_2CO_3.10H_2O$
α ($^oC^{-1}$)	5.46×10^{-5}	6.45×10^{-5}	7.91×10^{-5}	6.40×10^{-5}	4.26×10^{-4}
β (per wt. fraction)	9.16×10^{-2}	7.30×10^{-2}	7.91×10^{-5}	6.40×10^{-5}	8.59×10^{-1}
$\left(\frac{\partial T}{\partial S}\right)_{liq}$	7.01×10^{2}	7.14×10^{2}	6.89×10^{2}	7.95×10^{1}	5.07×10^{1}
ν ($m^2\ s^{-1}$)	4.63×10^{-2}	1.66×10^{-2}	3.77×10^{-3}	7.65×10^{-1}	1.79×10^{-5}
η (poise)	1.21×10^{2}	4.38×10^{1}	1.01×10^{1}	1.99×10^{3}	1.89×10^{-2}
ρ ($kg\ m^{-3}$)	2.61×10^{3}	2.64×10^{3}	2.71×10^{3}	2.62×10^{3}	1.11×10^{3}
Rs_f/Ra_f	7.33×10^{7}	4.29×10^{7}	2.13×10^{7}	2.90×10^{7}	1.87×10^{6}
Rs/Ra	7.92×10^{5}	5.30×10^{5}	3.14×10^{5}	3.95×10^{5}	5.06×10^{4}

[a] Irvine *et al.* (1983)
[b] Wilson (1982)
[c] Elthon (1979)
[d] Great Dyke parent after fractional crystallization of 23 wt.% olivine
[e] 30 wt.% solution, parameters derived from International Critical Tables

TABLE 4.2

Values of parameters used in calculations

Symbol	Units	Value
c_p	$J\ kg^{-1}\ ^oC^{-1}$	1.1×10^{3}
C	-	0.2
g	$m\ s^{-2}$	9.81
L	$J\ kg^{-1}$	8.4×10^{5}
κ_T	$m^2\ s^{-1}$	8×10^{-7}
κ_S	$m^2\ s^{-1}$	1×10^{-10}
α	$^oC^{-1}$	5×10^{-5}
ρ	$kg\ m^{-3}$	2.5×10^{3}

Variations of the liquidus slope have only a small effect. Because the value of the latent heat of crystallization, L, used in the preparation of figure 4.2 was that appropriate to olivine, figure 4.2 strictly only applies to olivine crystallization. However, as minerals crystallizing after olivine have lower latent heats of crystallization, the values of Rs/Ra shown may be regarded as minimum estimates for magmas saturated with other minerals.

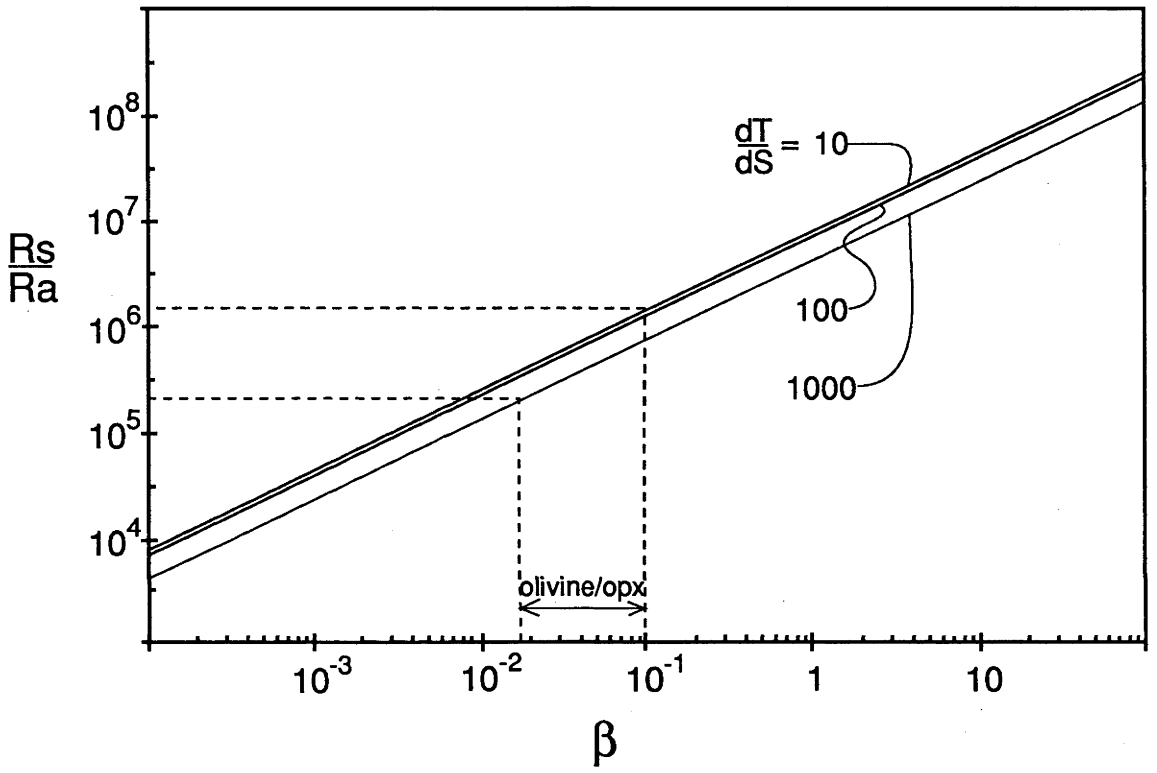

Figure 4.2. The ratio of conventional Rayleigh numbers, Rs/Ra, plotted against β (in "per weight fraction") for various values of $\left(\frac{\partial T}{\partial S}\right)_{liq}$ (°C per weight fraction) using parameters given in table 4.2.

An effective Rayleigh number, Ra_e, when both compositional and thermal buoyancy forces are destabilizing may be defined by

$$Ra_e = Ra + Rs \qquad (4.12)$$

(Turner, 1973, p.255). Since Rs is predicted to be orders of magnitude greater than Ra, $Ra_e \approx Rs$. Taking values of Ra from figure 3.3 and the ratio of Rs/Ra from figure 4.2, it is found that the effective Rayleigh number for mafic magmas crystallizing olivine-orthopyroxene assemblages lies between 10^{16} and 10^{21} for chamber depths between 1 and

10km. At these Rayleigh numbers convection is highly unsteady and disordered, cellular convection should only be possible for layer depth of well below 1m.

Bottom crystallization also releases latent heat, providing a second source of thermal buoyancy. However, since the rate of crystallization is controlled by the heat loss through the roof, the latent heat flux, q_L, must be less than the heat flux, q, though the roof. (In the case of olivine crystallization $q_L \approx q/2$.) Thus the buoyancy flux due to latent heat release at the floor is smaller than the thermal buoyancy flux due to cooling through the roof and has a negligible effect on the magnitude of the effective Rayleigh number.

The compositional and latent-heat boundary layers

Latent heat is generated at the crystal/liquid interface as crystallization proceeds so that not only is compositional buoyancy produced at the lower boundary, but thermal buoyancy as well. There are thus two superimposed boundary-layers at the base of the magma chamber: the compositional boundary-layer and the latent-heat boundary-layer.

The latent-heat flux is related to the heat flux through the roof by the following equation:

$$q_L = fL = \frac{qL}{\left(L + c_p\left(\frac{\partial T}{\partial S}\right)_{liq}\right)} \qquad (4.13)$$

and q_L is generally of order q/2 when olivine is crystallizing from a mafic magma.

If the timescale t_L^* for the conductive growth and sweeping away of the latent-heat boundary-layer alone is shorter than the corresponding timescale t_S^* for the compositional boundary-layer alone, then the compositional boundary-layer will never reach its maximum thickness calculated assuming the absence of the latent-heat boundary-layer: instability of the latent-heat boundary-layer on the shorter timescale will sweep away the buoyant (but always stable) compositional boundary-layer. Conversely, if the intermittent timescale for the chemical boundary-layer is smaller than t_L^*, the latent-heat boundary-layer will not reach its full thickness due to instability of the chemical boundary-layer. The smaller of the two timescales calculated for the independent boundary-layers is the timescale applicable to the double boundary-layer, since the large disparity in lengthscales (d_L, like d_T, is of order one hundred times larger than d_S) ensures that the buoyancy

contained in one boundary-layer has little effect on the stability of the other. For independent (uncoupled) boundary-layers the timescale t^* can be calculated using the definition of the flux Rayleigh number, but substituting $d_S = \sqrt{\pi\kappa_S t^*}$ or $d_T = \sqrt{\pi\kappa_S t^*}$ as the lengthscale in place of the layer depth, h. The ratio of the critical timescales for the two boundary-layers, assuming no coupling is found from (3.27), (4.2) and (4.13):

$$\frac{t_S^*}{t_L^*} = \left(\frac{\alpha q_L}{c_p \beta f}\right)^{1/2} = \left(\frac{\alpha L}{\beta c_p}\right)^{1/2} \qquad (4.14).$$

For magmas crystallizing olivine we find $t_S^*/t_L^* \approx 0.8$. Hence the timescales for the latent-heat boundary-layer and the compositional boundary-layer are almost identical, and parameters governing each boundary-layer can be determined as if the other boundary-layer were not present.

Having established the effective independence of the superimposed boundary-layers, d_S and ΔS can now be calculated in a manner directly analogous to the calculation of d_T and ΔT in (3.31) and (3.32). Thus

$$d_S = \frac{h}{Nu_S} = \frac{h}{CRs^{1/3}} = \frac{h}{C^{3/4}Rs_f^{1/4}}$$
$$= \left(\frac{\rho\nu\kappa_S^2}{C^3 g\beta q}\left(L + c_p\left(\frac{\partial T}{\partial S}\right)_{liq}\right)\right)^{1/4} \qquad (4.15)$$

using (4.2), (4.5) and (4.8), and from (4.15) and (4.5)

$$\Delta S = \frac{f d_S}{\rho\kappa_S}$$
$$= \left(\frac{\nu}{g\beta\kappa_S^2}\left(\frac{q}{\rho C\left(L + c_p\left(\frac{\partial T}{\partial S}\right)_{liq}\right)}\right)^3\right)^{1/4} \qquad (4.16).$$

Figure 4.3 illustrates the values found for d_S and ΔS when olivine is crystallizing from a mafic magma chamber. The compositional boundary-layer is roughly one hundred times thinner than the (upper) thermal boundary-layer with d_s ranging from 2mm to 2cm for conductive cooling rates. Corresponding values of ΔS are 0.2 to 7 wt.%.

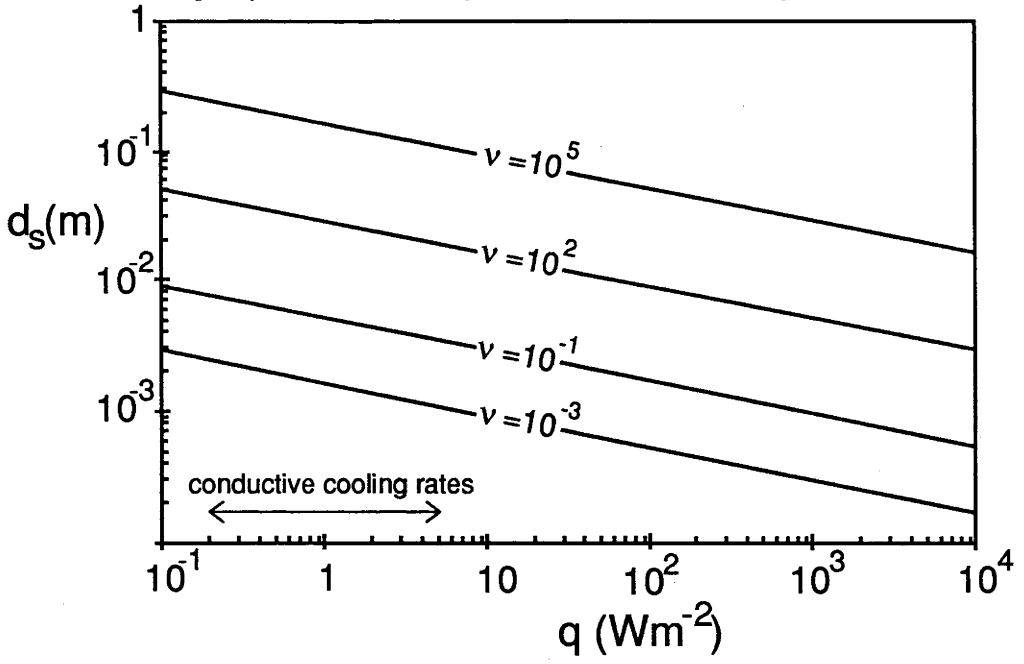

Figure 4.3.a The thickness of the compositional boundary-layer.

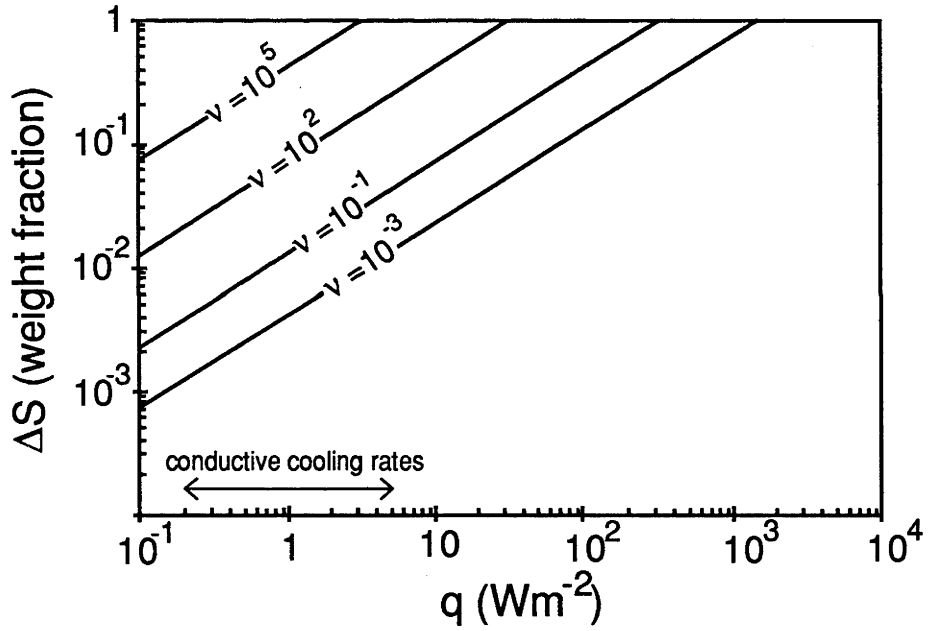

Figure 4.3.b. The compositional drop across the compositional boundary-layer as a function of cooling rate for different viscosities (in $m^2\ s^{-1}$) for mafic magmas crystallizing olivine. Figures 4.3a and b calculated using parameters specified in table 4.2 and with $\left(\frac{\partial T}{\partial S}\right)_{liq} = 700$ and $\beta = 7 \times 10^{-2}$. Note that ΔS is expressed in weight fraction dissolved olivine, to convert to weight per cent multiply by 100. The likely normal range of conductive cooling rates is indicated.

It is interesting to note that the density deficit βΔS is two orders of magnitude greater than the density difference αΔT, since

$$\frac{\beta\Delta S}{\alpha\Delta T} = \left(\frac{\kappa_T}{\kappa_S}\right)^{1/2}\left(\frac{\beta c_p}{\alpha\left(L+c_p\left(\frac{\partial T}{\partial S}\right)_{liq}\right)}\right)^{3/4} \approx \left(\frac{\kappa_T}{\kappa_S}\right)^{1/2}$$

Together with the disparate boundary-layer thicknesses this implies that the compositional boundary-layer and the (upper) thermal boundary layer contain roughly equal amounts of buoyancy.

As in the previous chapter, caution should be advised owing to the neglect of viscosity variations in the above calculations. The computer simulation of fractional crystallization referred to above suggests that the viscosity of olivine saturated magmas increases by some 20% for every 1wt.% fractionally crystallized. For the low values of ΔS predicted for conductively cooled magma chambers, variable viscosity is unlikely to be important. However, for more rapidly cooled magma chambers a thicker compositional boundary-layer is to be expected than that predicted for the isoviscous case, and with a larger compositional drop across it.

The form of the lower boundary-layer is perhaps best shown by considering a specific example. The example sketched in figure 4.4 is that of a chamber containing the parental magma of the Great Dyke cooled at 0.4 Wm^{-2}. The liquidus temperature of the magma is calculated to be $\approx$1337 $^{\circ}C$. The following points are noteworthy.

(i) The temperature increases towards the top of the crystal pile (here considered to be a planar surface) because crystallization at the floor results in the release of a significant amount of latent heat.

(ii) The thickness of the latent heat boundary-layer is 110cm, compared with 1.1cm for the compositional boundary-layer.

(iii) The calculated temperature drop across the latent heat boundary-layer is 0.02 ^{o}C resulting in a very small thermal gradient.

(iv) The change in the olivine content of the magma across the compositional boundary-layer is 0.2 wt.%, resulting in a strong compositional gradient close to the growing crystals.

(v) The depletion of the olivine component of the melt within the compositional boundary-layer lowers the liquidus temperature of the magma adjacent to the growing crystals by 1.5 ^{o}C compared with the liquidus temperature of the far-field magma.

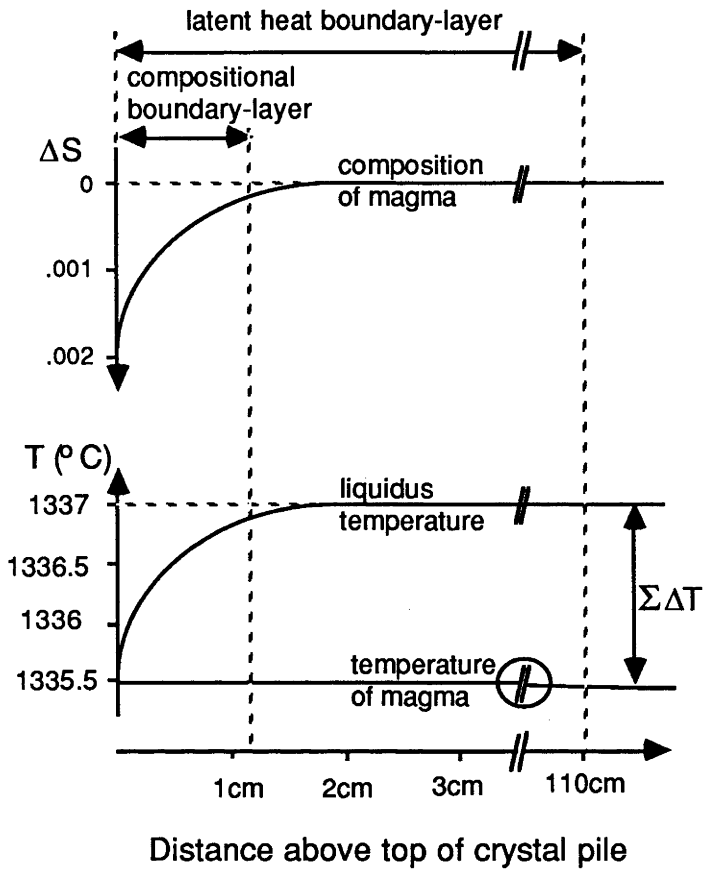

Figure 4.4. A sketch of chemical and thermal profiles in the compositional and latent-heat boundary-layers at the base of a magma chamber undergoing *in situ* crystallization. The numbers shown are those calculated for the parental magma of the Great Dyke (Wilson, 1982) cooling at 0.4 Wm^{-2}, but the qualitative form of the diagram is likely to be appropriate to all magmas which release a light fluid on crystallization. Note that the depletion of the magma in the crystallizing components across the compositional boundary-layer leads to a sharp decrease in the liquidus temperature close to the growing crystals. Also note that the total amount of supercooling ($\Sigma\Delta T$) always increases away from the crystal/liquid interface, and that compositional effects contribute by far the largest portion of this supercooling. The slope of the line representing magma temperature is reflected in the (small) drop across the break between 3cm and 110cm (circled in the diagram).

(vi) If the melt adjacent to the crystals at the top of the crystal pile is assumed to be in equilibrium with the crystals, the far-field magma is supercooled by 1.5°C, almost all of which (1.48 °C) is due to compositional depletion in the boundary-layer and only 0.02 °C is due to thermal differences. That is, the supercooling of the magma outside the boundary-layers (*i.e.* in the bulk of the magma) is dominated by compositional effects and is more appropriately described as supersaturation (or, equivalently, as constitutional supercooling).

(vii) Supersaturation (supercooling) increases with distance from the crystal-liquid interface.

The influence of the compositional boundary-layer on crystal habit

The calculations presented above suggest that for crystals growing at the bottom of a conductively cooled convecting silicate melt, the lengthscale for the compositional boundary-layer will normally be much greater than that of the crystals (observed to be ≤3 mm), although thin boundary-layers are possible at faster cooling rates. Similar calculations show that when crystals are grown from aqueous solutions in laboratory tanks the thickness of the compositional boundary-layer will always be very much less than the size of the crystals. The latter crystals, if growing at the bottom of a convection tank, are large and elongated regardless of whether cooling is from the top or bottom of the tank. Crystals in cumulate rocks, on the other hand, are more equant. It is possible that this fundamental difference in crystal habit is due to the difference in the relative thickness of the compositional boundary-layer in the fluid from which the crystals grew, and can therefore be predicted from a knowledge of the convection régime and crystal size.

An example of a relatively thin compositional boundary-layer is illustrated in figure 4.5a. Thin compositional boundary-layers "cling" to the sides of the growing crystal and are inhibited from breaking away by viscous stresses. Since the fluid within the compositional boundary-layer is light it flows upwards, as illustrated in figure 4.5a, and eventually leaves the crystal from its highest point as a plumes. Removal of the depleted fluid from the growing crystal is a continuous process and the system quickly evolves to a steady-state. The compositional profiles within the boundary-layer are controlled by a balance between diffusion and advection of the boundary-layer, with the melt adjacent to the growing crystal being strongly depleted in those components which are required to form the solid. The heterogeneous nucleation of new crystals within the boundary-layer requires the supercooling adjacent to the crystal to exceed some finite value. If crystal growth and the steady-state condition of the boundary-layer maintain the degree of supercooling of the fluid at a level below that required for the nucleation of new crystals the existing crystals continue to grow outward, resulting in the formation of elongate crystals.

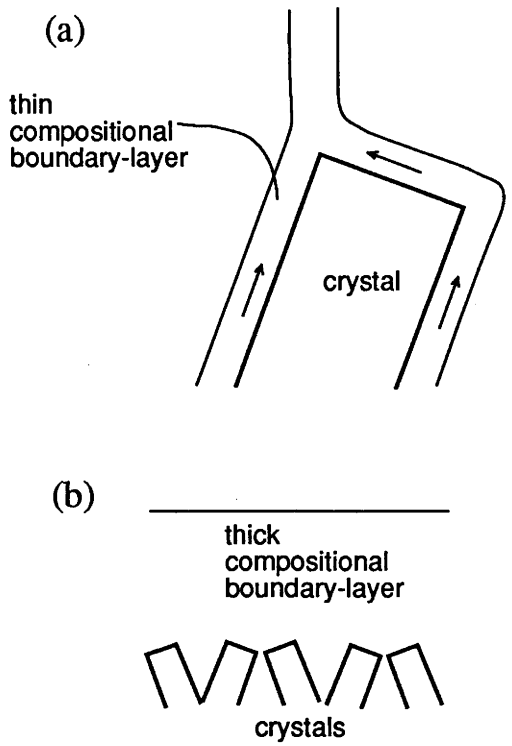

Figure 4.5. Sketches of the two possible configurations of compositional boundary-layer and growing crystals. (a) At high cooling rates the crystals are large compared with the thickness of the boundary-layer. (b) For conductively cooled magmas the crystals are small compared with the thickness of the boundary-layer, which in this case grows by diffusion and breaks down periodically.

The relationship between the compositional boundary-layer and the growing crystals when the boundary-layer thickness is greater than the size of the crystals is very different. This configuration is illustrated in figure 4.5b. Under these conditions there is no continuous, steady flow of buoyant fluid away from the growing crystals. Molecular diffusion spreads the chemical depletion through a relatively much greater distance before the boundary-layer acquires enough buoyancy to become unstable and to rise as a plume. As a consequence the boundary-layer thickness is continuously changing and is intermittently thinned each time it is "swept" by a plume. It then thickens slowly by diffusion as crystallization proceeds. The composition of the fluid adjacent to the growing crystals must change constantly in response to the irregular fluctuations in the thickness of the boundary-layer. When the boundary-layer is at its thinnest, the composition of the magma adjacent to the crystal is closer to that of the undepleted far-field magma outside the boundary-layer. When the boundary-layer is at its maximum

width, near the end of the diffusive growth, the magma next to the crystals is most depleted and closest to the equilibrium composition. This means that the degree of supercooling of the magma adjacent to the crystals is constantly changing, being highest early in the growth cycle and lowest immediately before the end of the cycle. These fluctuations might allow the supercooling at the crystal-liquid interface to occasionally exceed that required for the nucleation of new crystals, even though the average supercooling may be less than that in the case of the narrow boundary-layer. The result will be that new crystals can nucleate against existing crystals, leading to a more equant crystal habit.

The influence of the compositional boundary-layer on trace-element partitioning

Transport of material to the growing crystal is ultimately by diffusion across the compositional boundary-layer. Trace elements which partition preferentially into the crystal will become depleted within the boundary-layer by an amount which is dependent both on the diffusion coefficient (κ_{tr}) and the partition coefficient (D) for the element. This process can be approximated by assuming steady-state diffusion across the time-averaged thickness (2/3 d_S) of the compositional layer. The apparent distribution coefficient, D', which is defined as the ratio of the element concentration in the crystal to that in the far-field magma outside the boundary-layer, is then given by

$$D' = \frac{D}{1+\frac{2Dfd_S}{3\rho\kappa_{tr}}} \qquad (4.17),$$

where, from (4.5) and (4.15),

$$\frac{Dfd_S}{\rho\kappa_{tr}} = D\left(\frac{\kappa_S^2 q^3 \nu}{C^3\rho^3 g\beta\kappa_{tr}^4\left(L+c\left(\frac{\partial T}{\partial S}\right)_{liq}\right)}\right)^{1/4} \qquad (4.18).$$

This D' will be appreciably less than D when $\frac{Dfd_S}{\rho\kappa_{tr}}$ is of order one or greater. For example, for Ni in olivine which is crystallizing from a basaltic melt, $\kappa_{tr}\approx\kappa_S$ and D≈10. Putting appropriate values into equation (4.17) reveals that D' in significantly less than D for cooling rates greater than about $10Wm^{-2}$. For trace elements with small diffusivities (*i.e.* ions with large charges and small radii) the effect is even greater. The appropriate partition coefficient for *in situ* crystallization from silicate melts is therefore not the

equilibrium partition coefficient, D, but the apparent coefficient, D', which depends not only on the composition of the magma and the temperature of crystallization, but also on the nature of the convection. It should also be pointed out that similar considerations apply to incompatible trace elements, although the equation giving D' for these elements is not the same as for compatible elements. It is suggested that the use of equilibrium partition coefficients in geochemical modelling may lead to significant errors in some situations.

Detailed studies of the chemistry of minerals in rhythmically-layered sequences from the Skaergaard intrusion by McBirney and Noyes (1979) support these arguments concerning the nature of the boundary-layer, if it is assumed (as these authors suggest) that these rocks formed by *in situ* crystallization. McBirney and Noyes have shown that the concentration of elements with high partition coefficients into a mineral, or group of minerals, depends on the abundance of that mineral, or group of minerals, in the rock. For example, the concentration of Ni in olivine is lowest at the bottom of a rhythmic layer and increases towards the top. The bottoms of the rhythmic layers are rich in olivine, pyroxene and oxides and grade into a top which is plagioclase-rich. (Note that since iron-oxide, olivine and plagioclase are the major phases in the crystallizing assemblage the magma released by crystallization is light.) The partition coefficient for Ni into olivine, pyroxene and the oxides is greater than one but for plagioclase it is very low. Thus there is an inverse correlation between the Ni content of olivine in a rock and the abundance of Ni-rich phases in that rock. This observation requires the Ni content of the melt from which the olivines are growing to vary systematically with the amount of Ni-rich phases crystallizing. Because the amount of Ni-rich phases in an individual layer is small compared with the size of the main body of the magma, the Ni concentration of the far-field magma is unlikely to change significantly during the crystallization of a single-layer. The crystallization of Ni-rich phases can, however, influence the Ni content of a narrow boundary-layer.

There are two cases to consider: the first when the lengthscale for the boundary-layer is less than that of the crystal and the second when it is greater.

If the boundary-layer is thin it is influenced only by the adjacent crystal. The boundary-layer on each olivine crystal at the top of the crystal pile will be depleted in Ni so that the Ni content of the crystallizing olivines will be less than the equilibrium value. Because the lengthscale of the boundary-layer is small compared with that of the crystals, boundary-layers will rarely overlap. Hence the Ni content of the boundary-layer on a given olivine crystal will not normally be affected by the crystallization of other Ni-rich phases. If the boundary-layers are thin, there should therefore be no correlation between the Ni content of olivine in a rock and the abundance of Ni-rich phases in that rock.

If the compositional boundary-layer is thicker than the crystals, the boundary-layer is not specific to an individual crystal but forms a continuum (as shown in figure 4.5b). Growth of each crystal influences the Ni content of the boundary-layer, so that the higher the percentage of Ni-rich phases crystallizing (and the higher their partition coefficients), the lower becomes the Ni content of the boundary-layer fluid. Thus the observed inverse correlation between the Ni content of olivines and the abundance of Ni-rich phases in the Skaergaard intrusion is consistent with the lengthscale of the boundary-layer being greater than that of the crystal. Similar observations have been made in the Jimberlana intrusion (Campbell, 1978).

Zoning in crystals

As pointed out earlier, if the compositional boundary-layer is thick compared with the crystals the composition of the melt adjacent to the crystal/liquid interface is continually changing on a cyclic basis. Cycles are not periodic in this highly unsteady, chaotic flow, but have a timescale $t_S^* \sim d_S^2/\pi\kappa_S$. Taking d_S=1 cm and $\kappa_S=10^{-10}$ m^2 s^{-1} gives $t_S^* \sim$ 3 to 4 days. By way of comparison the rate of advance of the crystal pile is of the order 10 cm per year for conductive cooling rates, making the timescale for the growth of a 3mm crystal about 10 days. The similarity of the two timescales suggests that crystals growing *in situ* in magma chambers should show compositional banding.

This model can be tested by looking for oscillatory zoning in crystals from layered intrusions. Unfortunately, diffusion is rapid in most crystals and any zoning which forms during primary crystallization is likely to be annealed during the slow cooling of a

large intrusion. Diffusion rates in plagioclase, however, are slower and plagioclase crystals do preserve their primary zoning. Campbell (1973) made a detailed study of zoning in cumulus plagioclase crystals in gabbros from the Jimberlana intrusion. He found that cores of plagioclase crystals from both pyroxene- and plagioclase-rich layers showed complex oscillatory zoning. An example from a mesocumulate pyroxene-rich layer is illustrated in figure 4.6. Note that the predicted oscillations are present and of a magnitude corresponding to the ΔS predicted (albeit for olivine) in figure 4.3b.

Figure 4.6. Compositional variations determined by electron microprobe along a traverse *IJ* across a zoned plagioclase crystal from a pyroxene-rich layer in the Jimberlana intrusion. (Taken from Campbell, 1973.)

The effect of heat loss from the floor

Experimental and theoretical studies of the effect of cooling a magma chamber from the floor as well as the roof are reported in Jaupart *et al.* (1984) and Jaupart and Brandeis (1986). These studies describe experiments conducted using a non-crystallizing fluid and emphasize the diffusion-controlled growth of a cold, dense stagnant layer at the base of the experimental tank. However, the situation when crystallization is occurring on the floor of the chamber or tank is quite different. Superimposed on the stabilizing (negative) buoyancy flux due to cooling are two fluxes of destabilizing (positive) buoyancy: the light depleted fluid released by crystallization and the hot, light fluid resulting from the concomitant release of latent heat. Note that both of these destabilizing buoyancy fluxes would be enhanced by heat loss through the floor (in addition to that through the roof). The stabilizing effect of cooling through the floor is overwhelmed by the destabilizing effects of crystallization (*i.e.* $(\beta f/\kappa_S^2) >> (\alpha q'/\kappa_T^2)$, where q' is the heat

flux through the floor less the latent heat flux). This would be true even if the heat flux through the floor were comparable with the heat flux through the roof.

SUMMARY AND CONCLUSION

Magma chambers cool and crystallize at a rate determined by the heat flux from the chamber. The *in situ* model for magmatic crystallization suggests that, although the heat is lost predominantly through the roof, crystallization takes place mainly at the floor. When a light residual fluid is generated by crystallization both processes provide destabilizing buoyancy fluxes which drive highly unsteady, chaotic convection in the magma. Since the compositional and thermal buoyancy fluxes are directly related it can be shown that the compositional Rayleigh number is very much greater than the thermal Rayleigh number. In the case of a basaltic melt crystallizing olivine Rs is about 10^6 times greater than Ra. However compositional and thermal buoyancy fluxes are roughly equal.

The latent-heat thermal boundary-layer at the floor of a conductively cooled basaltic chamber is of the order of 1m thick, with very low thermal gradients, whereas the compositional boundary-layer is about 1cm thick with large compositional gradients. As a consequence, the variation in the degree of supercooling in front of the crystal-liquid interface is dominated by compositional effects. The habit and composition of the growing crystals may also be controlled by the nature of the compositional boundary-layer. Elongate crystals are suggested to form when the thickness of the compositional boundary-layer is small compared with the crystal-size (as in laboratory experiments with aqueous solutions). In contrast, equant crystals may form when the boundary-layer is thicker than the crystals (as in most conductively cooled magma chambers). Instability of the boundary-layer in the latter case gives rise to zoning within crystals. Diffusion of trace elements through the boundary-layer can also explain an inverse correlation, observed in layered intrusions, between Ni concentration in olivine and the proportion of Ni-bearing phases in the crystallizing assemblage.

CHAPTER FIVE

CONVECTIVE FRACTIONATION: CRYSTALLIZATION ON SLOPING FLOORS

In this chapter I extend the study of convective fractionation, begun in the previous chapter, to include magma chambers with sloping floors. Since many layered intrusions have a funnel-shaped cross-section (*e.g.* Jimberlana, Muskox, Great Dyke) understanding the influence of sloping floors on compositional convection is of obvious geological importance.

I begin this chapter by describing the formation of plumes at a heated sloping floor during turbulent thermal convection. By combining a simple scaling argument with experimental results I derive equations describing the convective boundary-layer above an inclined plane. These equations are then applied to compositional convection in magma chambers.

The second half of this chapter is concerned with the possibility that crystallization against sloping floors may give rise to stratification in the overlying magma. That crystallization against vertical and inward-sloping walls may produce, at least some, stratification is now well established (*e.g.* Turner, 1980; McBirney, 1980; Nilson *et al.*, 1985). It has recently been suggested by Huppert *et al.* (1986b, 1987) that compositional convection from sloping floors may also lead to compositional zonation. This suggestion is addressed below by modelling compositional convection from sloping floors in magma chambers with thermal convection from a sloping heat exchanger in laboratory tanks.

The fluid mechanics of convection above sloping boundaries

There are few studies of convection above sloping boundaries in the fluid-dynamical literature. Most deal with convection in tilted rectangular boxes (*e.g.*, Hart, 1971), although Poulikakos and Bejan (1983) studied a wedge-shaped enclosure (in the context of an attic space). All of these studies, however, are at relatively low Rayleigh number compared with the situation studied here. Previous investigations at higher Rayleigh number have dealt with transitions in the flow within the thermal boundary-layer

(Tritton, 1963; Sparrow and Husar, 1969; Lloyd and Sparrow, 1970) but not with the formation of plumes at the boundary.

Convection above sloping boundaries can be considered as a case lying between the two extremes of convection from horizontal boundaries and convection from vertical boundaries. In the former case there is no component of gravity parallel to the boundary so that buoyant fluid produced at the boundary has no tendency to move in any direction other than the vertical. In this situation a useful description of turbulent convection is in terms of a boundary-layer of buoyant fluid which grows by diffusion until its thickness reaches a critical value, at which time it becomes unstable and breaks away to join convection in the interior of the fluid. In contrast, in the case of convection from a vertical boundary there is no component of the gravity vector perpendicular to the boundary: buoyant fluid produced at the boundary has no tendency to move away from it. However, buoyant fluid will always move parallel to the boundary in response to gravity no matter how small the buoyancy force is. In this situation the boundary-layer never breaks away from the boundary, growing all the time by diffusion while the fluid within it moves upward parallel to the wall.

Turning now to the case of sloping boundaries, there are components of the gravity vector both parallel to the boundary and normal to it. As in the case of the vertical wall, the fluid within the boundary-layer will always have a tendency to move up the slope parallel to the boundary, and as in the case of the horizontal boundary, the boundary-layer will tend to break away from the boundary once its thickness has exceeded a certain critical value. Figure 5.1a is a shadowgraph of an experiment on convection from a sloping boundary (a sketch bringing out the important features of figure 5.1a is given in figure 5.1b). The boundary can be divided into two regions: a lower region in which no plumes are observed to break away and an upper region in which several plumes are observed. In the lower region the boundary-layer, which grows with distance along the slope, is always below its critical thickness, and the fluid within it merely moves upward parallel to the boundary. The boundary-layer in this region is broadly similar to that at a vertical boundary. In the upper region the boundary-layer has been able to grow enough to exceed the critical thickness and peels away to form plumes which sweep up the boundary.

Figure 5.1a. Shadowgraph of an experiment in which an aqueous solution containing 60 wt.% glycerol (ν=9.5x10^{-6} m^2 s^{-1}) was supplied with a heat flux of 6.2x10^2 Wm^{-2} at a sloping floor.

Convection in this region can be considered as broadly similar to high-Ra convection above a horizontal boundary except that the fluid within the boundary-layer moves up the slope as the boundary-layer grows. The boundary-layer in both regions is too thin to be visible in figure 1a.

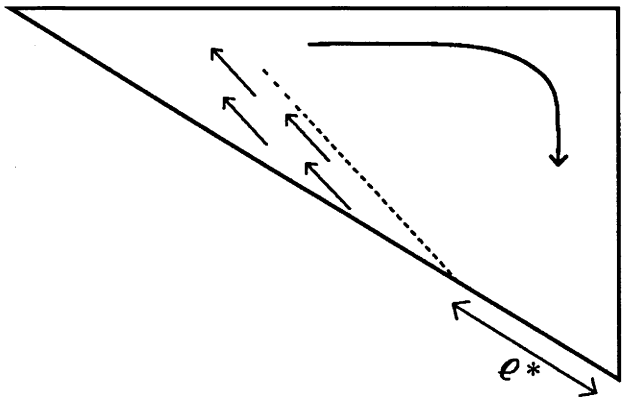

Figure 5.1b. Sketch intended to illustrate the important features of figure 5.1a

A flux-based Rayleigh number for a sloping boundary may be defined by

$$R_f = \frac{\alpha q \ell^4 g \cos\theta}{\nu \kappa_T^2 \rho c_p} \qquad (5.1)$$

where ℓ is the distance up the slope, g is the acceleration due to gravity, θ is the angle of inclination of the boundary to the horizontal, q is the heat flux, α is the thermal expansion coefficient, ν is the kinematic viscosity, κ_T is the thermal expansion coefficient, ρ is the density, and c_p is the specific heat capacity. Experiments show that the length of the lower stable region corresponds to a critical flux Rayleigh number.

A series of experiments was undertaken to determine the value of this critical Rayleigh number and its Prandtl number dependence. Mixtures of glycerol and water were supplied with known heat fluxes via a heat exchanger inclined at 30° to the horizontal using the apparatus described below. Flow visualization was by shadowgraph except for pure water where a pH-indicator technique was used. The viscosity was measured from samples taken after each experiment, while the values of other parameters were taken from Segur (1953). The results are illustrated in figure 5.2 and demonstrate that the critical Rayleigh number is independent of Prandtl number (at least in the range 10^1 to 10^4) and is approximately equal to 3×10^8.

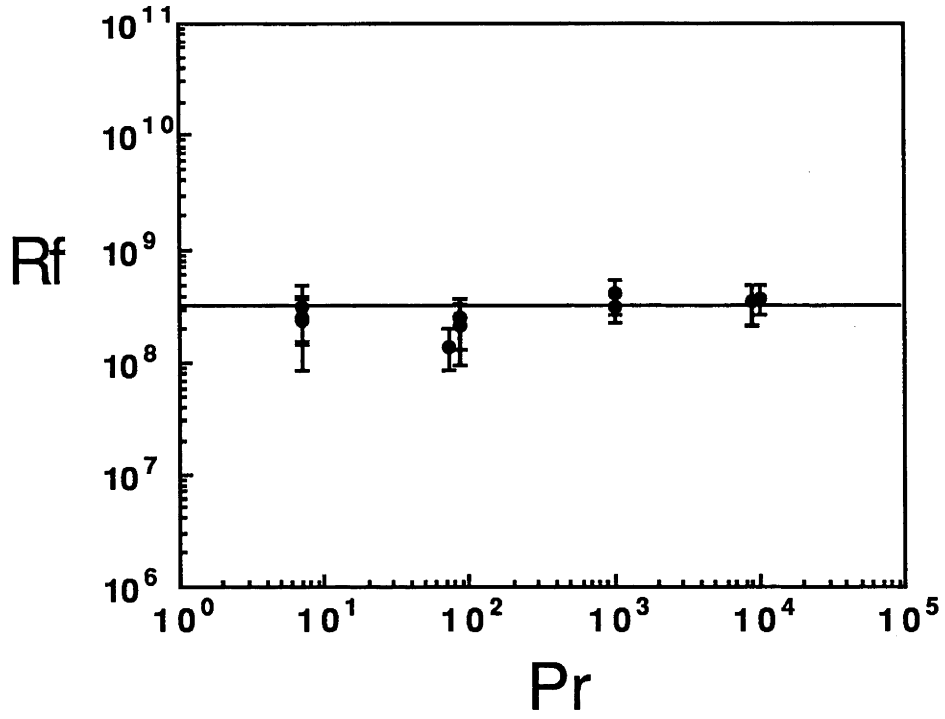

Figure 5.2. Experimental results of critical Rayleigh number based on the length up the slope and its dependency on Prandtl number. R_f is independent of Pr and is approximately equal to $3x10^8$. Error bars are based on the estimated uncertainty of the measured values of ℓ^*.

A simple scaling argument describing the growth and heat content of the boundary-layer is presented in the appendix. Given that the critical Rayleigh number, R_f^* is approximately $3x10^8$, ℓ^* can be calculated using equation (5.1). A rough idea of the critical boundary-layer thickness d_T, can then be gained by using equation (A5.4). d_T is thus given by

$$d_T^* \sim \left(\frac{\nu\kappa_T^2\rho c_p}{g\alpha q}\right)^{1/4} \left(\frac{3x10^8}{\sin^4\theta\cos\theta}\right)^{1/20}$$

$$= 3.1\left(\frac{\nu\kappa_T^2\rho c_p}{g\alpha q}\right)^{1/4} \qquad (5.2).$$

The critical boundary-layer thicknesses at the onset of instability for convection from a horizontal boundary can be compared with that estimated here for convection from an inclined boundary. The thickness of the boundary-layer in the horizontal case is obtained by equating the appropriate Rayleigh number, based on the boundary-layer thickness, to 10^3:

$$d_T^* \sim \left(\frac{10^3\nu\kappa_T^2\rho c_p}{g\alpha q}\right)^{1/4}$$

$$= 5.6\left(\frac{\nu\kappa_T^2\rho c_p}{g\alpha q}\right)^{1/4} \qquad (5.3)$$

Within the resolution of these calculations, the critical boundary-layer thickness for convection above an inclined surface is identical to that for convection above a horizontal surface.

Application to magma chambers

In this section the results presented above are applied to compositional convection in magma chambers. The problem of crystallization against sloping floors releasing a light residual fluid is considered, using (as in chapter four) the specific example of an olivine-saturated magma.

The stability of the compositional boundary-layer in front of the crystals growing on a sloping boundary can be considered irrespective of the stability of the thermal boundary-layer which would be produced by any heat loss through that boundary. This is because the thermal boundary-layer is much thicker than the compositional boundary-layer, and thermal gradients in the compositional boundary-layer are therefore very much weaker than compositional gradients. Because of this the equations derived in the appendix for single-component convection are also applicable to compositional convection in magma chambers.

First, typical values are determined of the compositional Rayleigh number, R_{fs}, which is the compositional equivalent of R_f defined in (5.1). The mass flux, f, onto the crystal pile is related to the the heat flux out of the chamber by

$$f = \frac{q}{r\left(L+c_p\left(\frac{\partial T}{\partial S}\right)_{liq}\right)} \qquad (5.4)$$

(cf. equation (4.5)), where q is the heat flux, r is the ratio of the area over which the heat flux is being lost to the area over which crystallization is occurring, L is the latent heat of crystallization, and $(\partial T/\partial S)_{liq}$ is the slope of the liquidus ($^\circ$C per weight fraction). The compositional flux Rayleigh number, R_{fs}, is then given by

$$R_{fs} = \frac{\beta q l^4 g\cos\theta}{r\nu\kappa_S^2\rho\left(L+c_p\left(\frac{\partial T}{\partial S}\right)_{liq}\right)} \qquad (5.5).$$

Figure 5.3 shows values for R_{fs} calculated for mafic magmas crystallizing olivine, assuming r=1. The minimum cooling rate of 0.1W m^{-2} (see chapter four) was used in the construction of this diagram, with other parameters being taken from Table 5.1. Thus the values of R_{fs} illustrated are minimum values.

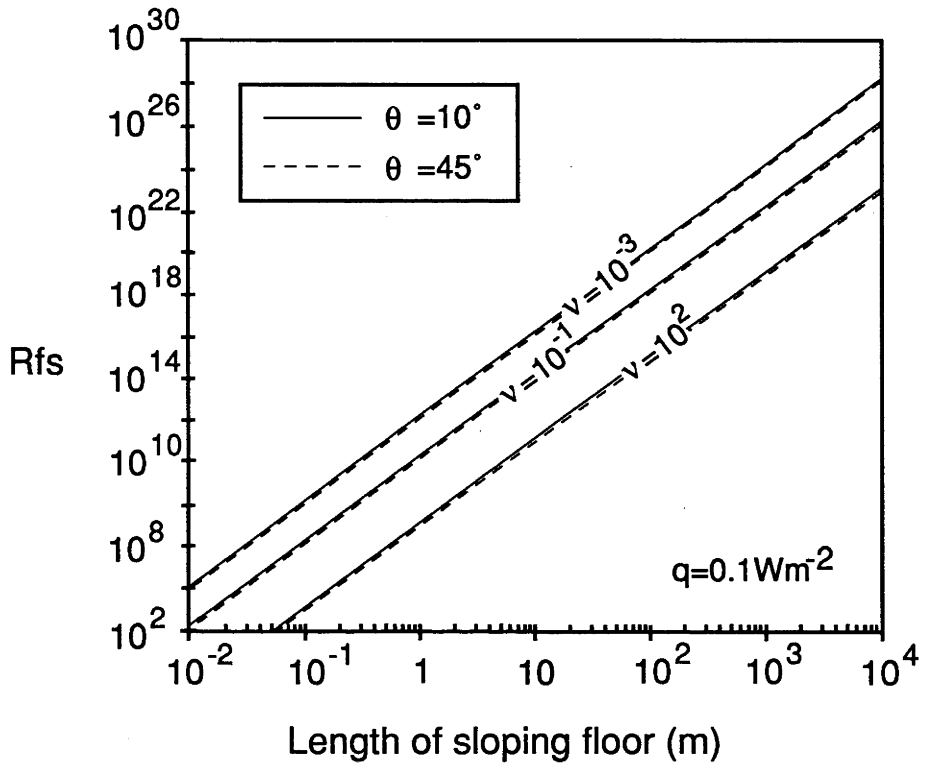

Figure 5.3. Graph showing typical values of R_{fs} appropriate to mafic magmas crystallizing olivine. The solid lines are for a sloping floor inclined at 10° to the horizontal and the dashed lines (which almost overlap with the solid lines) are for an angle of inclination of 45°.

TABLE 5.1

Values of parameters used in calculations

Symbol	Units	Value
c_p	J kg^{-1} $^oC^{-1}$	$1.1x10^3$
g	m s^{-2}	9.81
L	J kg^{-1}	$8.4x10^5$
κ_S	m^2 s^{-1}	$1x10^{-10}$
β	(weight fraction)$^{-1}$	$7x10^{-2}$
ρ	kg m^{-3}	$2.5x10^3$
$\frac{\partial T}{\partial S_{liq}}$	°C (weight fraction)$^{-1}$	$7x10^2$

Note that for mafic magmas R_{fs} is always larger than the critical value for ℓ greater than about 10 cm; in other words, the length ℓ^* along the boundary that the fluid in the boundary-layer flows before breaking away is of the order of 10cm. Basaltic magma chambers between 1km and 10km deep are typically characterized by an R_{fs} in the range 10^{24} to 10^{28} for this minimum cooling rate.

Having established the supercriticality of the sloping-boundary Rayleigh number for compositional convection in magma chambers, the thickness of the compositional boundary-layer, d_S, and the drop in concentration, ΔS, across the boundary-layer can now be estimated. These are approximated by the critical value of these quantities at the onset of instability of the boundary-layer and are given by equations (A5.9) and (A5.10). Typical values for olivine-saturated magmas are illustrated in Figure 5.4, which shows that the thickness of the compositional boundary-layer is commonly in the range 2 mm to 2 cm for conductively cooled magma chambers, while the drop in composition across the boundary-layer is between about 0.2 and 7 wt.% (in terms of dissolved olivine). Both quantities show only a weak dependence on the angle of inclination of the floor.

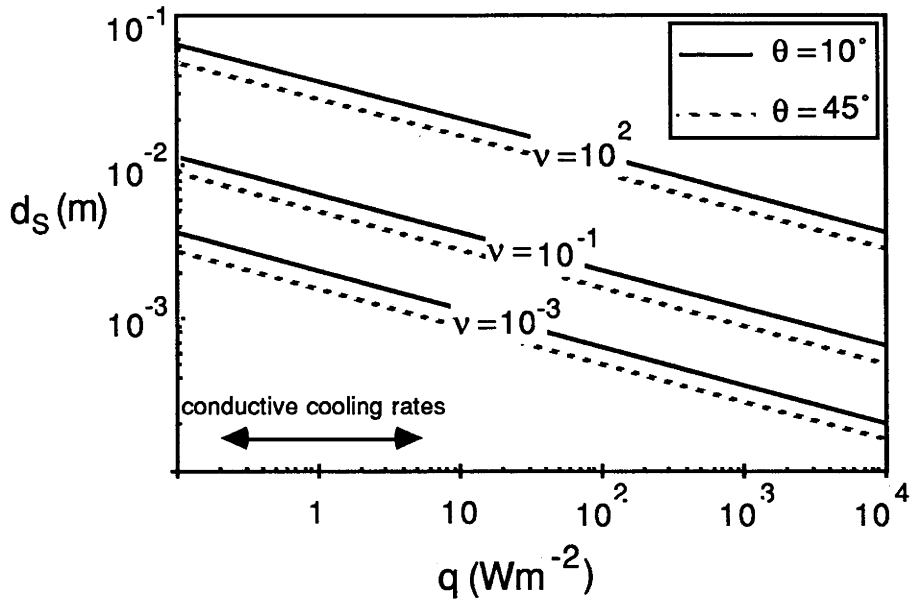

Figure 5.4a. The thickness of the compositional boundary-layer, d_S. See caption for figure 5.4b.

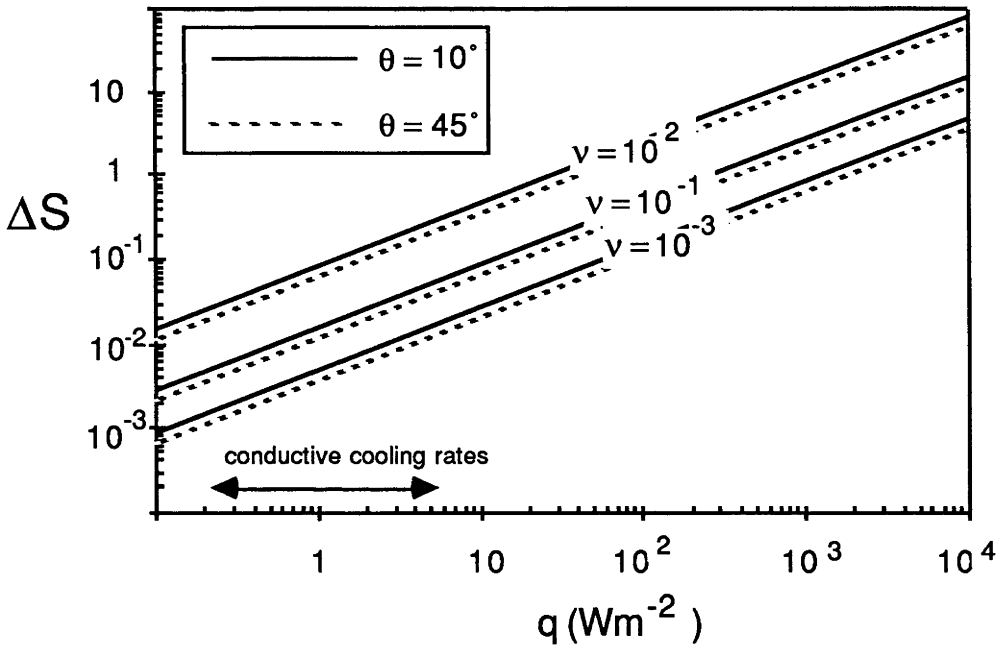

Figure 5.4b. The drop in concentration, ΔS, (in weight fraction dissolved olivine) across the compositional boundary-layer. The solid lines are for θ=10° and the dashed lines are for θ=45°. Calculated using parameters appropriate to olivine crystallization taken from table 5.1.

The predicted magnitudes of d_S and ΔS for compositional convection driven from sloping floors are very similar to the horizontal-floor case examined in chapter 3. The suggested petrological consequences of the calculations in chapter three therefore apply equally to the sloping-floor case.

Experiments investigating stratification produced by convection driven by heating at a sloping floor.

Once the plumes have broken away from the boundary, it might be expected that they should move vertically in response to the buoyancy force (*i.e.* parallel to the gravity vector). In the present series of experiments this is not the case, and the reason for this is geometrical. Because the region above the sloping boundary is wedge shaped, plumes rising from near the top of the slope mix with comparatively little ambient fluid before they reach the top of the fluid. Fluid at the top of the tank near the heat exchanger is therefore less dense than fluid further away, and this horizontal density gradient drives a flow outward from the top of the slope. In order to conserve mass, fluid from further down the heat exchanger is drawn in and up, so creating a broad upslope current.

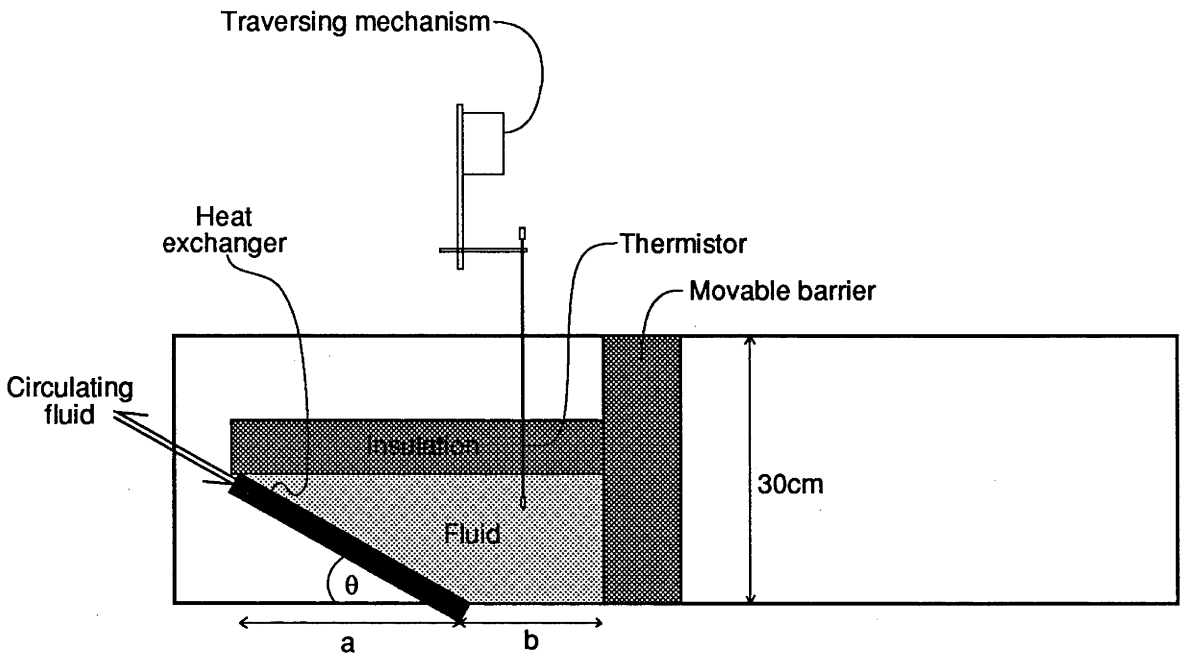

Figure 5.5. Schematic diagram of experimental apparatus.

The flow of this current raises the possibility that convection from sloping boundaries may give rise to stratification of the main body of the fluid. A series of experiments was conducted to investigate the stratifying effect of the upslope current in various geometrical configurations. The apparatus in which most of the experiments were conducted (illustrated in figure 5.5) consisted of a perspex tank, 15cm wide and 30cm deep, one end of which is formed by a movable P.V.C. barrier with an inclined heat exchanger clamped in place to form the other. The whole tank was insulated using expanded polystyrene which could be removed to make observations. The heat exchanger (surface area 30 cm x 15 cm) comprised a 3cm thick aluminium block with a 1cm thick copper block above it and a 1mm thick polypropylene sheet sandwiched between them. A maze of 12mm channels through which hot or cold fluid could be circulated was cut into the aluminium block. The temperature difference across the polypropylene sheet could be determined by means of two thermistors adjacent to the sheet embedded in the copper and aluminium blocks. The temperature of the fluid circulated through the heat exchanger was controlled by a cooling unit and a Braun 1480 Thermomix which was linked to a PDP11 computer programmed in such a way as to maintain a constant temperature difference across the polypropylene sheet, with the intention of providing a fixed heat flux which

could be calculated from previous calibration experiments. Temperature profiles through the experimental fluid (water) were determined by slowly traversing (~1 mm s^{-1}) one or two thermistors and logging the outputs from the thermistor(s) and the traversing mechanism on an I.B.M. A.T. computer. In these experiments the angle of inclination of the heat exchanger to the horizontal was fixed at 30°. Because this angle enters only very weakly into equations (A5.4) and (A5.5) and because of technical difficulties concerning the small volume of fluid at low angles of inclination, experiments covering a wide range of angles were not carried out. Later experiments were conducted using two heat exchangers in configurations described in the appropriate sections below.

In all cases the heat flux through the heat exchanger at the site of the thermistors was fixed at 6.2 x 10^2 Wm^{-2}, which gives a flux Rayleigh number, based on the entire length of the heat exchanger, of ~10^{11}. The temperature profiles illustrated are those at "quasi-steady state", taken when the profile had achieved a shape which did not change with time, the whole profile being moved along the temperature scale without distortion as time proceeded. This was always achieved in less than half an hour from the start of the experiment. Flow visualization was enabled by a pH technique which caused the buoyant fluid adjacent to the heat exchanger to be stained a dark colour for a short period, the subsequent motions of this dark fluid could then be followed.

When the sloping heat exchanger occupies the entire length of the tank. The apparatus was assembled so that the distance, b, in figure 5.5 was zero. A temperature profile taken close to the deepest part of the fluid is illustrated in figure 5.6, and figure 5.7 is a sequence of photographs showing the fluid motions.

In this configuration there is an overall circulation involving an overturning that affects all of the fluid in the tank. Because of this the thermal stratification observed is minimal, significantly less than the drop in temperature across the thermal boundary-layer for example. This is not greatly different from what would be expected for turbulent convection between horizontal plates: for example, Chu and Goldstein (1973) report a weak stratification in this configuration, although they found that it did not persist to a very high Rayleigh number.

Figure 5.7. A sequence of photographs showing the overall circulation produced in the experiments at A=0. Blue dye was produced at the boundary for a short period of time by a *p*H technique, enabling the subsequent motions of the dyed fluid to be observed.

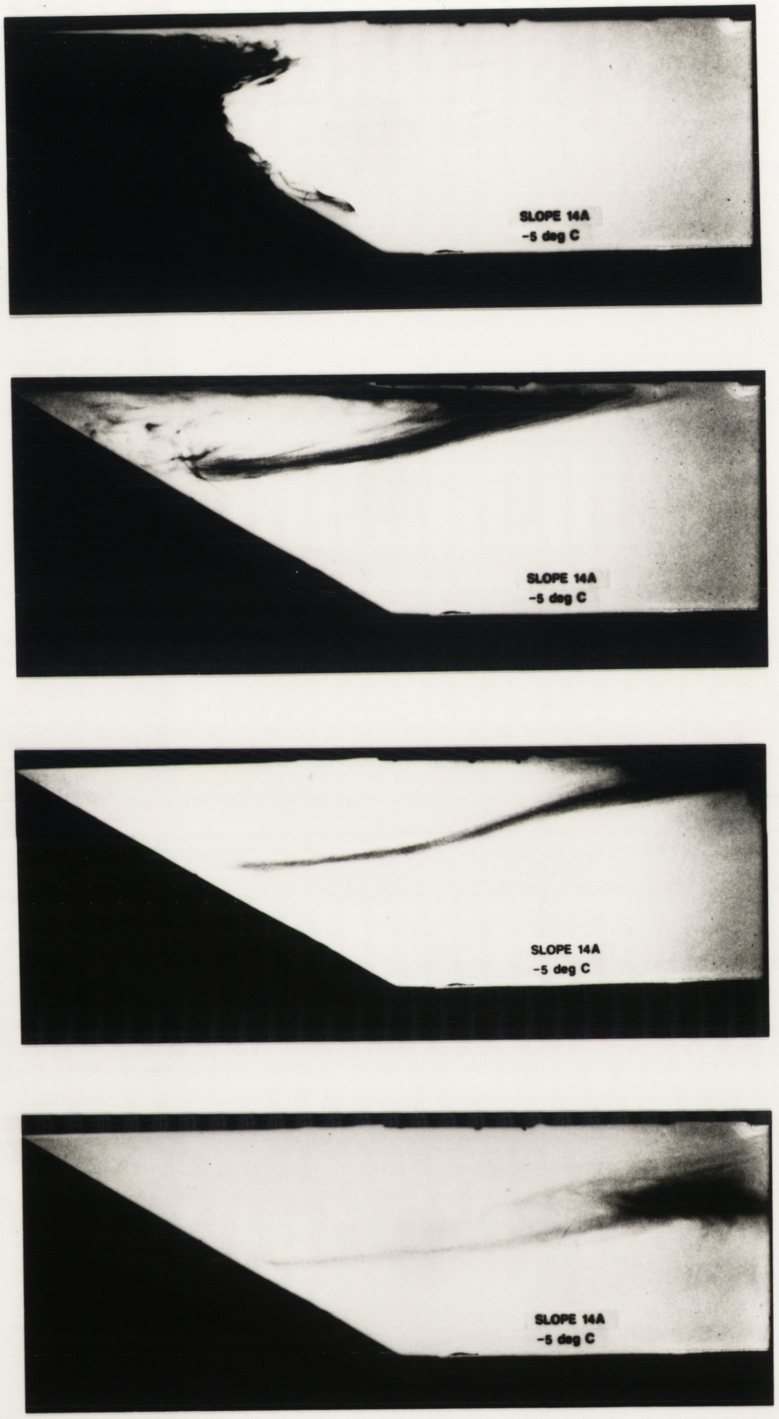

Figure 5.9. A sequence of photographs illustrating the filling-box process which operates in tanks with an unheated horizontal floor when heat is supplied at an outward-sloping wall.

(ii) The shape of the high-A profiles are more like those observed in a turbulent filling box (Baines and Turner, 1969) than the S-shaped profiles observed in a laminar filling box (Worster and Leitch, 1985). It is interesting to note, however, that in the evolution of the temperature profiles toward quasi-steady state no "first front" was observed, which is more in keeping with the experiments of Worster and Leitch than those of Baines and Turner.

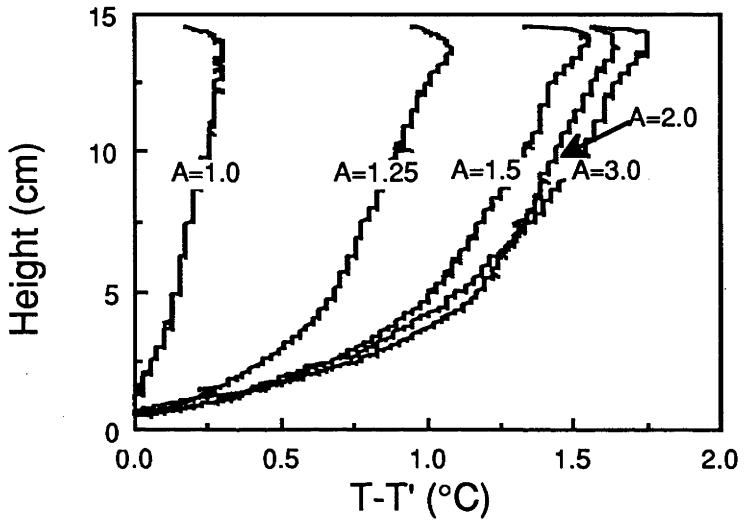

Figure 5.8. Quasi-steady state temperature profiles taken for the experiments involving a passive horizontal floor of varying length. Height in fluid plotted along y axis, with temperature of fluid, T, less temperature at base of profile, T', plotted along x axis.

(iii) Stratification of the fluid leads to a greater heat flux though the bottom half of the heat exchanger than the top half. The heat flux was only controlled at the height of the thermistors in the heat exchanger (*i.e.*, halfway up the slope). When the fluid is stratified by 1.5°C, the heat flux at the bottom is 15% greater than the desired value and the heat flux at the top is 15% less.

When there is an active (heated) horizontal floor occupying part of the tank. In the series of experiments described above the highest stratifications were achieved at the highest A. High-A configurations were produced by adding a passive, unheated, horizontal floor to the tank extending out from the bottom edge of the heat exchanger. This situation, however, is not a realistic representation of a magma chamber where buoyant fluid is likely to be released by crystallization on the floor as well as the walls. The experiment now described represents an attempt to reproduce more closely the geometry of a magma

chamber. The passive floor of the tank illustrated in figure 5.5 was replaced by a similar heat exchanger to that used in the previous experiments. The precise geometry in this case was restricted by the available apparatus so that A=2.4 and θ=45°, and the heat flux through the floor was constrained to be (roughly) equal to that through the sloping wall.

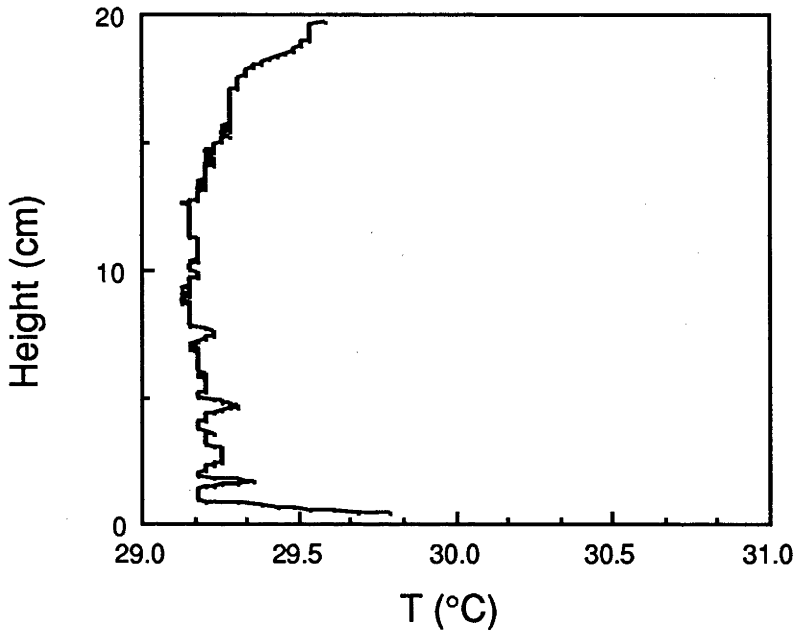

Figure 5.10. Steady state temperature profiles observed in an experiment at A=2.4 in which both the sloping wall and the base of the tank were heated at the same rate.

Observations of the fluid motion indicated that the filling-box process observed previously at high-A was unable to operate due to the homogenizing influence of light fluid released at the horizontal floor. This fact is reflected in the temperature profile illustrated in figure 5.10 which shows a weak thermal stratification in the top few centimetres of the fluid, while the lower 15 cm are dominated by the homogenizing influence of convection from the horizontal boundary. The large fluctuations in temperature close to the floor of the tank can be attributed to the thermistor passing through plumes rising off the base and, at the very bottom, to it approaching the thermal boundary-layer.

The effect of two sloping boundaries. In a further attempt to replicate the geometry of magma chambers, the two heat exchangers were joined at 90° along their short ends and clamped so that both heat exchangers made an angle of 45° to the horizontal. This configuration then resembled a cross section across a funnel-shaped intrusion. Not

surprisingly the effect was similar to the case with A=1 discussed above. An overall circulation up the slopes and down in the middle is observed resulting in a similar small degree of thermal stratification, illustrated in figure 5.11.

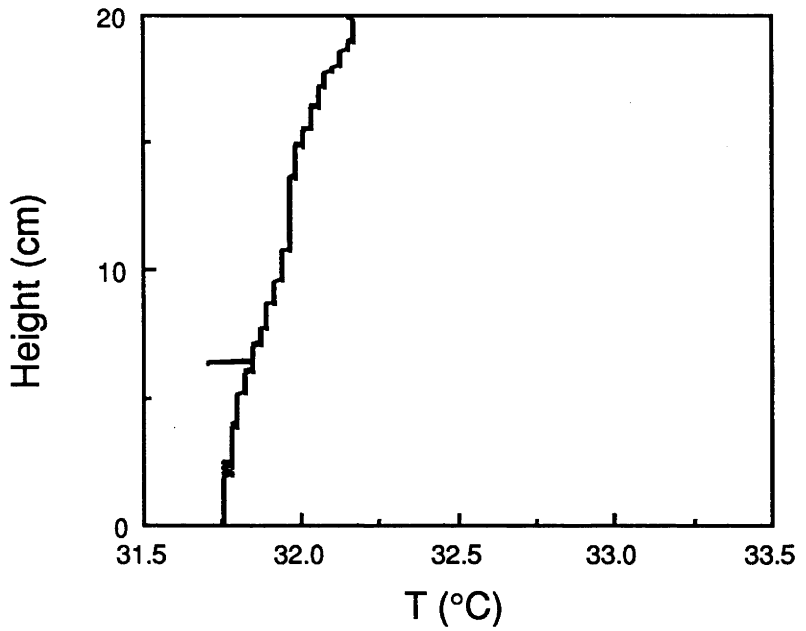

Figure 5.11. Steady state temperature profiles observed in an experiment involving supplying the same heat flux at two sloping floors inclined at 45° to the horizontal and joined along their lower edges.

Comparison of filling-box processes

In this section I compare the filling-box process observed in the high-A experiments involving an unheated horizontal floor with two filling-box mechanisms that have previously been studied, namely: turbulent convection from a line source (Baines and Turner, 1969) and laminar convection against a vertical wall (Worster and Leitch, 1985).

The analysis of Baines and Turner refers to buoyancy continuously supplied from a line source in the form of a turbulent plume which rises through the ambient fluid, entraining it at a rate proportional to the local mean upward velocity. When the plume (plus entrained ambient fluid) reaches the top of the fluid it spreads out to become part of the environment so that the box is filled from the top downward and stratification is built up. This process has been applied to magma chambers undergoing replenishment by buoyant inputs by Campbell *et al.* (1983), Huppert *et al.* (1986a), and Turner and Campbell (1986).

The analysis of Worster and Leitch considers a convective boundary-layer produced by heating at a vertical wall. As buoyant fluid is produced at the boundary it moves upward in a boundary-layer, always clinging to the boundary except at the very top when it spreads out laterally to fill the box from the top downward. In the experiments studied by Worster and Leitch, and probably also in magma chambers, the velocities are such that the flow within the boundary-layer is always laminar.

Convection from sloping floors at high A has features in common with both processes. Like the filling box of Worster and Leitch the flow within the boundary-layer is likely to be laminar; however, it is not the flow within the boundary-layer that leads to stratification of the fluid but rather the turbulent flow of the upslope current. Unlike the vertical-wall case, the thermal boundary-layer does not cling to the heated boundary indefinitely but breaks away when its thickness (and hence buoyancy content) exceeds a critical value and then undergoes turbulent mixing with ambient fluid to form the upslope current. Stratification induced by convection from outward sloping boundaries will therefore always be less than if the boundary were vertical.

The upslope current constitutes a turbulent filling-box process, as evidenced by the shape of the temperature profiles, but there are major differences with the turbulent process analyzed by Baines and Turner. Specifically, the heated boundary is an extended source of buoyancy, not a line or point source. Plumes are released at different heights in the fluid so that plumes released near the top of the boundary entrain less fluid than plumes released near the bottom. Second, plumes released above the critical distance ℓ^* are released into a mixture of previously released plumes and ambient fluid, and it is this mixture of fluid that they entrain, not purely ambient fluid. For these reasons, stratification induced by the upslope current will always be greater than that produced if the buoyancy flux were concentrated into a turbulent line plume at the base of the fluid.

The conclusion reached by the above discussion is that the stratification resulting from the present filling-box mechanism should be intermediate between that which would be produced by the two previously studied mechanisms for the same total buoyancy flux. Although I have been unable to develop a quantitative theory describing the sloping-boundary filling-box process, this conclusion can at least be tested, given the

experimental results above and equations describing the vertical-wall process and the line-plume process.

For the vertical wall case, a rough estimate of the stratification induced can be obtained by assuming that the amount by which the temperature of the fluid is changed during its journey through the boundary-layer is equal to the vertical drop in temperature across the depth of the fluid:

$$T\text{-}T' \sim \left(\frac{\nu q^4 \ell}{g\alpha\kappa_T^3 \rho^4 c_p^4}\right)^{1/5} \tag{5.6}$$

which is equation (A5.5) with $\theta=90^o$, where T-T' is the drop in temperature across the fluid. Putting in appropriate parameters the drop in temperature predicted by (5.6) for the same buoyancy flux as in the experiments reported above is of the order of 2°C.

For the process analyzed by Baines and Turner an estimate of the drop in buoyancy Δ across the depth h of the fluid due to a line source of buoyancy of equivalent strength to the heated sloping boundary is given by

$$\Delta = 2^{1/6} F_0^{2/3} a^{-2/3} h^{-1} f(\zeta) \tag{5.7}$$

where F_0 is the buoyancy flux per unit length of the equivalent line plume ($F_0=g\alpha q\ell/\rho c_p$), a is the entrainment constant ($a\approx 0.1$), and $f(\zeta)$ is a function of order 1. In this case $\ell\sin\theta$ is the appropriate length scale, and this is substituted for h. Then converting buoyancy to temperature ($\Delta=g\alpha(T-T')$) gives

$$T\text{-}T' \sim \frac{1}{\sin\theta}\left(\frac{q^2}{10^{-2} g\alpha l \rho^2 c_p^2}\right)^{1/3} \tag{5.8}$$

which yields 0.3°C for values of parameters appropriate to the experiments reported above.

The stratification observed in our experiments at high A with a passive floor was close to 1.5°C, slightly less than that predicted by equation (5.6) but greater than that predicted by equation (5.8), in agreement with the preceding discussion.

Comparison with experiments involving the cooling and crystallization of aqueous solutions against a sloping floor

Huppert *et al.* (1986b, 1987) reported a series of experiments in which aqueous solutions were cooled and crystallized at a sloping boundary. They found that compositional stratification with prominent double-diffusive layering always developed in the solution. Figure 5.12 shows the evolution with time of compositional stratification in a typical experiment.

I believe there are two reasons why stratification develops in these experiments. The first reason is the presence of an unheated horizontal extension to the tank. Huppert *et al.* conducted all of their experiments in a tank with a passive horizontal floor (*i.e.* in apparatus similar to that illustrated in figure 5.5, but always with b>0). As noted above for thermal convection experiments, in such geometries a filling-box process is able to operate. However, it is significant that the shape of the compositional profiles observed by Huppert *et al.* is quite different to the shape of the thermal profiles observed above at high A. Whilst the shape of the latter profiles are characteristic of a turbulent filling-box process, the former profiles are S-shaped, suggesting the operation of a laminar filling-box process. I attribute this additional laminar process to thin laminar compositional plumes which rise off the tips of growing crystals. As noted in chapter four, in crystallizing aqueous solutions the width of the compositional boundary-layer is much smaller than the typical size of the crystals. Crystals growing in aqueous solutions present an array of predominantly steep surfaces on which growth takes place and from which compositional convection is driven. Buoyant fluid produced by crystallization clings to the growing crystals and streams off continuously from the tips of the crystals. My own experience with crystallizing aqueous solutions and the photographs of Huppert *et al.* (1986b, 1987) indicate that these plumes can rise through the ambient fluid for a few centimetres before going unstable and mixing with it. Inevitably, since the sloping floor occupies the entire depth of the tank, some of these plumes must reach the top of the fluid before they go unstable and hence before they can mix with an appreciable amount of ambient fluid. This laminar process is suggested to be the origin of the strong stratification at the top of the fluid in the Huppert *et al.* experiments.

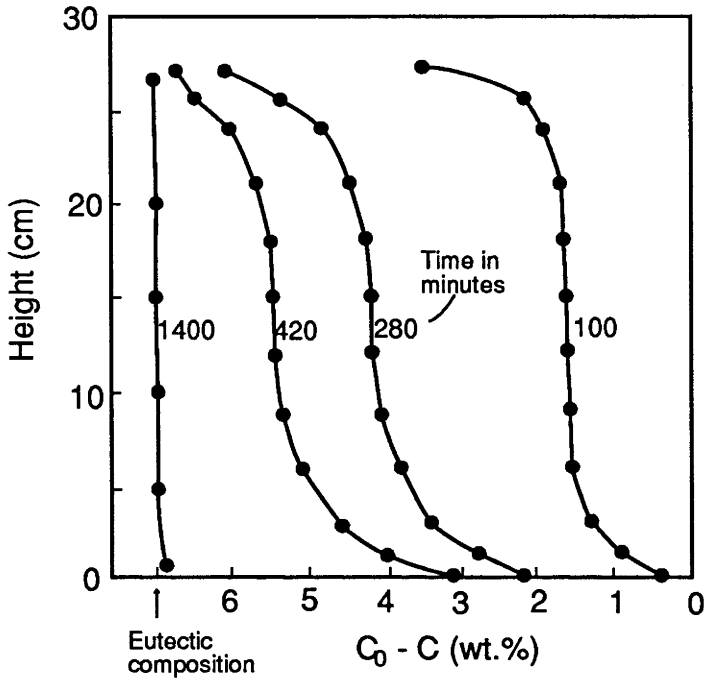

Figure 5.12. The evolution of compositional profiles with time during the crystallization of Na_2CO_3 solution against a floor sloping at 45°. The initial concentration of Na_2CO_3 less the observed concentration is plotted along the x-axis and the profiles are labelled with time after the start of the experiment (in minutes). Taken from Huppert *et al.* (1986b).

In aqueous solutions there are thus two mechanisms which can contribute to compositional stratification during crystallization against sloping floors. First, when the tank has a passive horizontal extension, a similar filling-box process to that observed in the above thermal-convection experiments may operate. Second, steady plumes rising from the tips of growing crystals may stratify the fluid directly.

Application to magma chambers

It is suggested that the thermal-convection experiments reported in this chapter more closely capture the features of compositional convection from sloping floors in magma chambers than the experiments with crystallizing aqueous solutions reported by Huppert *et al.* (1986b,1987). This suggestion is supported by two considerations.

(i) *The geometry of the container.* The Huppert *et al.* experiments were conducted in tanks with geologically unrealistic shapes, with A>1 and a passive horizontal floor. As shown in the experiments reported above (see figure 5.8), even a very small passive horizontal extension has a large influence on the nature of the flow. For this geometry to be reproduced in magma chambers requires that crystallization take place over the upper

parts of the sloping floor but not where the floor levels out toward the centre of the chamber. It is hard to imagine how this could be the case. In fact it is more likely that the reverse is true, since the influence of pressure on the melting point of minerals ensures that supersaturation increases with depth. Further, observations from layered intrusions show that crystallization takes place over the entire floor. In the thermal-convection experiments described above, when buoyancy is supplied over a sloping floor that covers the entire width of the chamber (i.e., A=1), an overturning circulation on the scale of the entire tank results and convection therefore has a homogenizing effect rather than a stratifying effect. Similarly, if the horizontal floor is active, then the filling box process is unable to operate because of the homogenizing influence of convection from that boundary.

(ii) *The smoothness of the surface from which convection is taking place.* In aqueous solutions the thickness of the compositional boundary-layer is very small compared with the size of the crystals. In thermal-convection experiments, however, the thickness of the thermal boundary-layer is greater than the lengthscale of the roughness of the boundary. The smooth surface in these latter experiments may be closer to the magmatic situation than the extremely rough surface produced in experiments with aqueous solutions. The predicted thickness of the compositional boundary-layer while olivine is crystallizing (given above) compares with olivine crystal sizes usually in the range 0.2-4 mm (Brandeis *et al.*, 1984). The compositional boundary-layer is usually thicker than the crystal size. Therefore if crystal size is an adequate indication of roughness, which is certainly appropriate to irregularities of horizontal wavelength of the order of the crystal size, the compositional boundary-layer is usually just thicker than the roughness of the crystal pile. However, there are likely to be much larger irregularities when the surface of the pile is viewed at larger horizontal wavelengths. There are two points to be made here. First, it is estimated above that the fluid forming each plume 'sees' only about 10cm of the surface of the crystal pile so that irregularities of wavelength larger than 10cm are not important, i.e., they are 'filtered out'. At wavelengths of order 10cm or less, crystal size is often an adequate estimate of roughness, as is shown by many of the figures of Wager and Brown (1968) (*e.g.* figures 38, 44, 51, 63, 158, 187, 188, and 197). Second,

when there are significant irregularities at wavelengths below 10cm, figures of Wager and Brown (1968) (*e.g.* figures 68, 85, and 160) also show that these are relatively gentle undulations compared with the extremely jagged aggregate of vertically oriented crystals produced in aqueous solution experiments. In this case the situation in magma chambers may be more closely approximated by a smooth surface.

Before the one-component thermal convection experiments described above can be applied to compositional convection in magma chambers, however, some discussion is necessary of the effect of the superposed thermal convection in magma chambers. Figure 5.13 shows a sketch of a cross-section through a funnel-shaped magma chamber, with arrows indicating heat loss. Consider first the situation in which all of the heat is lost through the roof (*i.e.* $q_f = 0$). In this case, in addition to the positive buoyancy flux due to crystallization against the floor, there is another positive buoyancy flux due to the release of latent heat. Both of these buoyancy fluxes will tend to drive a similar upslope current and an overall circulation which will homogenize the fluid. At the same time, heat loss through the roof drives a further homogenizing circulation, although in this case the natural tendency will be for a circulation in the opposite direction.

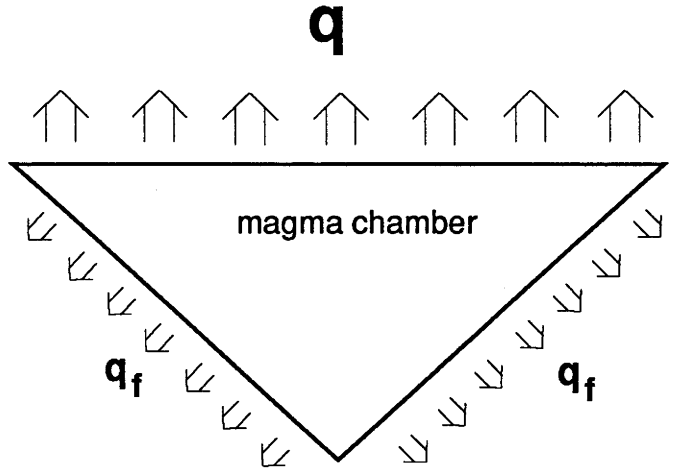

Figure 5.13. A sketch cross-section through a funnel-shaped magma chamber. The arrows are intended to indicate heat loss, with q being the heat flux through the roof and q_f being the heat flux through the floor.

Consider now the effect of increasing the magnitude of q_f relative to q. As q_f is increased there will always be a net positive thermal buoyancy flux from the boundary until $q_f = q_L$ where q_L is the latent heat flux. As shown in chapter four, this occurs when

$q_f \approx q/2$ for magmas crystallizing olivine. Until this point is reached the situation will be similar to that described in the preceding paragraph.

As q_f is increased still further a negative thermal buoyancy flux is produced at the sloping floor. In this case the magnitude of this negative buoyancy flux, F_T, should be compared with magnitude of the positive compositional buoyancy flux, F_S. The ratio of these two fluxes is given by:

$$\frac{F_S}{F_T} = \frac{\beta f c_p}{\alpha q_f} \qquad (5.9).$$

Only when all the heat is lost through the sloping floor (*i.e.* when q is close to zero) are the two buoyancy fluxes of similar magnitude.

In practise, it is likely that the heat flux driving crystallization against the floor will be lost predominantly through the roof (Irvine, 1970). For most magma chambers, therefore, the effects of the superposed thermal convection will be homogenizing. Taking thermal convection into account will not normally alter the conclusions reached here.

Because the Rayleigh numbers appropriate both to compositional convection in magma chambers and the thermal convection experiments reported here are much larger than the critical value and because the details of the production of buoyant fluid at the boundary are similar, it is reasonable to extrapolate from these experiments to compositional convection in magma chambers. Compositional convection from outward sloping boundaries in magma chambers will not lead to a filling box process; instead convection will be characterized by overturning on the scale of the depth of the fluid and significant stratification is unlikely to develop.

Such a conclusion is supported by geological evidence. The Columbia River Basalts are made up of flows of "remarkably uniform" tholeiitic magmas (Carmichael *et al.*, 1974) 20-30 m thick and, in some cases, several hundred kilometres in length. It is likely that these flows were fed by a magma chamber for two reasons. First, the flows are characterized by Mg numbers that are well below the accepted level for magma in equilibrium with the mantle and include highly evolved magmas such as ferrobasalts. Second, it is hard to imagine how such large volumes could be withdrawn from the mantle in a single event without first accumulating in a holding reservoir or magma

chamber. The existence of these lavas therefore suggests that magma chambers may contain large volumes of unzoned magma.

During *in situ* crystallization of a magma chamber, if the floor is horizontal the release of a light magma homogenizes the overlying magma, whereas the release of a dense magma has a stratifying influence. Therefore, if crystallization at a sloping boundary leads to zoning of the magma chamber regardless of whether a light or dense magma is released, large volumes of homogeneous magma can only be produced when light magma is released by crystallization at a horizontal floor. This is possible if the Columbia River Basalts are fed by a large, flat-bottomed sill. However, it is much more likely that the floor to the chamber that fed the Columbia River Basalts either sloped or was undulating. In this case the chamber would show some evidence of zoning. Alternatively, if the preceding discussion is correct and crystallization releasing a light liquid at a sloping floor has a homogenizing influence on the overlying melt, there is no necessity for the floor to be flat.

Models of crystallization of layered intrusions

Irvine *et al.* (1983) and Wilson and Larsen (1985) have proposed models of crystallization against inclined floors in zoned magma chambers which seek to explain observed features of layered intrusions. Of particular interest to this study is the observation of Wilson and Larsen that the composition of minerals from a given stratigraphic layer in the Hyllingen Series, Norway, become more evolved when traced up dip and their suggestion that this is due to crystallization at a sloping floor in a zoned chamber. A key question is whether the required zoning can be produced by crystallization at a sloping floor when a light depleted magma is produced or whether the required zoning is produced by some other mechanism. The experiments reported above show that the latter is the case: that zoning cannot be produced by crystallization at an outward sloping wall if a light magma is released.

The process most likely to lead to zoning in magma chambers when crystallization releases a light magma is replenishment of the chamber by hot dense magma (Huppert and Sparks, 1980; Turner and Campbell, 1986). If the new input takes the form of a

turbulent fountain, extensive mixing will occur between the new magma and the fractionated magma, leading to the development of a zoned hybrid layer at the bottom of the chamber that will break up into a number of double-diffusive convecting layers (Turner and Campbell, 1986). In order to be certain about the subsequent evolution of the chamber, further experiments are required, but it may be the case that such liquid layering is more persistent than previously thought. In the two-layer system discussed by Huppert and Sparks (1980) the density of the lower layer decreases as crystallization proceeds, eventually becoming equal to the overlying layer at which time overturning and homogenization occurs. However, if the magma in the different layers is related by the same liquidus, overturning may never occur. Consider a two-layer system in which both layers are crystallizing. Although the density of the lower layer will decrease, it may never become the same as the overlying layer because the upper layer is also crystallizing and evolving. If heat is being lost predominantly through the roof of the chamber, the overlying layer will always be colder and more evolved and its density less (provided the same degree of supersaturation is maintained in both layers). Complete overturning can only occur if the upper layer becomes more supersaturated than the lower layer.

It is suggested that the entry of hot, dense pulses of magma into chambers in the form of fountains may, under conditions likely to be common in magma chambers, lead to the formation of persistent layering in magma chamber even when light magma is being released during crystallization. A reasonable explanation, therefore, for the change in mineral compositions along stratigraphic layers observed by Wilson and Larsen (1985) may be that it results from crystallization at an inclined wall or floor of a chamber that was zoned during replenishments by fountains of hot, dense magma.

SUMMARY AND CONCLUSION

The Rayleigh numbers appropriate to compositional convection driven by crystallization at a sloping floor in magma chambers are sufficiently large to be highly supercritical. Convection from sloping boundaries under these conditions is very similar to that from a horizontal surface, in particular, in the thickness of the compositional

boundary layer and drop in composition across it, and there is only a weak dependence of these quantities on the angle of inclination of the sloping boundary.

Compositional convection from an inclined floor in magma chambers is appropriately modelled by thermal convection from an inclined heat exchanger because in both cases the surfaces are comparatively smooth. Laboratory investigations show that in geologically realistic configurations the convection is characterized by a large-scale overturning on the scale of the entire tank, and significant stratification is therefore not developed. This observation leads to the conclusion that in magma chambers crystallization at a sloping floor releasing a light depleted fluid will homogenize, rather than stratify, the overlying magma. Significant compositional zonation will not develop.

Three geological conclusions follow from this result:

1. The suggestions made in the preceding chapter concerning the consequences of *in situ* crystallization for the habit and composition of the crystals apply equally to crystallization against inclined floors.

2. Large volumes of homogeneous magma can exist in a magma chamber when crystallization is taking place against an inclined floor.

3. Models describing the crystallization of layered intrusions which involve the interaction of crystallization against an inclined floor with compositionally stratified magma require an external cause for the stratification when crystallization releases a light magma. For example, replenishment of the chamber by a hot, dense magma may lead to persistent compositional zoning.

APPENDIX

Heat content and thickness of the boundary-layer in convection driven from a sloping floor

The conservation of heat and momentum give

$$w\frac{\Delta T}{\ell} \sim \kappa_T \frac{\Delta T}{d_T^2} \qquad \text{(A5.1)}$$

and

$$0 \sim \frac{\nu U}{d_T^2} + g\alpha\Delta T \sin\theta \qquad \text{(A5.2)}$$

where U is the speed of the fluid in the boundary-layer parallel to the heated boundary, ΔT is the temperature drop across the boundary-layer, ℓ is the length along the heated boundary, κ_T is the thermal diffusivity, d_T is the boundary-layer thickness, g is the acceleration due to gravity, α is the thermal expansion coefficient, and θ is the angle of inclination of the heated boundary to the horizontal. The heat flux q is given by

$$q \sim \kappa_T \rho c_p \frac{\Delta T}{d_T} \qquad \text{(A5.3)}$$

where ρ is the fluid density and c_p is the specific heat capacity.

Eliminating U in (A5.1) and (A5.2) and substituting for ΔT using (A5.3) gives

$$d_T \sim \left(\frac{\nu \kappa_T^2 \rho c_p}{g \alpha q \sin\theta}\right)^{1/5} \qquad \text{(A5.4)}$$

with

$$\Delta T \sim \left(\frac{\nu q^4 \ell}{g \alpha \kappa_T^3 \rho^4 c_p^4 \sin\theta}\right)^{1/5} \qquad \text{(A5.5).}$$

The experiments described above suggest that buoyant fluid breaks way from the boundary at $R_f^* \sim 3 \times 10^8$, and using the definition of R_f (equation (5.1)), this gives the critical length along the heated boundary:

$$\ell^* \sim \left(\frac{3 \times 10^8 \nu \kappa_T^2 \rho c_p}{g \alpha q \cos\theta}\right)^{1/4} \qquad \text{(A5.6)}$$

The critical boundary-layer thickness at which the boundary-layer becomes unstable, d_T^*, and the excess temperature of the plumes, ΔT^*, are then given by substituting (A5.6) in (A5.4) and (A5.5):

$$d_T^* \sim \left(\frac{\nu \kappa_T^2 \rho c_p}{g \alpha q}\right)^{1/4} \left(\frac{3 \times 10^8}{\sin^4\theta \cos\theta}\right)^{1/20} \qquad \text{(A5.7)}$$

and

$$\Delta T^* \sim \left(\frac{\nu q^3}{g \alpha \kappa_T^2 \rho^3 c_p^3}\right)^{1/4} \left(\frac{3 \times 10^8}{\sin^4\theta \cos\theta}\right)^{1/20} \qquad \text{(A5.8).}$$

Analogous equations apply to compositional convection:

$$d_S^* \sim \left(\frac{\nu \kappa_S^2 \rho}{g \beta f}\right)^{1/4} \left(\frac{3 \times 10^8}{\sin^4\theta \cos\theta}\right)^{1/20} \qquad \text{(A5.9)}$$

and

$$\Delta S^* \sim \left(\frac{\nu f^3}{g \beta \kappa_S^2 \rho^3}\right)^{1/4} \left(\frac{3 \times 10^8}{\sin^4\theta \cos\theta}\right)^{1/20} \qquad \text{(A5.10).}$$

CHAPTER SIX

CRYSTAL SETTLING IN CONVECTING MAGMAS

In the last two chapters I have examined a model for magmatic differentiation which relies on *in situ* crystallization. This model has become increasingly popular in the last ten years. Nevertheless, strong evidence in favour of the alternative crystal-settling model can be found in some layered intrusions (*e.g.* Irvine, 1974; Parsons and Butterfield, 1981) and this model is also supported by observations on lavas (Cox and Mitchell, 1988). In addition, the occurrence of cogenetic phenocrysts in erupted magmas shows, at least, that not all crystallization takes place *in situ*. In this chapter I shall consider the fluid mechanics of crystal settling. I shall proceed under the assumption that crystals either grow in, or are transported into, the convecting magma before they accumulate on the floor of the chamber. Circumstances under which crystals are likely to form in suspension in the magma are outlined in the following chapter.

Some simple theoretical considerations are presented first, and I shall then describe a series of laboratory experiments on particle settling in turbulent convection. Finally some geological applications are discussed.

The problem of crystal settling in convecting magmas

I begin by comparing typical crystal settling velocities with typical thermal-convective velocities in magma chambers. Such a comparison is given in figure 6.1. Stokes' Law gives the terminal settling velocity of a spherical particle:

$$v_s = \frac{g\Delta\rho x^2}{18\rho\nu} \qquad (6.1),$$

where x is the diameter of the crystal and $\Delta\rho$ is the density contrast between the crystal and the magma. The shaded area on figure 6.1 shows the range of likely crystal-settling velocities in magma chambers. Also shown are predicted values of the mid-depth r.m.s. vertical component of convective velocity, W, calculated using equations given in chapter 3. The convective velocities were calculated using parameters given in table 3.2 and assuming a cooling rate of 0.1 Wm^{-2}, which is the minimum likely cooling rate, hence the

convective velocities illustrated are minimum estimates. Despite this fact it can be seen from the graph that convective velocities are almost always much larger than crystal-settling velocities. Only for the largest olivine crystals in the least viscous magmas, such as picrite or komatiite, is the settling velocity comparable to the mid-depth r.m.s. vertical component of the convective velocity. .

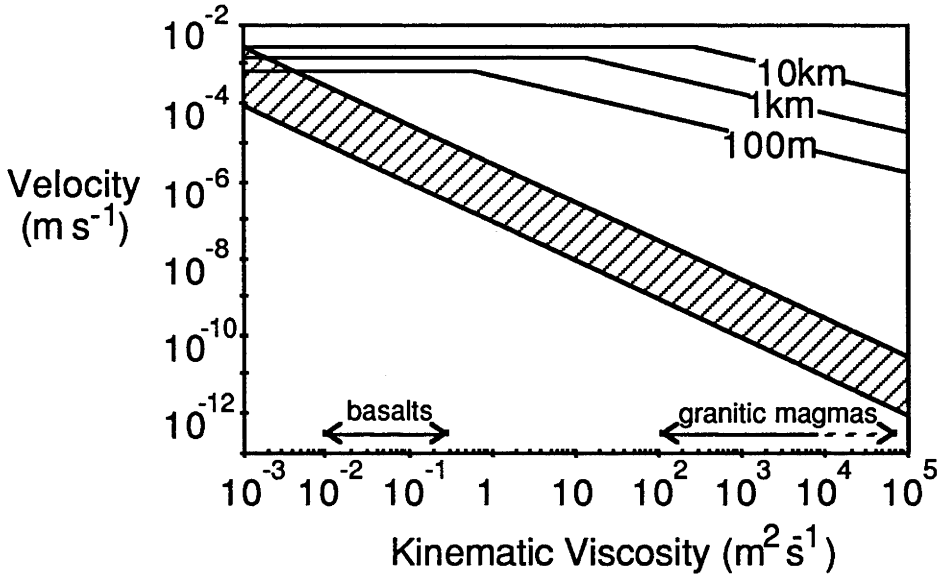

Figure 6.1. Predicted velocities in magma chambers. The crooked lines are predictions of mid-depth r.m.s. vertical component of convective velocity from equations (3.24) and (3.25), using q=0.1Wm^{-2} and other parameters from table 2. The lines are labelled with the depth of the chamber. The shaded area is the range of predicted Stokes' Law settling velocities for spherical crystals, bounded on the low-velocity side by the velocities predicted for 1mm diameter crystals which are 0.05 g cm^{-3} more dense than the magma (appropriate to small plagioclase crystals), and on the high-velocity side by 5mm diameter crystals which are 0.6 g cm^{-3} more dense than the magma (appropriate to large olivine crystals).

Such a conclusion was also reached by Sparks *et al.* (1984), who made the suggestion that convective velocities may be sufficiently large in most magma chambers, when compared with the crystal-settling velocities, to ensure that all crystals are kept in suspension indefinitely. Thus, Sparks *et al.* questioned whether crystal settling could normally be possible. Similarly, doubts have been raised about the possibility of crystal settling in rapidly convecting ponded komatiite lavas (Turner *et al.*, 1986). However, while a parameter s, defined as

$$s = \frac{v_s}{W}, \qquad (6.2)$$

is generally very small ($10^{-5}<s<1$ for basaltic magmas and $10^{-10}<s<10^{-3}$ for granitic magmas) the convective velocities must tend toward zero as the boundaries of the flow are

approached. This raises the possibility, also noted by Huppert and Sparks (1980) and Sparks *et al.* (1984), that crystal settling will be effective at the bottom boundary of the fluid. A simple theory of particle settling in turbulent convection arising from this possibility is presented in the following section.

Simple theory of particle settling in turbulent convection

In this section an equation describing the rate at which particles settle out of a turbulently convecting fluid is derived. Three major assumptions are made:

(i) The system is one dimensional; in other words the turbulent convection guarantees that the particles are mixed homogeneously across the flow.

(ii) There is no re-entrainment of particles into the flow once they have settled out.

(iii) Particle concentrations are sufficiently low so that the particles neither influence each other nor the nature of the flow. The limitations imposed by these assumptions are discussed later.

Consider the case of particles of uniform size suspended in a fluid undergoing turbulent thermal convection driven by cooling from above. If the ratio s is very much less than one, throughout the bulk of the fluid the particles behave as passive tracers and are very nearly uniformly mixed by the turbulent motions. However, at the base of the fluid, where the convective velocities vanish, the particles are free to settle out from the fluid with their full Stokes' Law settling velocity. Therefore the rate at which the number of particles in the flow, N, decreases with time is given by

$$\frac{dN}{dt} = -A_b v_s c(0) \qquad (6.3)$$

where A_b is the area of the base of the fluid and c(z) is the number concentration of particles at height z above the bottom boundary. To a first approximation, as the particles are uniformly distributed throughout the majority of the flow it may be assumed that c(0) is simply given by $\frac{N}{A_b h}$, the depth-averaged concentration. The integration of equation (6.3) then yields

$$N = N_0 \exp\left(\frac{-v_s t}{h}\right) \qquad (6.4)$$

where N_0 is the initial number of particles in the flow. The number of particles decays according to an exponential law where the decay constant is given by the ratio of v_s and h.

The ratio s does not appear in the result but its magnitude has been used in the assumption of particle uniformity.

This simple analysis is quite satisfactory provided s is very much less than unity, ensuring that the convective velocity, although everywhere less than or equal to W, is still very much greater than the particle settling velocity throughout nearly all of the flow. However, it is clearly of interest to know how large s must be before this analysis becomes invalid. In Martin and Nokes (1989) a more sophisticated analysis, due to Roger Nokes, is presented in which the variation of particle concentration with height in the flow as a function of s is calculated. The calculations described in that paper suggest that equation (6.4) should hold to a very good approximation even when s approaches unity.

The above model differs from those of Bartlett (1969) and Huppert and Sparks (1980) in that the fact that convective velocities vanish at the lower boundary is a key feature. The analyses of Bartlett and Huppert and Sparks, on the other hand, do not take the depth-dependence of convective velocity into account.

Experimental investigation of particle settling in turbulent convection

In this section experimental support for the reasoning presented above is described. The experiments were conducted using a perspex tank 20cm high and measuring 15cm x 30cm across the base (internal dimensions). Both the top and the base of the tank were fitted with metal heat exchangers similar to that described in chapter five. The heat flux through the heat exchangers, the temperature of the upper and lower boundary and the temperature at mid-depth in the fluid were monitored during the experiments. The experiments were performed using one or both heat exchangers either to cool from above only, to cool from both above and below, or to cool from above and heat from below.

The experimental fluids consisted of water with various amounts of additives. NaCl was used to increase the density, and C.M.C. (sodium carboxymethyl cellulose) was used to increase the viscosity. Both of these properties were measured in the laboratory. The particles used in the experiments were unexpanded round polystyrene beads (measured density 1.033±0.001 g cm^{-3}) in three size ranges: 0.21-0.31mm, 0.31-

0.42mm and 0.42-0.50mm. The tank was illuminated by slide projectors shining through two 1cm wide vertical slits on the two 15cm wide walls of the tank, and photographs were taken looking through one of the 30cm wide walls.

The experiments involved introducing particles into the convecting fluid (depth 20cm) and monitoring the subsequent evolution of the system by taking short (1/4 s) exposure photographs (one such photograph is shown for illustration in figure 6.2). The number of particles in suspension was determined by counting the number of dots in a representative area of each photograph. In all except one experiment (in which re-entrainment of particles was observed) the number of particles decayed with time according to an exponential law. Figure 6.3 shows the number of particles plotted against time for a typical experiment (involving cooling from above only) and confirms that an exponential law is obeyed (equation (6.4)). In addition several streak photographs were taken, which enabled W to be determined (as described in chapter 3).

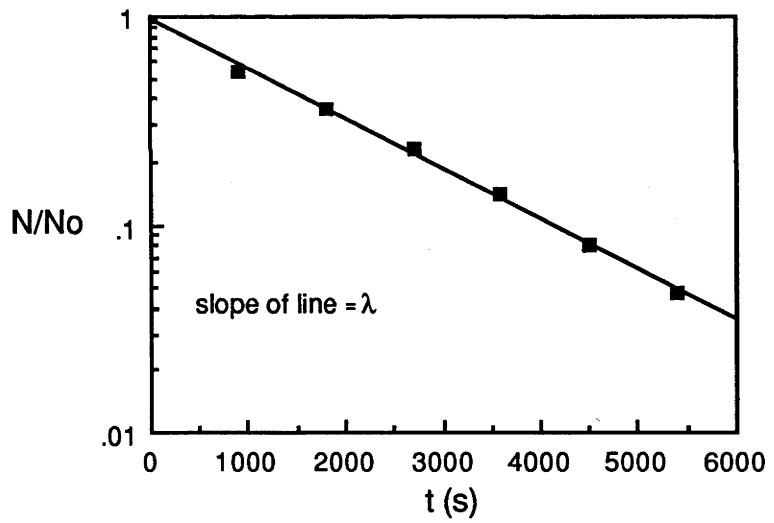

Figure 6.3. Graph of ratio, N/N_0, of number of particles at time t to number of particles at time t=0, against time, t, confirming exponential decay law (equation (6.4)).

The experimental investigation attempted to cover as wide a range of s as was practically possible, and to study the effect of changing the heat-transfer condition at the bottom boundary. Coolant was circulated through the top heat exchanger in all experiments, whilst the bottom heat exchanger had either hot, cold or no fluid circulated through it. Figure 6.4 shows streak photographs showing the structure of convection in all three configurations, and reveals that a large-scale circulation is present in keeping with

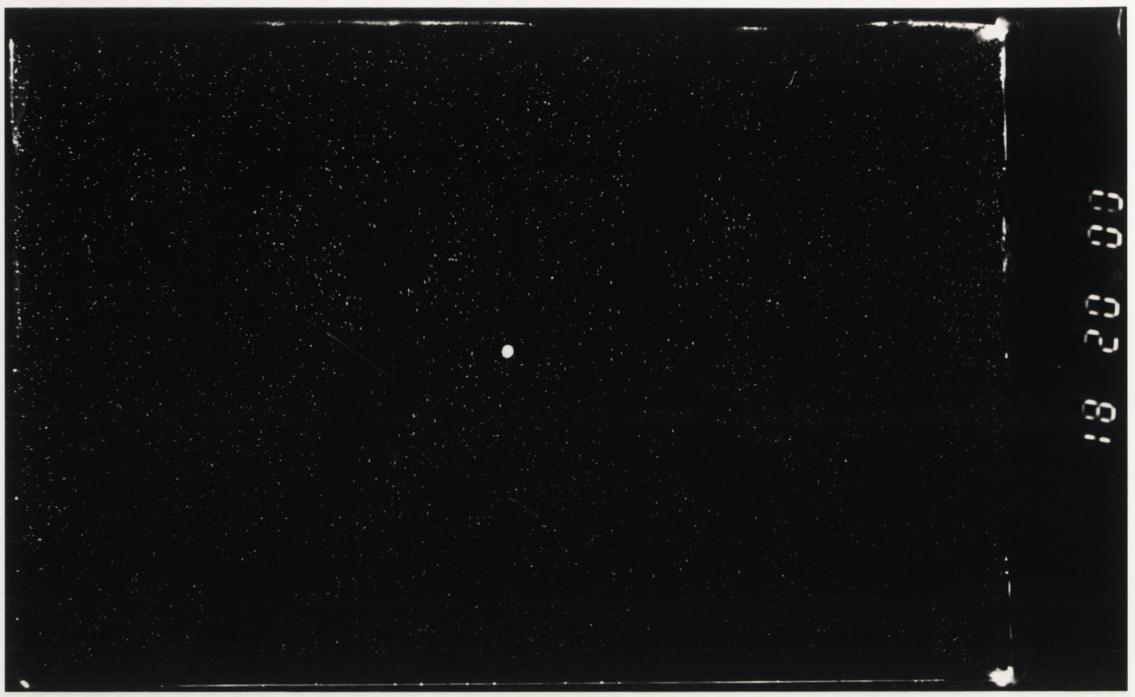

Figure 6.2. 0.25 second exposure photograph of a typical experiment. The polystyrene particles show up as white dots. The clock at the left shows the experiment number (18) and the time in minutes and seconds and the large white blob in the centre of the photograph is a thermistor.

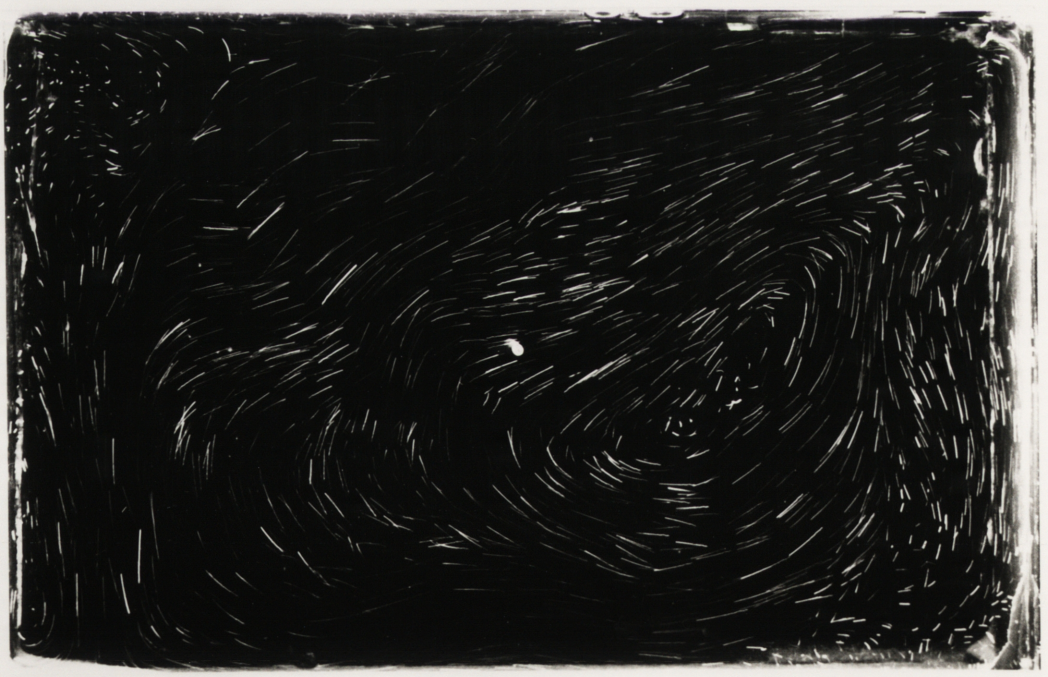

Figure 6.4a. Streak photograph showing the structure of convection driven by cooling from above when $Ra=2x10^8$ and $Pr=7$.

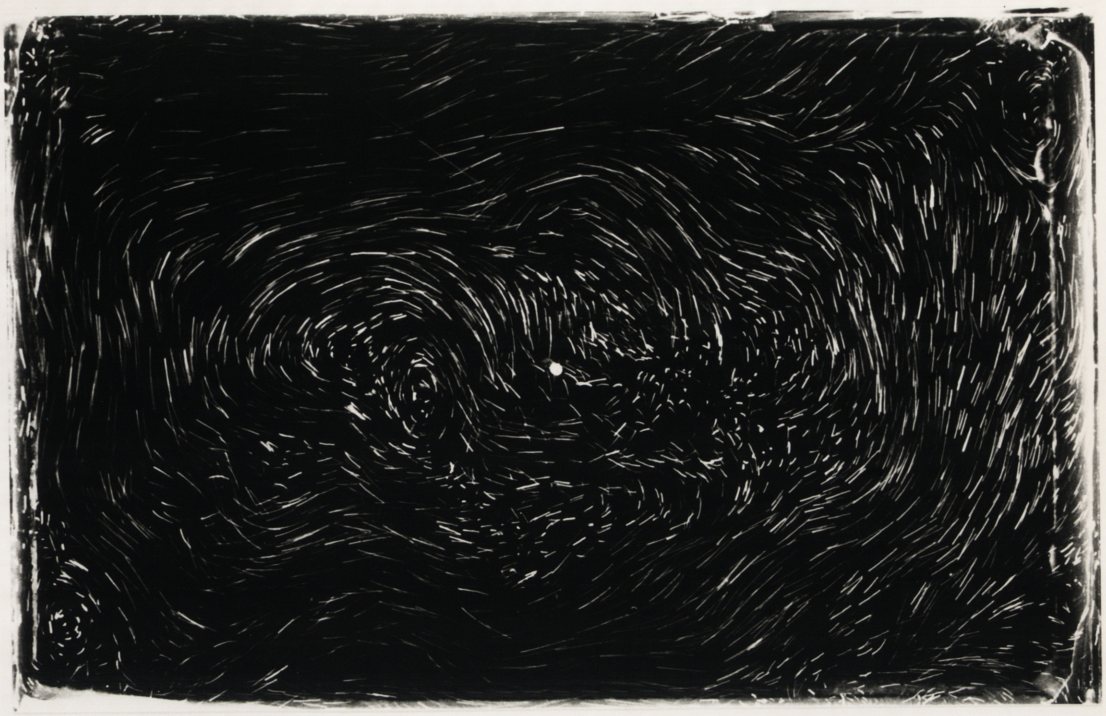

Figure 6.4b. Streak photograph showing the structure of convection driven by cooling from above and heating from below when $Ra=1x10^9$ and $Pr=7$.

Figure 6.4c. Streak photograph showing the structure of convection driven by cooling from above and cooling from below when $Ra=6x10^8$ and $Pr=7$.

previous studies of high-Ra convection (Deardorff and Willis, 1967; Fitzgerald, 1976; Krishnamurthi and Howard, 1981). Plumes forming at the upper and lower boundaries descend or rise into the interior of the fluid and combine to form an overall circulation. The structure of convection revealed by the streaks is similar in all cases, except that when the bottom boundary is cooled a ponded layer of cool fluid is observed. The major difference when the bottom boundary is heated is that plumes of buoyant fluid rise off the heat exchanger providing an additional driving force for convection in the interior of the fluid.

From the decay of the number of particles in suspension with time it was possible to determine an exponential-decay constant for each experiment. For each experiment this decay constant was normalized by multiplying by the settling velocity calculated for the middle of the particle-size range and by dividing by the depth of the fluid. Thus a dimensionless decay constant , λ', was determined which, according to the analysis presented above, should be equal to unity. The parameter s was also determined for each experiment using the calculated settling velocities and convective velocities determined from streak photographs. The results are given in table 6.1, and in figures 6.5 and 6.7 the experimentally determined values of λ' are plotted against s. It is estimated that the error in the determination of λ' is approximately ±25%, and that the error in s is roughly ±20%. Taking each set of experiments in turn:

Cooling from above only. This set of experiments was intended to simulate a magma chamber in which convection is driven only by heat loss through the roof with no additional heat loss through the floor. The results are plotted in figure 6.5. The average value of λ' deduced from the experiments when $s<0.5$ is 0.83. When $s>0.5$ the apparent λ' appears to be significantly less than unity. This is explained by the breakdown of the assumption of one-dimensionality. As illustrated in figure 6.6, the particles are concentrated into the upwelling part of the mean flow so that the number of particles adjacent to the floor is reduced to less than the average particle concentration in the fluid.

TABLE (6.1)

Particle settling in turbulent convection - experimental results

Bottom boundary condition	Ra	Pr	s	λ'
passive	4.9×10^{8}	7	7.6×10^{-1}	0.66
"	4.9×10^{8}	7	7.6×10^{-1}	0.55
"	4.9×10^{8}	7	6.2×10^{-1}	0.69
"	4.9×10^{8}	7	4.0×10^{-1}	0.85
"	2.9×10^{7}	60	2.2×10^{-1}	0.77
"	4.9×10^{8}	7	2.0×10^{-1}	0.81
"	1.9×10^{7}	266	1.8×10^{-1}	0.65
"	3.7×10^{7}	43	1.5×10^{-1}	0.70
"	1.1×10^{8}	43	1.3×10^{-1}	0.72
"	1.1×10^{7}	266	1.3×10^{-1}	1.03
"	1.9×10^{7}	266	1.2×10^{-1}	0.94
"	1.1×10^{7}	266	1.1×10^{-1}	0.84
"	8.4×10^{7}	64	9.4×10^{-2}	0.84
"	1.9×10^{7}	266	6.2×10^{-2}	0.98
"	1.1×10^{7}	266	5.8×10^{-2}	1.11
"	2.5×10^{7}	71	4.4×10^{-2}	0.56
heated	1.4×10^{9}	7	2.6×10^{-1}	1.02
"	5.0×10^{8}	7	2.6×10^{-1}	0.82
"	1.7×10^{9}	7	2.4×10^{-1}	1.11
"	1.9×10^{9}	7	1.4×10^{-1}	0.91
"	8.1×10^{7}	199	4.8×10^{-2}	0.74
"	3.9×10^{7}	199	4.6×10^{-2}	0.71
"	1.1×10^{7}	1890	1.9×10^{-2}	1.05
"	2.1×10^{7}	851	1.5×10^{-2}	0.74
"	5.1×10^{6}	4070	5.4×10^{-2}	(re-entrainment occurred)
cooled	2.4×10^{8}	7	2.8×10^{-1}	0.89
"	5.9×10^{8}	7	2.0×10^{-1}	0.75
"	2.1×10^{8}	85	1.0×10^{-1}	0.71
"	1.0×10^{8}	234	5.0×10^{-2}	0.73

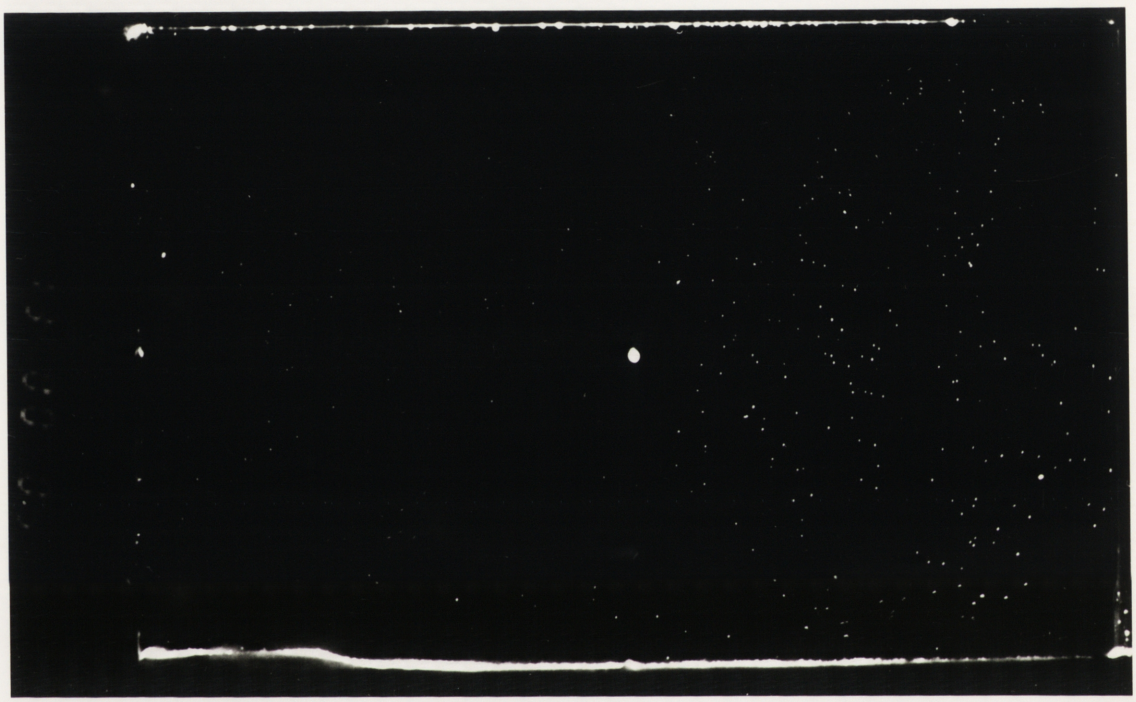

Figure 6.6. 0.25 second exposure photograph illustrating the breakdown of the assumption of one-dimensionality at S>0.5. Here the distribution of particles is not horizontally uniform. Instead particles are concentrated in the right-hand side of the field of view where there is a broad upwelling region in the flow.

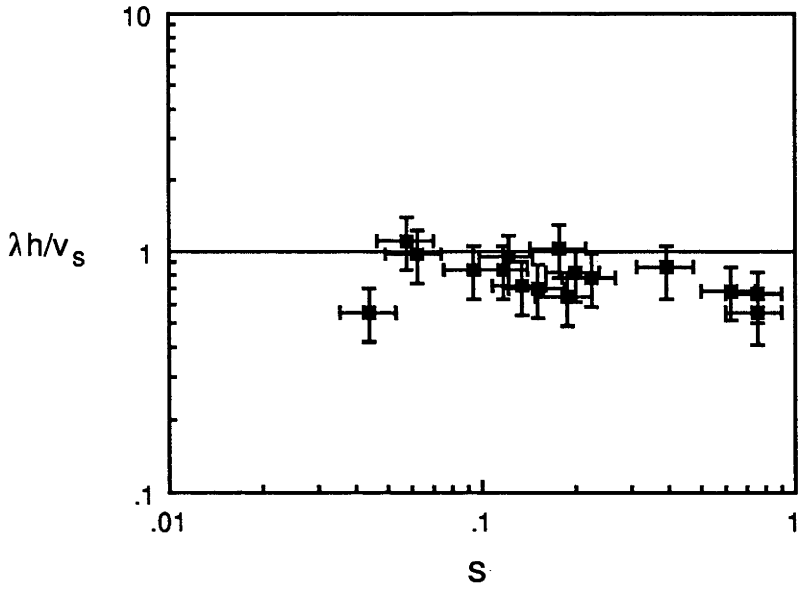

Figure 6.5. Experimentally determined values of λ' plotted against s for cooling from above. The theoretically predicted value (λ'=1) is indicated by the horizontal line.

Cooling from above and heating from below. The geological situation which these experiments model is that of a magma chamber in which convection is driven from above by cooling and from below by crystallization on the floor releasing a light, depleted melt. In these experiments, because the fluid did not cool down with time and ultimately freeze, it was possible to conduct longer experiments than for those involving cooling only, so that fluids of a higher viscosity could be investigated. Most of the experiments behaved identically to the experiments in which the bottom boundary was passive. The results from these experiments are plotted on figure 6.7 (solid squares). The average value of λ' from these experiments is 0.89. The experiment using the most viscous fluid (and hence the lowest particle settling velocities) behaved quite differently, however. In this experiment the plumes rising off the floor were able to re-entrain particles which had previously settled out.

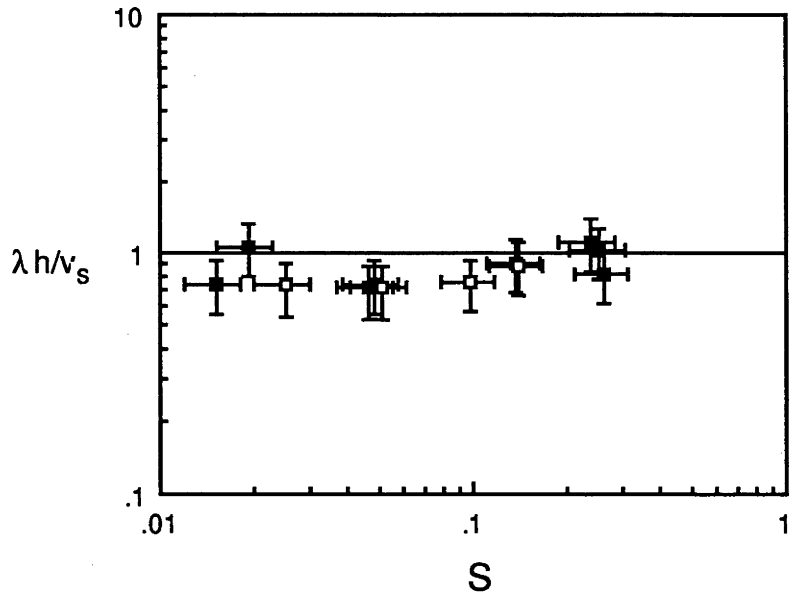

Figure 6.7. Experimentally determined values of λ' plotted against s for cooling from above and heating from below (solid squares) and cooling both from above and below (open squares). The theoretically predicted value (λ'=1) is indicated by the horizontal line.

The evolution of the number of particles remaining in suspension with time is shown in figure 6.8, which shows that the number initially decays but ultimately reaches a steady-state at which the rate at which particles are re-entrained is equal to the rate at which they settle out. If the re-entrainment rate is constant (say M particles per second) throughout the experiment then the decay in the number of particles in suspension will be given by

$$\frac{dN}{dt} = M - \frac{v_s}{h}N \qquad (6.5)$$

which can be integrated to give

$$N = \frac{Mh}{v_s} + N_0 \exp\left(\frac{-v_s t}{h}\right)\left(1-\frac{Mh}{v_s}\right). \qquad (6.6)$$

Plotted on figure 6.8 is the line given by equation (6.6) for 0.26mm diameter particles and for M=0.22 particles per second. The value of M was chosen by averaging the last five values of N. Also plotted on figure 6.8 is the line calculated assuming no re-entrainment (equation (6.4)). Within experimental error the behaviour of this experiment is adequately described by equation (6.6).

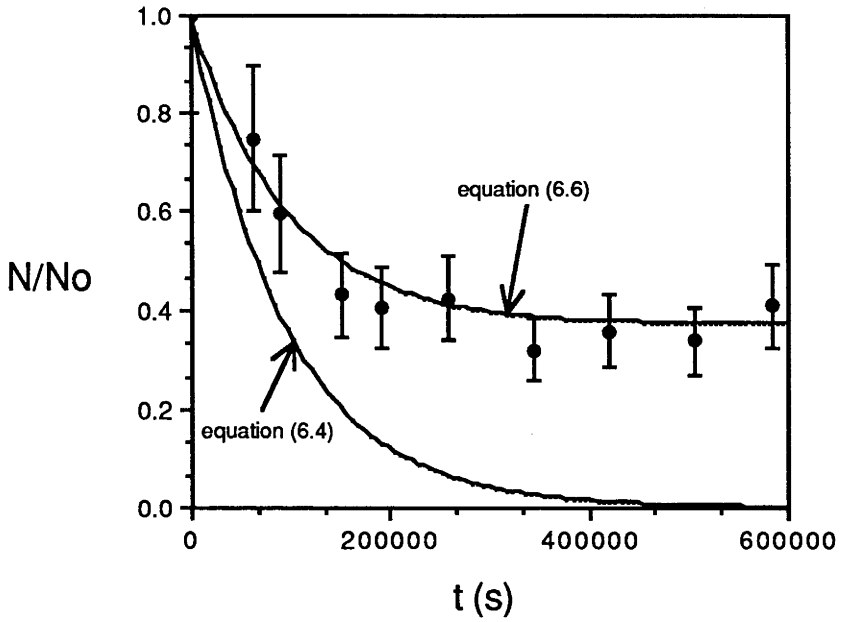

Figure 6.8. Graph showing the evolution of the experiment in which re-entrainment was observed. Also shown are theoretical lines calculated according to equation (7) and equation (22). Re-entrainment appears to occur at a constant rate of 0.22 particles per second.

Cooling from above and below. These experiments modelled magma chambers undergoing heat loss from through the roof and the floor. In these experiments with a stagnant bottom layer the value of viscosity used to calculate the settling velocity took into account the temperature dependence of viscosity for the two C.M.C. solutions. This was done by using the measured viscosity of the solutions at the temperature of the base of the tank. The results are plotted on figure 6.7 (open squares). The average λ' from these experiments is 0.77.

The above experimental results show that, when the assumptions of one-dimensionality and no re-entrainment hold, λ' is close to unity. In fact the experiments consistently suggest that λ' is just less than unity, with a value around 0.8 being more appropriate. One possible reason for this is that there is a range of particles sizes present in each experiment. If the exponential decay law (equation (7)) is applied to a range of particle sizes then the the total number of particles remaining in suspension at time t is given by

$$N(t) = \int_{x_1}^{x_2} \frac{N_0}{x_2 - x_1} \exp\left(\frac{-v_s t}{h}\right) . dx \qquad (6.7)$$

where a uniform distribution of particle sizes between diameters x_1 and x_2 has been assumed. Equation (6.7), on integration, gives

$$N(t) = P t^{-1/2} \left[\mathrm{erf}(Q x_2 t^{1/2}) - \mathrm{erf}(Q x_1 t^{1/2})\right] \qquad (6.8)$$

with $P = \frac{N_0}{x_2 - x_1} \sqrt{\frac{9\pi h \nu}{2 g \Delta\rho}}$ and $Q = \sqrt{\frac{g \Delta\rho}{18 h \nu}}$.

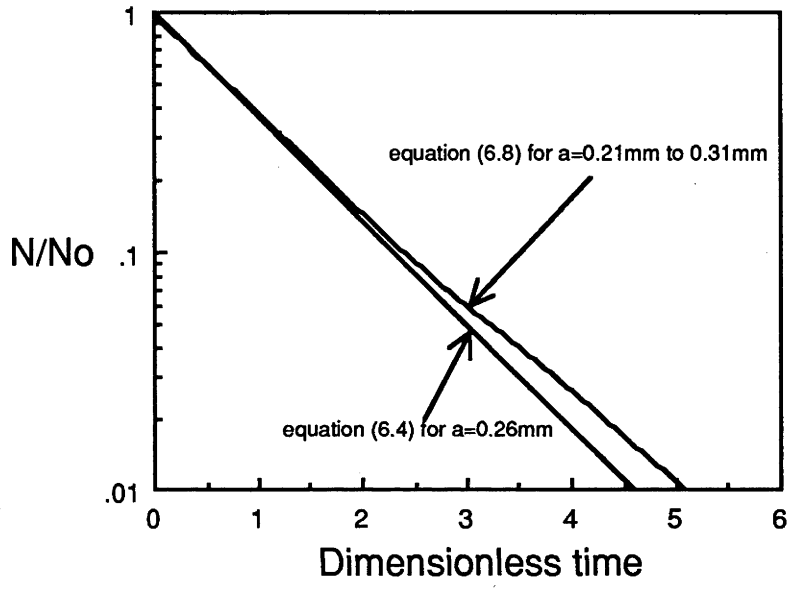

Figure 6.9. Comparison of exponential-decay law for 0.26 mm diameter particles with decay law for uniform distribution of particles between 0.21 mm and 0.31 mm diameter. Although the deviation of the latter from a straight line on this plot is negligible compared with experimental error, a systematic error resulting in an underestimation of λ' by about ten percent is introduced. This systematic error results in the data points in figure 6.5 falling below the line $\lambda'=1$.

Plotted on figure 6.9 are the exponential decay law for particles of 0.26 mm diameter, and the decay law for a uniform distribution of particles between 0.21 mm and 0.31mm diameter. For the duration of the experiments reported above the deviation of equation (6.8) from a straight line when the logarithm of the number of particles in suspension is plotted against time is negligible. Typically the results were determined over 4 or 5 dimensionless time-units, beginning one or two time-units after the introduction of particles into the flow. Over this time interval the rate of decay is biased towards the slower-settling particles, and calculations show that the values of λ' determined by fitting an exponential decay law underestimate the true experimental values of λ' by about ten per cent or so.

Experimental study of particle settling in rotating turbulent convection

Griffiths (1987) predicted that the Earth's rotation is likely to have a strong effect on convection in basaltic magmas greater than 100m thick at high and intermediate latitudes. The purpose of this section is to consider the phenomenon of crystal settling in such magmas.

In non-rotating turbulent convection, the dominant motion is an overturning with lengthscale of the order of the fluid depth. However, when rotation has a strong effect on convection the dominant lengthscale of motions is reduced and intense vortices are formed the axes of which are nearly vertical. How will this affect particle settling? Like the non-rotating case it can be expected that, when s is small, the distribution of crystals in the magma will be almost uniform and, in the absence of re-entrainment, a similar decay law will be obeyed. In the presence of rotation, however, the possibility of re-entrainment is increased: Griffiths suggested that the intense vortices produced by rotating convection might re-entrain particles from the floor in a manner analogous to 'dust devils'.

I have conducted a short series of experiments to demonstrate the effect that rotation might have on crystal settling. The apparatus described earlier was mounted on the rotating table at the Australian National University and experiments were performed at various rotation rates. Only experiments involving heating from below and cooling from above were conducted since this is when rotation is most likely to have an effect. These experiments confirm Griffiths' suggestion that the vortices can re-entrain particles. Figure 6.10 is a streak photograph showing the structure of convection at $Ra = 1.0 \times 10^9$, $Ta = 1.4 \times 10^{10}$, $Pr = 7$, whilst figure 6.11 shows vortices re-entraining particles in the same experiment. Experimental results are presented in table 6.2. For the experiments in which there is no re-entrainment of particles, the number of particles in suspension decays according to equation (6.4), as in the non-rotating case. Experiments in which re-entrainment was observed are better described by equation (6.6) in which a constant rate of re-entrainment is assumed.

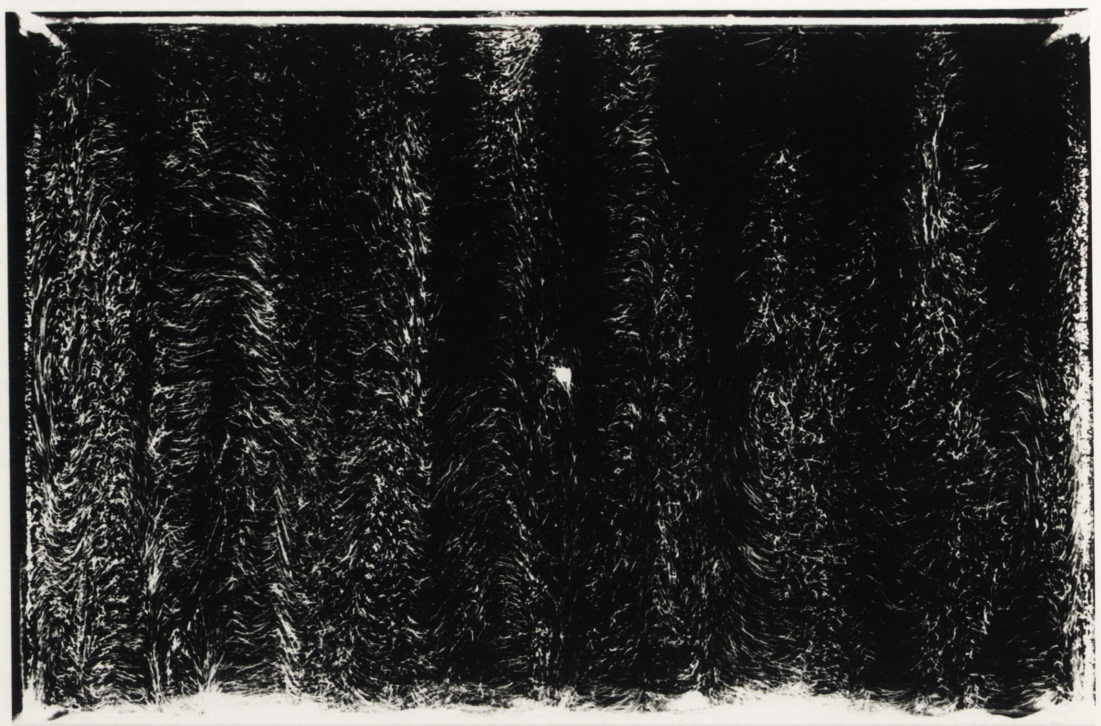

Figure 6.10. Streak photograph showing the structure of convection driven by cooling from above and heating from below when $Ra=1x10^9$, $Pr=7$ and $Ta=1.4x10^{10}$. Instead of a large-scale circulation as was observed in the non-rotating case, the fluid motions form an array of unsteady vortices the axes of which are nearly vertical.

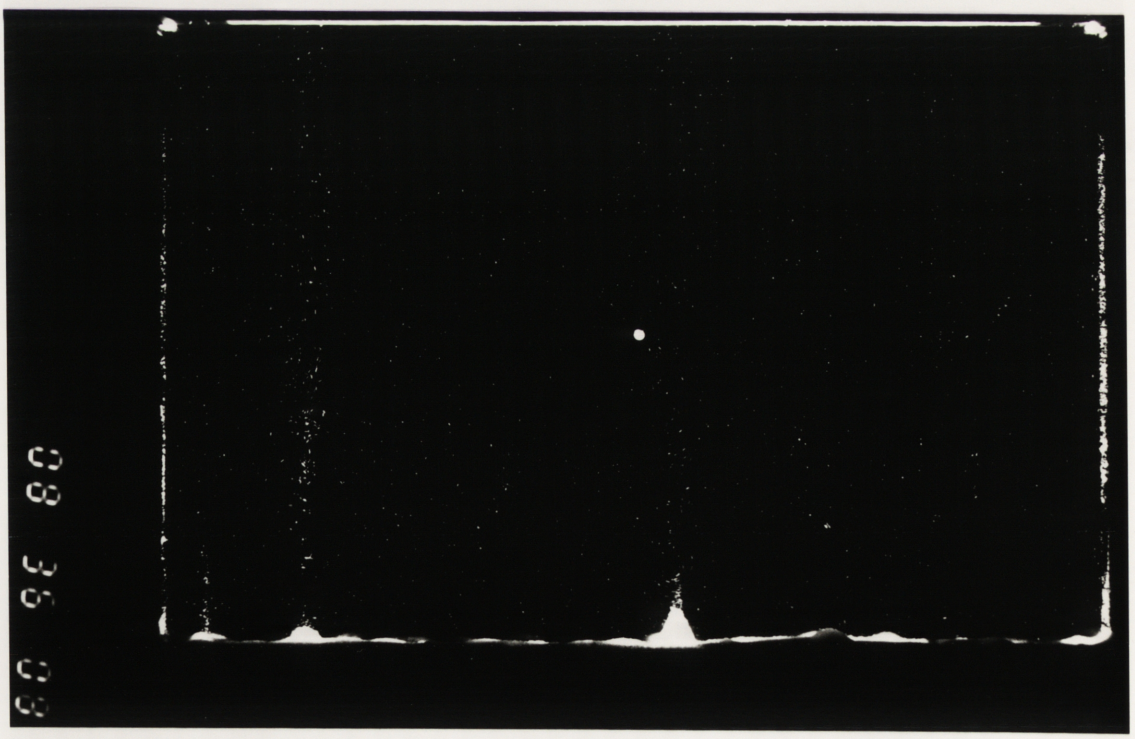

Figure 6.11. 0.25s exposure photograph of the experiment shown in figure 6.10. Three vortices can be seen re-entraining particles from the floor of the tank.

TABLE (6.2)

Particle settling in rotating turbulent convection - experimental results

Ra	Pr	Ta	s	comments
1.0×10^{9}	7	1.4×10^{10}	1.1×10^{-1}	re-entrainment; M=3.50
1.0×10^{9}	7	5.8×10^{8}	1.1×10^{-1}	re-entrainment; M=3.24
1.0×10^{9}	7	1.6×10^{7}	1.1×10^{-1}	re-entrainment; M=1.20
3.1×10^{8}	7	1.4×10^{10}	1.6×10^{-1}	no re-entrainment; $\lambda h/v_s=0.73$
3.1×10^{8}	7	5.8×10^{8}	1.6×10^{-1}	no re-entrainment; $\lambda h/v_s=0.90$
3.1×10^{8}	7	1.6×10^{7}	1.6×10^{-1}	no re-entrainment; $\lambda h/v_s=0.96$

Figure 6.12 shows the number of particles plotted against time for the experiment at Ra = 1.0×10^{9}, Ta = 1.4×10^{10}, Pr = 7. Also shown on figure 6.12 is the exponential decay law (equation (6.4)) assuming no re-entrainment and the line corresponding to equation (6.6) with v_s calculated using Stokes' Law and M calculated so as to give the best fit. In this case equation (6.6) describes the results well, in other cases the fit is less good reflecting the transient nature of the 'dust devils' and the consequent varying rate of re-entrainment.

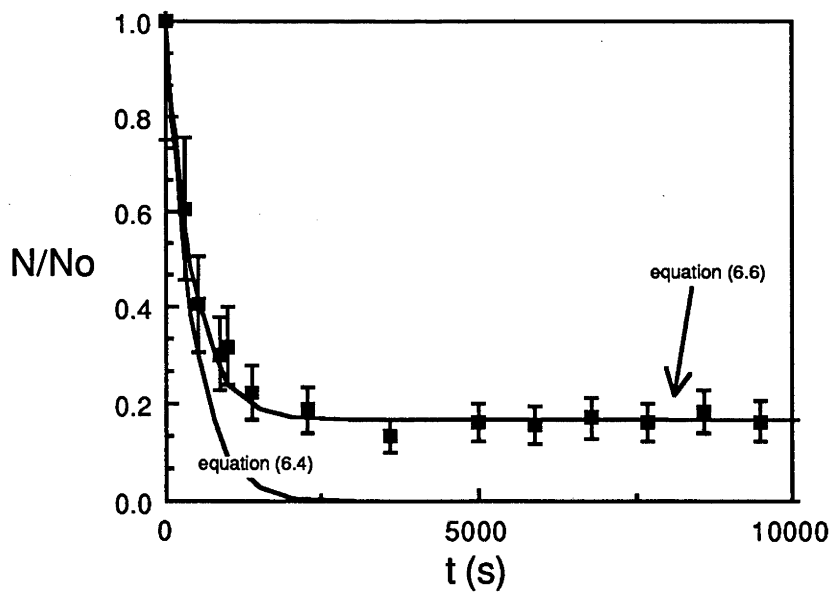

Figure 6.12. Graph of number of particles against time for particle settling in rotating turbulent convection at Ra=1.0×10^{9}, Ta=1.4×10^{7}, Pr=7. Also plotted are the line calculated from equation (6.4), which assumes no re-entrainment of particles, and the line calculated from equation (6.6), which assumes a constant rate of re-entrainment.

Summary of main results and limitations on their applicability

Mid-depth convective velocities in magma chambers often greatly exceed settling velocities of typical crystals (*i.e.* s<<1). However particles may still settle out of such a vigorously convecting fluid since the convective velocities diminish as the boundaries are approached. Because particles settle out from the base of the fluid with their full settling velocities and because the particles are kept uniformly distributed in the fluid by the turbulent convection, the number of particles remaining in suspension decays with time according to an exponential law. The decay constant is predicted to depend only on the settling velocity, v_S, and the depth of the fluid, h.

The experimental investigation modelled the following three geological situations:

(i) Crystal settling with no additional crystal growth once the crystals have settled out. (Cooling from above only).

(ii) Crystal settling with additional crystal growth on the chamber floor releasing a light depleted melt which drives compositional convection. (Cooling from above and heating from below).

(iii) Crystal settling with no additional crystal growth on the floor, but with heat loss through the floor as well as the roof so that a stagnant layer forms adjacent to the floor. (Cooling from above and below).

The experiments are adequately described by the theoretical analysis, except when the assumptions behind the analysis break down.

From theory and experiments it is therefore concluded that the rate at which particles settle out of suspension is given by

$$\frac{dN}{dt} = -\frac{v_s}{h} N .$$

Similarly, it is expected that this equation will apply to crystal settling in magma chambers. However, when applying this result to magmatic situations the limitations imposed by the assumptions behind it should be borne in mind. Thus:

(i) *The assumption of one-dimensionality.* I have assumed that the problem can be treated as one-dimensional. The experiments show that this assumption is invalid for s>0.5, when settling operated too rapidly for convection to keep the distribution of particles uniform in the horizontal. Instead particles were concentrated into the upwelling parts of

the mean circulation. It is expected that a similar limit will apply in magmas. For s>0.5, settling is less efficient than would be expected if the one-dimensionality assumption were valid because the concentration of particles immediately above the bottom boundary is less than the average concentration of particles in the fluid. If the convective velocities were higher, so that s<0.5, the particles would settle out more rapidly - a somewhat surprising result.

(ii) *The assumption of low particle concentrations.* I have assumed that the concentrations of particles are low enough so that the particles settle independently of each other, and the presence of the particles does not affect the flow. For high particle concentrations Stokes' Law is modified (Barnea and Mizrahi, 1973; Marsh and Maxey, 1985). However, little is known about the possible modification of convection by high concentrations of particles, but it seems likely that some damping of turbulence may occur. In addition there is the possibility that significantly stable density gradients will be set up as a result of particle concentration gradients. The assumption of low particle concentrations definitely holds for our experiments, in which the initial concentration was usually around 0.3 vol.%. However caution should be exercised in extrapolation of these results to high particle concentrations.

(iii) *The assumption of no re-entrainment of particles from the floor.* Convective velocities at the base of the fluid must vanish. However, the analysis requires in addition that convective velocities just above the base of the fluid are not large enough to cause re-entrainment of particles from the floor. Re-entrainment was only observed in one non-rotating experiment. This experiment was conducted using the most viscous fluid with the smallest particles, and involved cooling from above and heating at the floor. That re-entrainment occurred implies that the plumes breaking away from the heated floor had a sufficiently large velocity compared with the settling velocity of the particles. Unfortunately, because the fluid velocities associated with the peeling away of the boundary layer fluid to form a plume are unknown, I am unable to derive a re-entrainment criterion. It must therefore be considered that the re-entrainment of crystals is a possibility in magma chambers, especially when compositional convection is occurring due to the release of a light depleted melt by further crystal growth on the floor of the

chamber. Re-entrainment will be enhanced when the Earth's rotation has a strong effect on convection. However, it is not necessarily the case that re-entrainment prevents crystal settling. Providing the number of particles in the fluid is greater than $\frac{Mh}{\lambda' v_s}$ where M is the rate of re-entrainment, particles will still settle out.

The efficiency of crystal settling in the presence of re-entrainment is reduced, and it is true that all the particles will not eventually settle out, but unless the number given by $\frac{Mh}{\lambda' v_s}$ is too large it is expected that crystal settling will still occur, although individual crystals may have a complex history of several phases of deposition and re-entrainment.

GEOLOGICAL APPLICATIONS

In the remainder of this chapter I suggest some geological applications of this work. These applications are made under the assumption that magmas do not possess significant yield strength at liquidus temperatures.

Residence times of crystals in magma chambers and komatiites

The results described above show that particles can settle out of a rapidly convecting fluid even when the settling velocities are greatly exceeded by the convective velocities throughout most of the fluid. Extension of this result to magma chambers requires a comparison of the relevant timescales. The time taken for crystals to settle out of magmas needs to be compared with the time taken for the magma to solidify. Since particle settling obeys an exponential decay law (equation (6.4)), a half-life, or residence time, can be calculated for typical crystals in typical magmas. This is given by $\frac{\ln 2.h}{v_s}$ and is independent of the velocity of convection providing s is small.

Figure 6.13 shows the range of residence times (which are directly proportional to chamber depth) predicted for olivine and plagioclase crystals in a 1km deep chamber as a function of magma viscosity. For olivine crystals in basaltic chambers typical residence times range from as little as a month to a few tens of years, whilst plagioclase crystals have residence times in basaltic magmas of between one and a thousand years. These times are short compared with the many thousands of years that magma chambers take to

solidify when cooling is dominated by conduction through the country rock, so that on this timescale crystal settling is virtually instantaneous. However, cooling may be substantially enhanced when the magma is hot enough to cause melting of the surrounding country rock (Huppert and Sparks; 1988a,b), in which case solidification may only take hundreds, as opposed to thousands, of years. It should also be pointed out that in a double-diffusively layered magma chamber significant evolution can take place on timescales that are competitive with these predicted residence times (Huppert and Sparks, 1980; Turner *et al.*, 1983). In granitic magmas the range of residence times is from 1000 years to 10 million years: crystal settling may be able to operate in the least viscous granitic magmas, but not for the most viscous ones.

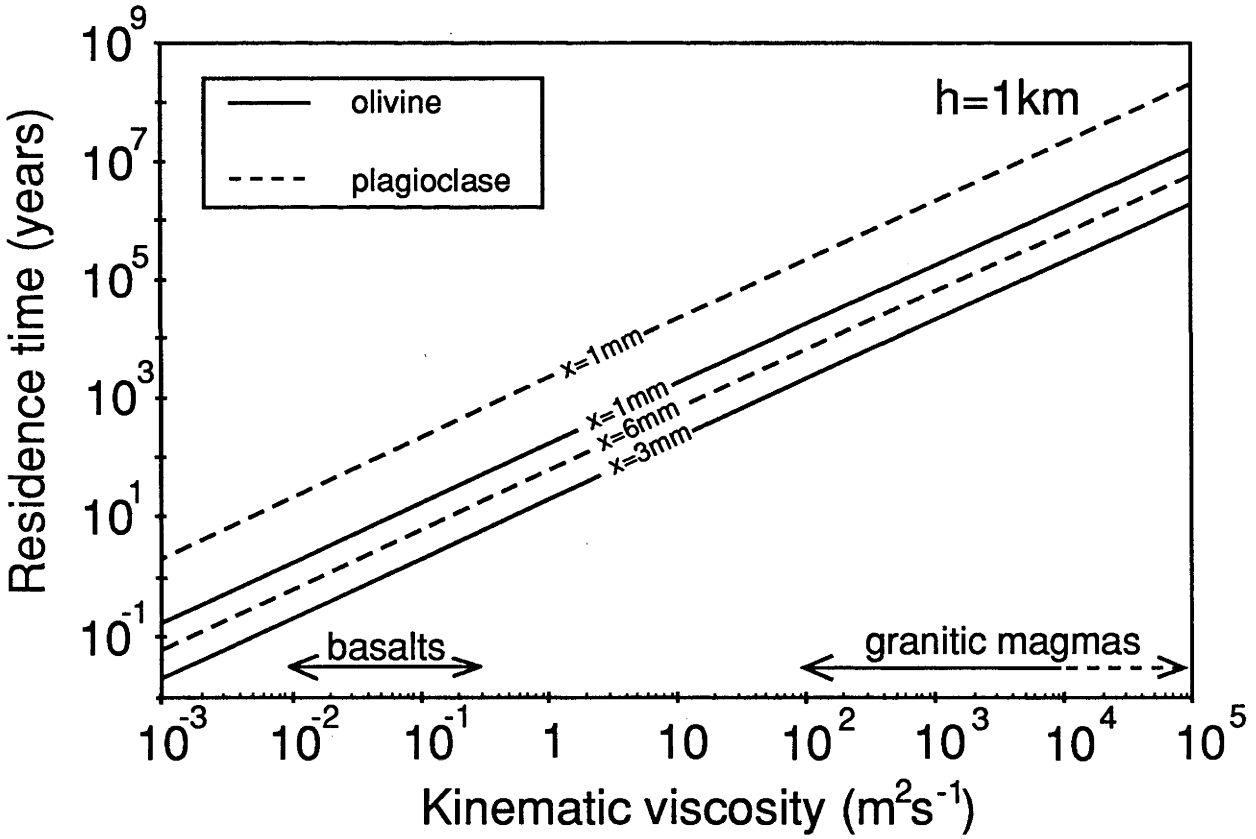

Figure 6.13. Graph of residence time of spherical phenocrysts plotted against viscosity for a 1km deep chamber. Solid lines: predictions for olivine (x=0.1 to 0.3 cm, ρ_c=3.3 g cm^{-3}, $\Delta\rho$=0.6 g cm^{-3}). Dashed lines: predictions for plagioclase (x=0.1 to 0.6 cm, ρ_c=2.7 g cm^{-3}, $\Delta\rho$=0.05 g cm^{-3}). Also shown are the typical ranges of basaltic and granitic magma viscosities.

This work should also be applicable to crystal settling in komatiitic lavas. Turner *et al.* (1986) calculated mid-depth r.m.s. vertical convective velocities for ponded

komatiite lavas, predicting that just after emplacement s ~ 10^{-2} and that this would increase with time. For typical Stokes' Law settling velocities of 10^{-3} m s^{-1} we predict that even for flows as thick as 100m, the residence time of crystals in the convecting magma will be barely longer than one day. Crystals are therefore expected to settle out readily and differentiation should be efficient.

Steady-state crystal settling

It is interesting to consider the consequences of crystal settling, as described above, when the rate-limiting step in the crystallization of magma chambers is the settling process, rather than the nucleation and growth process. If this is the case it can be expected that a steady-state will be achieved at which the crystal-settling rate is balanced by the rate at which crystals appear in the convecting magma due to crystallization. In this section examine the consequences of such a steady-state model for the properties of crystals in cumulates and lavas.

(i) *Proportions of crystals of different minerals in cumulates and lavas*

Jackson (1961) carried out a detailed study of the grain-size relations of cumulates in the Stillwater complex. He observed that sorting in rocks containing just one cumulus phase is generally good, however where there are two cumulus phases the distribution of grain-size is strikingly bimodal. Thus olivine chromite cumulates may consist of olivine grains from 1 to 4mm diameter together with chromite grains from 0.1 to 1mm diameter. Further, because these two crystal-types generally have different Stokes' Law settling velocity, Jackson described them as not being in 'hydraulic equivalence' and this led him to question whether convection currents could have been involved in the transport or deposition of cumulus minerals in the Stillwater Complex.

Consider a chamber containing convecting magma with more than one phase on the liquidus. When crystal settling in a magma chamber reaches steady-state, the rate at which crystals of the various phases are supplied to the chamber by crystallization is equal to the rate at which the crystals settle out of the chamber. (This situation is illustrated schematically in figure 6.14). In other words, since crystals of the different phases are supplied to the magma in cotectic proportions, they must also accumulate on the floor in

cotectic proportions regardless of their differing settling velocities. However, since crystals of different size and density settle out at different rates, the proportions in which minerals accumulate on the floor is not usually equal to the steady-state proportions of the various phases in the convecting magma.

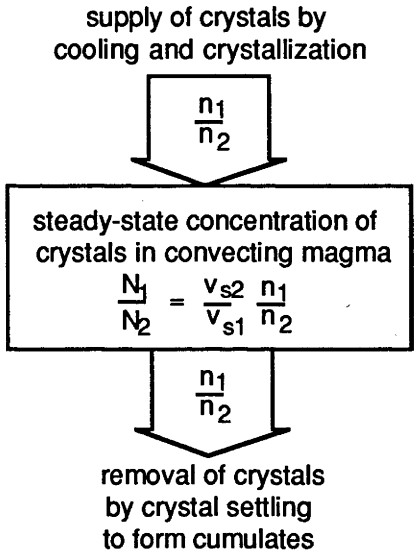

Figure 6.14. Schematic illustration of steady-state crystal settling, when the rate of supply of crystals into the convecting magma due to crystallization balances the rate at which they are removed by crystal settling.

At steady-state the composition of the cumulate is determined solely by phase equilibria, and not by the settling properties of the different types of crystal (these properties are only reflected in the concentration of the crystals in the convecting magma). For example if phase relations demand that two phases with settling velocities v_{s1} and v_{s2} crystallize in the proportion $\frac{n_1}{n_2}$, then at steady-state the proportion in the cumulate rock will be $\frac{n_1}{n_2}$, whilst the proportion in the convecting magma is given by:

$$\frac{N_1}{N_2} = \frac{v_{s2}}{v_{s1}} \cdot \frac{n_1}{n_2} . \qquad (6.9)$$

If a magma is undergoing steady-state crystal-settling there is thus no reason to expect 'hydraulic equivalence' of phases in the resulting cumulate. Cumulates in which the different mineral phases are in cotectic proportions despite different settling velocities can instead be interpreted as evidence supporting the idea of steady-state crystal settling. However, cumulates in which the different mineral phases are not in cotectic proportions (for example in rhythmically layered rocks) may suggest that the concept of a steady-state

is not always appropriate and instead may indicate that crystal nucleation and growth, rather than crystal settling, was the rate-limiting step during their formation.

The consequences of steady-state crystal settling for the proportions of phenocrysts in lavas are now considered. It is commonly assumed that the relative proportions of various phenocrysts in lavas are identical to the relative proportions of the phenocrysts in the magma chamber from which the lavas are derived. A further step that is often made is to equate the relative proportions of phenocrysts in lavas with the relative proportions of the different phases in the mineral assemblage that is being removed from the lavas to cause fractional crystallization. During steady-state crystal settling equation (6.10) suggests that this will only be the case when the different minerals have the same settling velocity. For minerals such as olivine and plagioclase, crystals of which may differ in settling velocity by a factor of up to ten or more, this assumption may be grossly incorrect. Plagioclase, being less dense than olivine, should be present in greater than cotectic proportions in magma chambers during steady-state crystal settling. In other words, if lavas are representative samples of such magma chambers, they should contain excess plagioclase phenocrysts.

Several authors have described basalts containing excess plagioclase phenocrysts, as predicted by this model (eg. Dick and Bryan, 1978; Shibata *et al.*, 1979; Krishnamurthy and Cox, 1980; Cox and Mitchell, 1988). For example, Cox and Mitchell (1988) calculate that fractionation of plagioclase, clinopyroxene and olivine in cotectic proportions of 0.5-06 : 0.3-0.4 : 0.10-0.15 (plag : cpx : ol) is required by basalts from the Deccan Traps with observed phenocryst proportions of 0.73 : 0.18 : 0.10. Similarly, Shibata *et al.* (1979) calculate that fractionation of plagioclase, clinopyroxene and olivine in the proportions 0.54 : 0.33 : 0.12 is required to produce the observed chemical variation basalts from the Oceanographer Fracture Zone. The observed phenocryst proportions in these basalts are 0.89 : 0.08 : 0.03 suggesting, from equation (6.10) that settling velocities are in the ratio 0.18 : 0.91 : 1.00 ($v_s^{plag} : v_s^{cpx} : v_s^{ol}$) which is in agreement with the expected mineral densities for similar-sized crystals.

(ii) *A 'first-order' calculation of steady-state crystal content of magma chambers*

First the rate at which crystals are formed due to crystallization is estimated. For a magma chamber cooling through its roof at a rate q, the crystallization rate, F (mass per second), is given by:

$$F = \frac{qA_r}{\left(L+c_p\left(\frac{\partial T}{\partial S}\right)_{liq}\right)} \tag{6.10}$$

(cf. equation (4.5)), where A_r is the area of the roof, L is the latent heat of crystallization, c_p is the specific heat capacity of the fluid and $\left(\frac{\partial T}{\partial S}\right)_{liq}$ is the slope of the liquidus. In order to convert the crystallization rate in mass per second to the crystallization rate in crystals per second I shall assume that crystallization results in crystals of a given size appearing in, or being transported into, the convecting magma on a timescale that is short compared with the predicted residence times. This is rather a crude approximation, but I believe it is sufficient to enable an order-of-magnitude estimate of the formation rate of crystals to be calculated. The rate at which crystals of diameter, x, and density, ρ_c, are formed is then

$$\frac{dN}{dt} = \frac{F}{\left(\frac{1}{6}\pi x^3 \rho_c\right)} \tag{6.11}$$

When settling balances crystallization, from equations (6.10) and (6.11), we have:

$$\frac{6qA_r}{\pi x^3 \rho_c\left(L+c_p\left(\frac{\partial T}{\partial S}\right)_{liq}\right)} = \frac{v_s}{h}N \tag{6.12}$$

so that, at steady-state, using Stokes' Law to substitute for v_s (assuming spherical crystals)

$$\phi = \frac{1800q\rho\nu}{gx^2\rho_c\Delta\rho\left(L+c_p\left(\frac{\partial T}{\partial S}\right)_{liq}\right)} \tag{6.13}$$

where ϕ is the concentration (volume per cent) of crystals in the magma.

Figure 6.15 illustrates predicted values of ϕ as a function of ν contoured for different values of heat flux, q (in Wm^{-2}), with other parameters as specified in the figure caption or taken from table 3.2. The hatched area on the graph gives the range of typically observed phenocryst concentrations in basaltic lavas. As can be seen, the calculations can reproduce the observed phenocryst proportions providing a cooling rate in the range 10 to 10^4 Wm^{-2} is used. These are much larger than the minimum cooling

rate estimated for conduction through the country rock many thousands of years after chamber emplacement (*i.e.* 0.1Wm^{-2}). However they are not impossibly large. Huppert and Sparks (1988a,b) have shown that, if the cooling effect of melting the roof of a basaltic magma chamber is taken into account, cooling rates may be very much larger than conductive cooling rates. Similarly if a magma chamber is heterogeneous due to the presence of double-diffusive layering extremely large heat fluxes may occur between the layers, especially just after replenishment of the chamber by hot, dense primitive magma (Huppert and Sparks, 1980).

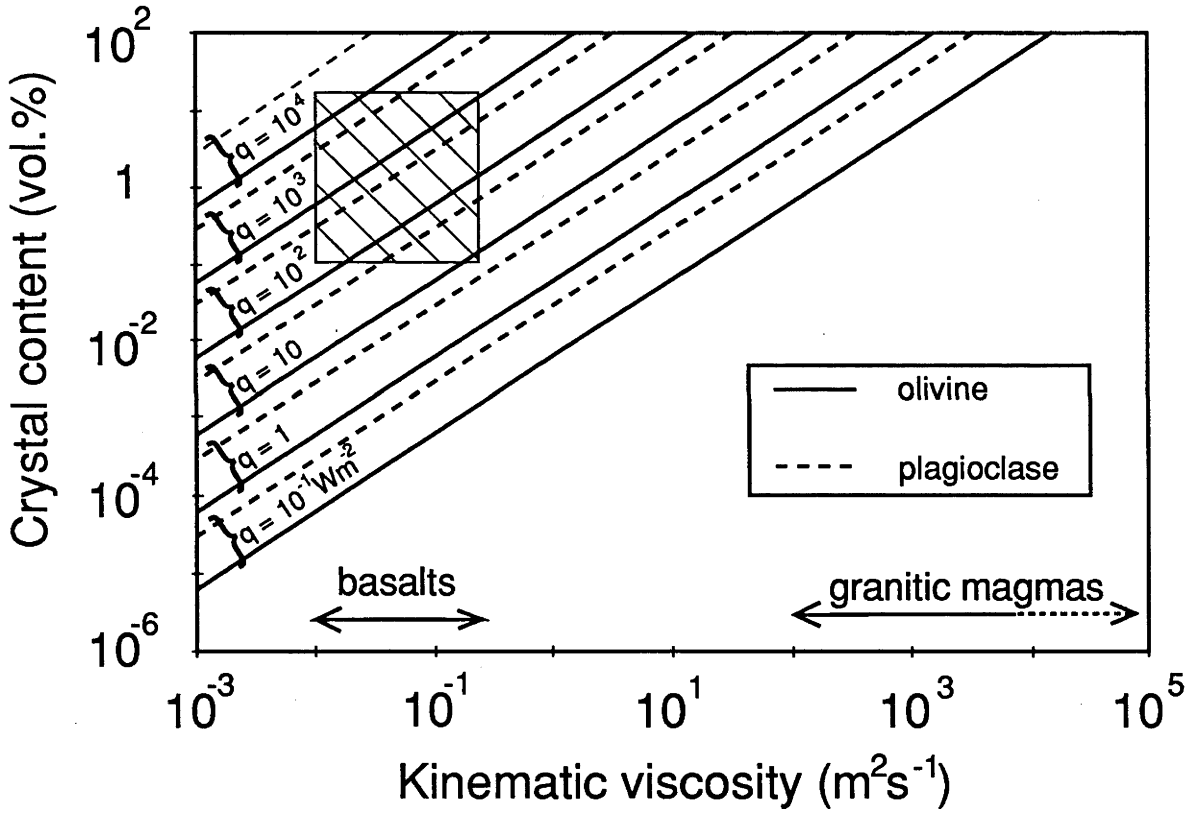

Figure 6.15. Graph of predicted steady-state crystal content of convecting magma against viscosity, calculated using equation (28). The graph is contoured for different values of cooling rate, q, ranging from the minimum estimate for slow conduction through the country rock (0.1 Wm^{-2}) to the likely maximum estimate for cooling across a double-diffusive interface just after replenishment (10^4 Wm^{-2}, Huppert and Sparks, 1980). Solid lines: predictions for olivine (x=0.1 to 0.3 cm, ρ_c=3.3 g cm^{-3}, $\Delta\rho$=0.6 g cm^{-3}). Dashed lines: predictions for plagioclase (x=0.1 to 0.6 cm, ρ_c=2.7 g cm^{-3}, $\Delta\rho$=0.05 g cm^{-3}). Both sets of predictions calculated assuming $(L+c_p(\frac{\partial T}{\partial S})_{liq}) = 10^6$ J Kg^{-1}, which is probably correct to within at least an order of magnitude. The box indicates the typical range of phenocryst concentrations in basaltic lavas.

Alternatively the calculations may be invalid, either because re-entrainment of crystals commonly occurs in magma chambers or because the assumption concerning the

manner of crystallization, which was made in order to derive an equation for ϕ, is grossly inadequate. For example it could well be the case that the time taken for crystals to grow is comparable with the predicted residence times, this would lead to an increase in the predicted crystal concentrations, but of probably not more than one order of magnitude.

Another possibility is that either erupted lavas are not representative samples of the magma resident in the chamber, or the eruptive process somehow concentrates or modifies the phenocryst content. Huppert and Sparks (1985) have calculated that, when basaltic magma ascends through dykes 1.6m wide, crystallization as a result of cooling during ascent increases the phenocryst content by some 7%. However, for dykes greater than about 4m wide, no increase in crystal content during ascent is predicted. Similarly, Blake (1986) has shown that crystals from the floor of a chamber are unlikely to be entrained into the magma during eruption.

The formation of chromitite layers and platinum-rich horizons in layered intrusions

An attractive model for the origin of both of these types of deposit is that they formed as a result of magma-mixing during chamber replenishment (Irvine, 1977, Campbell *et al.* 1983). Because of the necessity in both cases to scavenge the material from a very large volume of melt, Campbell *et al.* (1983) and Campbell and Turner (1986) suggested that the occurrence of these deposits implies that replenishment took place by means of a turbulent plume or fountain, since this enables large volumes of replenishing and host magma to be mixed intimately. Immiscible sulphide droplets, which act as collectors for the platinum-group elements (P.G.E.), or chromite crystals are envisaged to form within the turbulent fountain or plume, and ultimately to settle out of the magma to form laterally extensive deposits. Huppert *et al.* (1986a) have succeeded in modelling part of this process using aqueous solutions. However until now it has never been entirely clear, given the small settling velocities of chromite crystals and sulphide droplets, whether any model that relied on crystal settling can be really physically viable. The results presented above suggest that both chromite crystals and sulphide droplets can, indeed, settle out of rapidly convecting magmas on reasonable timescales. Further,

because the crystals or droplets are expected to be uniformly distributed in the convecting magma the uniformity of these deposits over wide areas is readily explained.

Steady-state crystal settling is not appropriate to these deposits. Instead it is expected that the injection of new magma causes a fixed amount of chromite or sulphide precipitation. The amount of chromite or sulphide remaining in suspension should then decrease exponentially with time (according to equation (6.4)). A corollary is that the rate of accumulation of chromite or sulphide on the floor of the chamber should also decrease exponentially with time. This prediction might be tested by examining these deposits in layered intrusions. Unfortunately, although it is straightforward to analyse the concentration of chromite or sulphide as a function of height in the chamber, it is not at all obvious how the transformation to concentration as a function of time should be made. Another problem is the lack of detailed analyses across typical deposits, and the strong probability of postcumulus modification for both chromite and sulphides. The only sufficiently detailed studies of which I am aware are those of Hiemstra (1985, 1986). He analysed the concentration of P.G.E. and chalcophile elements as a function of height in the UG-2 chromitite layer of the Bushveld Complex. The results showed that the concentrations decreased exponentially with height in two sequences, and between these sequences the concentrations are relatively constant. To model Hiemstra's data I assume that both chromite and the sulphides were precipitated at the same time during the same replenishment event which occurred over a short interval and the subsequent formation of the UG-2 layer is due to the settling of these, with chromite being completely volumetrically dominant. Thus the concentration of P.G.E., say, between 25 and 27cm height reflects the amount of time required to settle a 2cm thick layer of chromitite at that time, and the rate of settling of sulphides at that time. Hiemstra's data are consistent with this model if the following *ad hoc* hypotheses are made:

(i) The settling velocity of the sulphide droplets is about 10 times that of the chromite crystals. This requires that the diameter of the droplets to be about 3 times the diameter of the chromite grains. This is not necessarily inconsistent with the observed small grain size of sulphides in the solidified UG-2 chromitite since the liquid sulphide droplets must have been very susceptible to postcumulus modification.

(ii) A small amount of sulphide is carried down with the chromite grains in composite droplets. If there were no such composite droplets the concentration of P.G.E. in the chromitite would decay to zero. However, the concentration of P.G.E. in Hiemstra's profiles decays towards a constant, non-zero level.

(iii) There is a second phase of chromite and sulphide precipitation at 60cm height, corresponding to a second input of magma.

Figure 6.16b shows the variation of Pd with height which predicted according to the above model of crystal settling with these assumptions, and figure 6.16a shows Hiemstra's (1986) data. Other elements show similar features, although in many cases the scatter is greater.

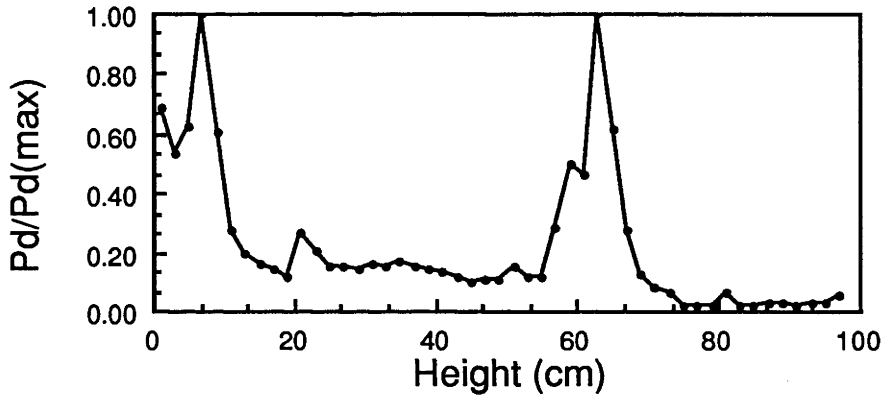

Figure 6.16a. Profile of Pd concentration in the UG-2 chromitite layer in the Bushveld Complex. Pd concentrations are normalized by their maximum value. (Data taken from Hiemstra (1986)).

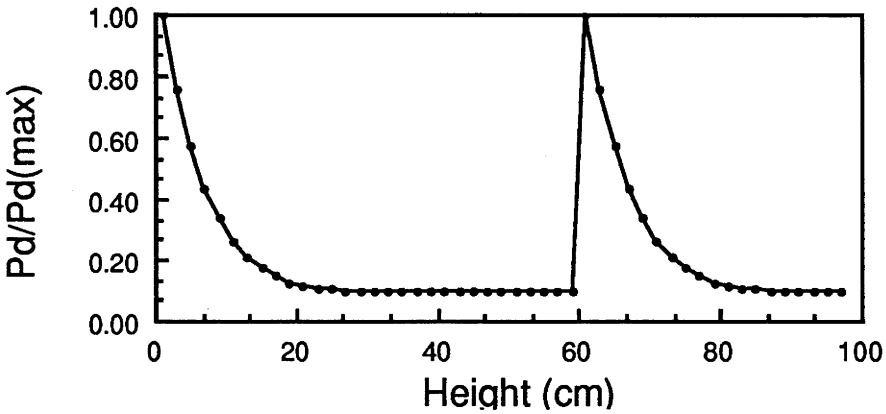

Figure 6.16b. Predicted profile of P.G.E. concentration under the assumptions discussed in the text.

Hiemstra (1985,1986) interpreted his data in terms of Rayleigh fractionation. He suggested that the concentration of a particular element at a particular height in the chromitite, C_r, reflects the bulk distribution coefficient, D, of that element and the

concentration of the element in the magma. C_r is related to the original concentration in the magma, C_0, by

$$C_r = DC_0 f^{(D-1)} \qquad (6.15)$$

where f is the proportion of the original magma which remains uncrystallized (which is inversely proportional to the height in the chromitite). This interpretation has the simple consequence that the rate of decay of concentration should be different for the different elements in proportion to the different values of D. My interpretation predicts that the rate of decay should vary slightly depending on how much of the particular element is carried down with the chromite crystals. The relative rates of decay have been determined by fitting an exponential decay law to the first 20cm of data given by Hiemstra (1986). It is found that, normalizing by the mean decay constant, the relative decay constants range from 0.61 to 1.45, with a standard deviation of 0.36. This small range seems consistent with my interpretation, whether it is also consistent with Hiemstra's interpretation is uncertain, since the bulk distribution coefficients are not known *a priori*. Another consequence of Hiemstra's interpretation is that the original magma thickness from which the UG-2 chromitite crystallized is required to be very low, of the order of 20m. This thickness is remarkably low, and is at variance with the calculations of Campbell and Turner (1986) who estimated from considerations of mass-balance that major chromitite layers must interact with a thickness of magma of at least about 2000m. My interpretation places no limits on the thickness of magma. Finally I note that my interpretation is consistent with the widely-held view that sulphide droplets act as the collector for P.G.E.. Hiemstra's interpretation, on the other hand, excludes this possibility and, instead, he suggests that chromite is the major collector.

SUMMARY AND CONCLUSION

Predicted convective velocities in magma chambers are commonly orders of magnitude larger than settling velocities for typical crystals calculated from Stokes' Law. The ratio, s, of the Stokes' Law settling velocity, v_s, to the r.m.s. vertical component of convective velocity, W, at mid-depth in the fluid is almost always less than unity. Although $v_s<W$, settling is still possible because convective velocities are height-

dependent and must decrease to zero at the boundaries of the fluid. Particles immediately adjacent to the bottom boundary settle out with their full Stokes' settling velocities. At the same time convection is vigorous enough to ensure that the distribution of particles in the fluid is uniform. It follows that the number of particles in suspension decays with time according to an exponential law, and the decay constant is simply the ratio of v_s to h, the depth of the fluid. Experiments confirm this relationship, at least for low particle concentrations, providing $s<0.5$ and there is no re-entrainment of particles from the floor of the tank.

This relationship has been applied to crystals in magma chambers, and residence times for typical crystals have been calculated. It was found that for basaltic magmas the predicted residence times are small compared with the many thousands of years that a chamber takes to solidify if cooling is dominated by conduction through the country rock. Crystal settling may therefore be an efficient differentiation mechanism. Significant magmatic evolution can, however, take place on timescales that are competitive with these residence times.

If the settling of crystals is the rate-limiting step during the crystallization of a magma chamber it is expected that a steady-state will be achieved at which the rate of supply of crystals into the convecting magma due to crystallization balances the rate at which crystals settle out. This idea can explain both the lack of hydraulic equivalence in cumulate rocks and the commonly observed discrepancy between the relative proportions of phenocrysts of various phases in fractionated basaltic lavas and the calculated relative proportions of these mineral phases in the fractionating assemblage. A comparison of the calculated steady-state crystal content of convecting magma chambers with the observed phenocryst content of typical basaltic lavas suggests that magma chambers may often cool more rapidly than would be expected for conduction through the country rock alone.

Application of this work to chromitite and P.G.E. deposits in layered intrusions supports a model in which the settling of crystals and/or sulphide droplets is envisaged to occur following precipitation in a turbulent plume during magma-mixing. The data of Hiemstra (1986) on the variation of P.G.E. content with height in the UG-2 chromitite of the Bushveld Complex can be interpreted in terms of this model.

CHAPTER SEVEN

CRYSTALLIZATION MECHANISMS OF AQUEOUS SOLUTIONS

In the preceding chapters I have examined, from a physical viewpoint, both the *in situ* crystallization model for magmatic differentiation and the crystal-settling model. The purpose of this chapter is to discuss the circumstances under which each differentiation mechanism operates. I will suggest that these two mechanisms are not mutually exclusive alternatives, but instead may both operate at the same time but to different extents under different conditions. From the point of view of the field geologist such a suggestion has its attractions, there being evidence from layered intrusions both in favour of *in situ* crystallization and in favour of crystal settling. To illustrate my arguments I have conducted a series of laboratory experiments with crystallizing aqueous solutions. I shall describe these first.

Experimental apparatus

Various aqueous solutions were cooled from above using the apparatus described in chapter six. Cooled alcohol was circulated through the heat exchanger which comprised the roof of the tank. The temperature of the alcohol was controlled by a PDP11 computer so as to maintain a constant temperature drop across the polypropylene sheet of either 3°C, 6°C or 9°C, thereby ensuring a constant heat flux throughout each experiment. The heat exchanger was not allowed to come into contact with the fluid. Instead a layer of kerosene was floated on top of the fluid between it and the heat exchanger. It was felt that this more closely approximated the geological situation, where cooling is likely to be through double-diffusive interfaces with the layers being produced either internally, by chamber replenishment or crystallization, or externally, by melting the roof. Allowing the copper surface of the heat exchanger to come into contact with the fluid would have provided an unrealistically easy nucleation site, and would have provided a solid surface to which the crystals could have adhered.

The solutions used were aqueous solutions containing ≈23wt.% KNO_3. In addition, in order to increase the viscosity, a small amount of sodium carboxymethyl

cellulose (C.M.C.) was added to some solutions. Viscosities were measured at room temperature at the start of each experiment, and densities were measured during the experiments by withdrawing a small sample of fluid and using an Anton-Paar densimeter. Temperature at mid-depth in the fluid was monitored by logging the output from a thermistor on the computer. By measuring the height of the crystal pile on the floor of the tank it was also possible to obtain a rough estimate of its porosity.

Description of experiments

(i) The basic experiment: 23wt.% KNO_3 , 0wt.% C.M.C., the lowest cooling rate

The viscosity of these solutions is close to that of pure water, *i.e.* about $1x10^{-6}$ m^2 s^{-1}. Crystallization did not begin until the temperature of the fluid had fallen to substantially below the liquidus temperature. Initially, elongate crystals of KNO_3 nucleated and grew on the fluid/kerosene interface. These crystals grew quickly but fell away from the interface while their length was still a fraction of a centimetre. The crystals dropped through the fluid and accumulated on the floor of the tank. Further, *in situ*, growth on these crystals was accompanied by compositional convection. This phase of the experiment, with crystals nucleating on the interface and falling through the fluid, lasted a little over half an hour.

For the remainder of the experiment, as long as the composition of the fluid remained above the eutectic, all the crystallization took place *in situ* on the floor of the tank. No further crystals were observed to grow on the interface and fall through the fluid. The growth of crystals on the floor of the tank drove vigorous compositional convection. A shadowgraph of the experiment at this stage is shown in figure 7.1.

Eventually, after about 24 hours, the composition of the fluid reached the eutectic composition. Eutectic solid, which is less dense than the experimental fluid, formed across the top of the fluid and proceeded to grow down into the interior of the fluid. No convective motions were observed in the fluid.

(ii) The effect of increasing cooling rate

Two experiments were carried out using a similar fluid but cooled two and three times as fast. These experiments were broadly similar to the basic experiment with the

Figure 7.1. Shadowgraph of the basic experiment. An aqueous solution of KNO_3 containing no C.M.C. is cooled from above. Crystallization takes place *in situ*, mainly on the floor of the tank, accompanied by vigorous compositional convection.

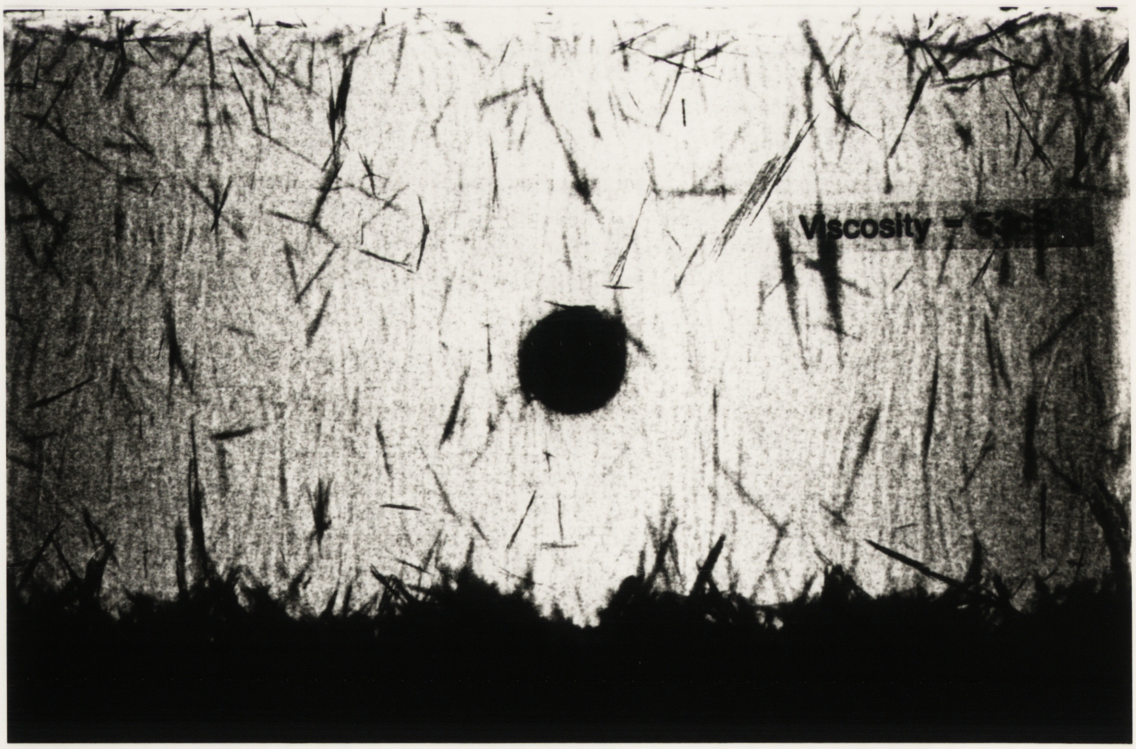

Figure 7.3. Shadowgraph of an experiment at higher viscosity. An aqueous solution of KNO_3 containing a small amount of C.M.C. is cooled from above. The viscosity of the solution is approximately 5.3×10^{-5} m^2 s^{-1}. Crystallization takes place by a combination of crystal settling and *in situ* crystallization.

exception that, throughout the crystallization of the above-eutectic fluid, crystals continued to nucleate, grow and fall away from the interface (again well before their size had reached the order of 1cm in length). In both of these experiments, however, vigorous compositional convection indicated that most of the crystallization took place by *in situ* growth on the floor of the tank.

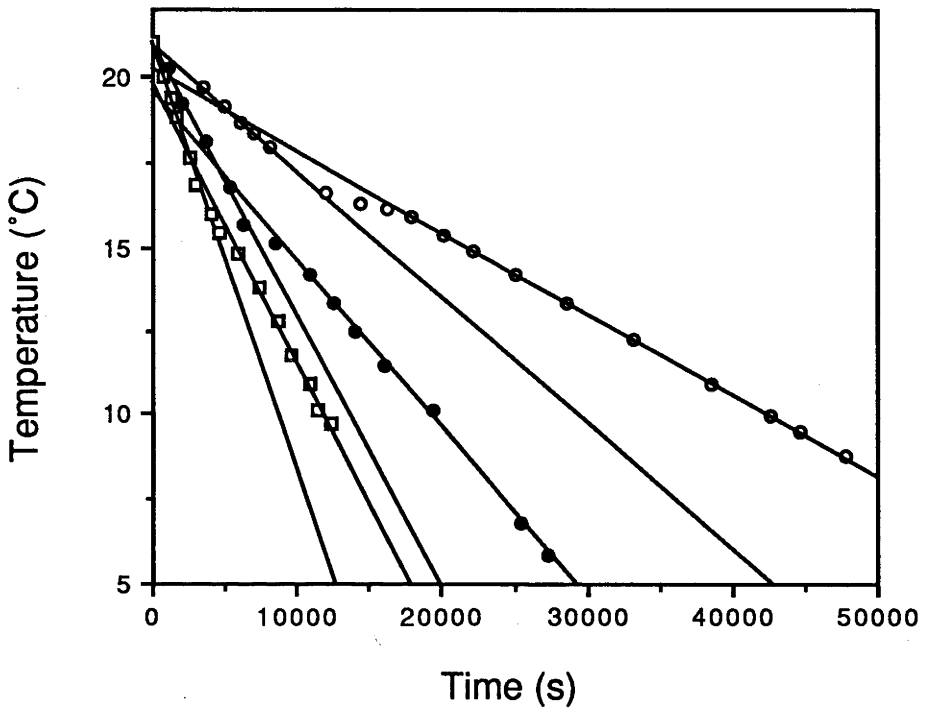

Figure 7.2. The temperature of the fluid at mid-depth as a function of time. The open circles are for the slowest cooling rate, the open squares are for the highest cooling rate and the solid circles are for an intermediate cooling rate. Before crystallization occurs, the fluid is cooled at a constant rate by the fixed heat flux extracted through the heat exchanger. When crystallization is well-established, cooling is again at a constant rate but with part of the heat flux offset by the release of latent heat due to crystallization.

The temperature of the fluid recorded at mid-depth in these three experiments is shown as a function of time in figure 7.2. All three experiments show a similar behaviour. Initially, before the onset of crystallization, the fluid cooled at a constant rate. The slope of the lines in figure 7.2 at this stage is simply $q/(\rho h c_p)$. After crystallization had become well-established, cooling again was at a constant rate with the heat flux from the fluid being balanced by cooling of the fluid and the latent heat of crystallization. The fact that straight lines are observed suggests that the change in the depth of the fluid, h, as a function of time due to the accumulation of crystals on the floor can be ignored. The slope of the lines at this stage is then given by $q/(\rho h[c_p+L(\partial S/\partial T)])$ where L is the latent

heat of crystallization and $\partial S/\partial T$ is the inverse of the liquidus slope. Using the data given on figure 7.2 it is possible to determine both q and L. Values of q=36, 72, and 108 Wm^{-2} were determined for the three experiments and L for KNO_3 was estimated to be about 370 kJ kg^{-1}. The *C.R.C. handbook of physics and chemistry* quotes a value of 345 kJ kg^{-1}, which, allowing for the likely experimental uncertainty, is in good agreement with the value measured here.

(iii) The effect of increasing viscosity

Further experiments were conducted using fluids of viscosities of, approximately, $7x10^{-6}$, $2x10^{-5}$, $5x10^{-5}$ and 10^{-4} m^2 s^{-1}. All of these experiments were cooled at the slowest rate.

At a viscosity of $7x10^{-6}$ most of the crystallization occurred *in situ* on the floor of the tank, again accompanied by vigorous compositional convection. However, unlike the basic experiment, crystals continued to nucleate and fall away from the kerosene/fluid interface throughout the period of above-eutectic crystallization. At $\nu=2x10^{-5}$ m^2 s^{-1} and $\nu=5x10^{-5}$ m^2 s^{-1} substantially more crystals formed on the kerosene/fluid interface. A shadowgraph of an experiment at $\nu=5x10^{-5}$ m^2 s^{-1} is shown in figure 7.3, in which settling crystals and compositional convection can both be seen. At $\nu=10^{-4}$ m^2 s^{-1} it was difficult to detect compositional plumes, and crystal settling seemed to dominate. In this experiment the crystals were able to grow to a size of a few cm long before falling away from the kerosene/fluid interface. Some crystals managed to adhere to the sides of the tank near the top of the fluid, eventually enabling falling crystals to be trapped and causing a network of crystals to form across the top of the fluid. The crystals accumulating on the floor formed an extremely porous crystal pile, half-filling the tank (and thereby covering the thermistor) in ~3 hours after the onset of crystallization.

Eventually, as in the basic experiment, eutectic solid formed across the top of the fluid and proceeded to grow down into the fluid.

The evolution of the fluid properties

In this section the evolution of the fluid composition and temperature in the above experiments is compared with the liquidus trajectory. The liquidi for the various solutions were calculated using the empirical equation

$$T = 153.3S - 16.15 - 165.8S_{C.M.C.} \qquad (7.1),$$

where T is temperature, S is the weight fraction of KNO_3 in the solution and $S_{C.M.C.}$ is the weight fraction of dissolved sodium carboxymethyl cellulose in the initial solution. The justification for this equation is given in the appendix to this chapter.

(i) The effect of increasing cooling rate

Figure 7.4 shows the evolution of the fluid in the three experiments at different

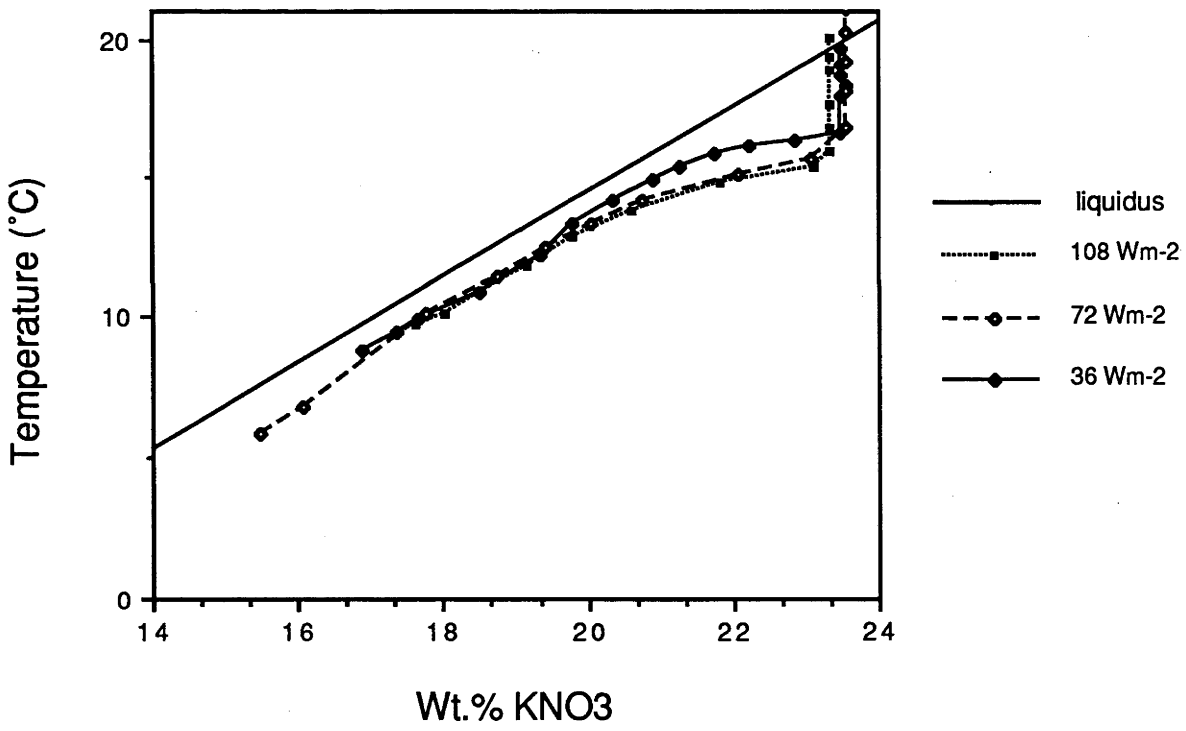

Figure 7.4. The evolution of the fluid during the experiments conducted using fluids without added sodium carboxymethyl cellulose, at three different cooling rates.

cooling rates. The trajectory of the fluid in all three experiments is rather similar, becoming parallel to, but offset from, the liquidus after an initial period. There is a tendency for increasing supersaturation with increasing cooling rate, although this

tendency is not very clear. Average supercoolings for the part of the experiment when the fluid evolves parallel to the liquidus are given in table 7.1.

(ii) The effect of increasing viscosity

Figure 7.5 a,b,c,d shows the evolution of the fluid in four of the experiments which investigated the effect of varying the viscosity. Also shown are the appropriate liquidi.

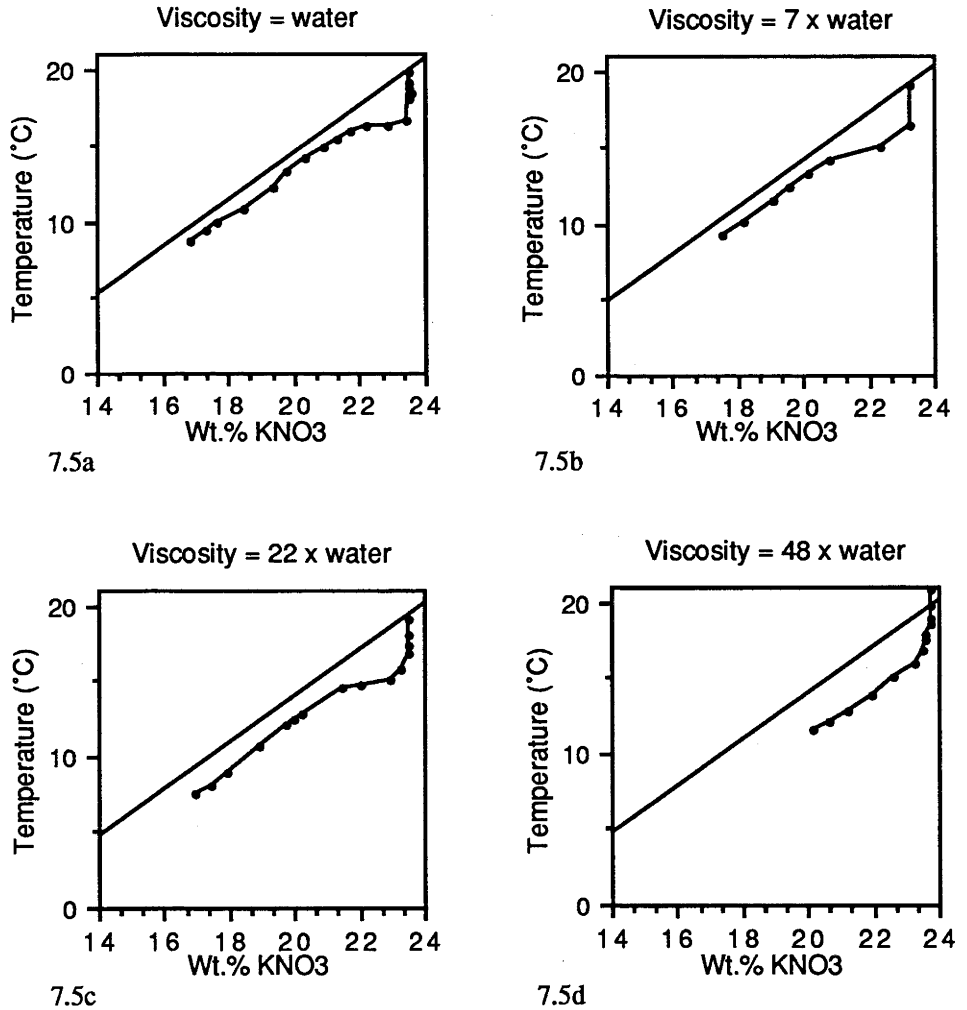

Figure 7.5. The evolution of the fluid in experiments at the same cooling rate (36 Wm^{-2}) for four different fluid viscosities. The experiment at the highest viscosity is not shown because the crystals buried the thermistor very early on in the experiment, during the initial stage of crystallization. For this experiment there were insufficient data to give a meaningful plot.

Figure 7.5 reveals a definite trend for increasing supercooling with increasing viscosity. Again average supercoolings have been determined for the period when the trajectory of the fluid in temperature-composition space is parallel to the liquidus. These are given in table 7.1.

TABLE 7.1

Experimental results

	ν ($m^2\ s^{-1}$)	q (Wm^{-2})	observed steady-state supercooling of main body of fluid	porosity (vol.%)
changing viscosity	10^{-6}	36	1°C	73
	$7x10^{-6}$	36	1.4°C	85
	$2x10^{-5}$	36	1.8°C	not determined
	$5x10^{-5}$	36	3°C	93
	10^{-4}	36	not determined	97
changing cooling rate	10^{-6}	36	1°C	73
	10^{-6}	72	1°C	81
	10^{-6}	108	1.4°C	87

Discussion of experimental results

These experiments show that aqueous solutions cooled from above in the laboratory display a range of crystallization mechanisms from pure *in situ* crystallization (at the lowest viscosity and cooling rate) to nearly pure crystal settling (at the highest viscosity and cooling rate). The experiments demonstrate that both crystal settling and *in situ* crystallization may occur at the same time. It appears also that a more porous crystal pile is produced by crystal settling than by *in situ* crystallization, suggesting that the porosity of the crystal pile might be a measure of the relative importance of crystal settling and *in situ* crystallization.

The controlling factor in determining the dominant crystallization mechanism is the amount of supersaturation of the fluid away from the crystals growing *in situ* . If thermal and compositional convection are able to keep the amount of supercooling low enough, crystallization will occur exclusively by *in situ* growth and heterogeneous nucleation on the floor of the tank. If not, homogeneous nucleation and crystal settling will occur in addition.

The fluid immediately next to the crystal/liquid interface will either be in compositional equilibrium with the crystal or supersaturated by an amount which depends on the crystal-growth rate. The fluid away from the crystal/liquid interface will always be more supersaturated than this fluid. There are two sources of this additional

supercooling, associated with thermal and compositional convection respectively. In a fluid cooled from above, the coldest fluid is found in the thermal boundary-layer at the top of the fluid. In the above experiments, the fluid in contact with the kerosene is therefore more supersaturated than the main body of the fluid by an amount ΔT. This is the reason why crystals nucleate on the interface. The value of ΔT may be predicted using equation (3.32) (see chapter three for more details). The other source of supercooling is the drop in composition across the chemical boundary-layer in front of the growing crystals. Fluid away from the crystal/liquid interface is more supercooled than fluid at the interface by an amount $\Delta S(\partial T/\partial S)$. If the fluid at the interface is in equilibrium, the supercooling of the main body of the fluid is equal to this 'constitutional supercooling', ΔS, due to the compositional boundary-layer. If the surface of the crystal pile is relatively flat and if no crystal settling is occurring, the value of ΔS may be predicted using equation (4.16). If, on the other hand, the surface of the crystal pile is rough, or if some crystal settling is occurring, equation (4.16) will overestimate the amount of supercooling (see chapter four for more details).

TABLE 7.2

ν ($m^2\ s^{-1}$)	q (Wm^{-2})	observed $\Delta S(\partial T/\partial S)$	predicted $\Delta S(\partial T/\partial S)$ eqn. (4.16)	predicted ΔT eqn. (3.32)	$\Sigma\Delta T$
10^{-6}	36	1°C	3.1°C	0.89°C	1.9°C
$7x10^{-6}$	36	1.4°C	5.1°C	1.45°C	2.9°C
$2x10^{-5}$	36	1.8°C	6.8°C	1.92°C	3.7°C
$5x10^{-5}$	36	3°C	8.3°C	2.35°C	5.4°C
10^{-4}	36	not determined			
10^{-6}	36	1°C	5.3°C	1.50°C	2.5°C
10^{-6}	108	1.4°C	7.1°C	2.03°C	3.4°C

The total amount of additional supercooling at the very top of the fluid in the thermal boundary layer is the sum of these two terms, ΔS and ΔT. In table 7.2 are shown the various supercoolings calculated for parameters appropriate to the experiments described above. ΔT was predicted using equation (3.32) while $\Delta S(\partial T/\partial S)$ was calculated using equation (4.16). The measured values of the supercooling in the main

body of the fluid is also given, together with the total amount of supercooling at the top of the fluid, $\Sigma\Delta T$, which is the sum of this measured value of ΔS and the predicted value of ΔT. As can be seen from this table, the values of $\Delta S(\partial T/\partial S)$ calculated using equation (4.16) are greater than the observed values as expected.

Exclusive *in situ* crystallization was observed only in the least viscous experiment at the lowest cooling rate. Therefore, for KNO_3, a supercooling of between 1.9°C and 2.9°C can be maintained in the fluid without nucleation occurring. As long as convection maintains the supercooling below this critical amount, crystallization can proceed exclusively by *in situ* growth. When this supercooling is exceeded, *in situ* crystallization is accompanied by crystal settling.

Application to magma chambers

Campbell (1978) stressed the importance of the kinetics of homogeneous and heterogeneous nucleation in determining whether crystal settling or *in situ* crystallization occurs in magma chambers. The experiments described above support Campbell's emphasis. Further, they suggest that crystal settling and *in situ* crystallization are not mutually exclusive. Both crystal settling and *in situ* crystallization may occur at the same time but to different extents. If a light depleted fluid is released by crystallization *in situ* crystallization may occur alone in magma chambers for sufficiently low supercoolings. At higher supercoolings, however, *in situ* crystallization will be accompanied by crystal settling, which may become dominant. The experiments demonstrate that high supercoolings, and hence crystal settling, are promoted by high fluid viscosities and high cooling rates.

A first step in the quantitative application of these experiments to magma chambers is to calculate the total amount of excess supercooling in the thermal boundary layer at the top of the chamber over that in the fluid at the crystal/liquid interface. This is given by

$$\Sigma\Delta T = \Delta T + \Delta S\left(\frac{\partial T}{\partial S}\right)_{liq} \qquad (7.2),$$

which using (3.32) and (4.16) gives

$$\Sigma\Delta T = \left(\frac{\nu q^3}{g\rho^3 C^3}\right)^{1/4} \left(\left(\frac{\left(\frac{\partial T}{\partial S}\right)_{liq}^4}{\beta\kappa_S^2 \left(L + c_p \left(\frac{\partial T}{\partial S}\right)_{liq}\right)^3} \right)^{1/4} + \left(\frac{1}{\alpha\kappa_T^2 c_p^3}\right)^{1/4} \right) \qquad (7.3).$$

Equation (7.3) assumes that the surface of the crystal pile is relatively smooth and that all crystallization is taking place *in situ*. The amount of excess supercooling is predicted to depend on viscosity weakly (to the one-quarter power) and somewhat more strongly on cooling rate (to the three-quarters power). Typical values of $\Sigma\Delta T$ when olivine is crystallizing *in situ* have been estimated from parameters given in table 7.3 and are shown in figure 7.6.

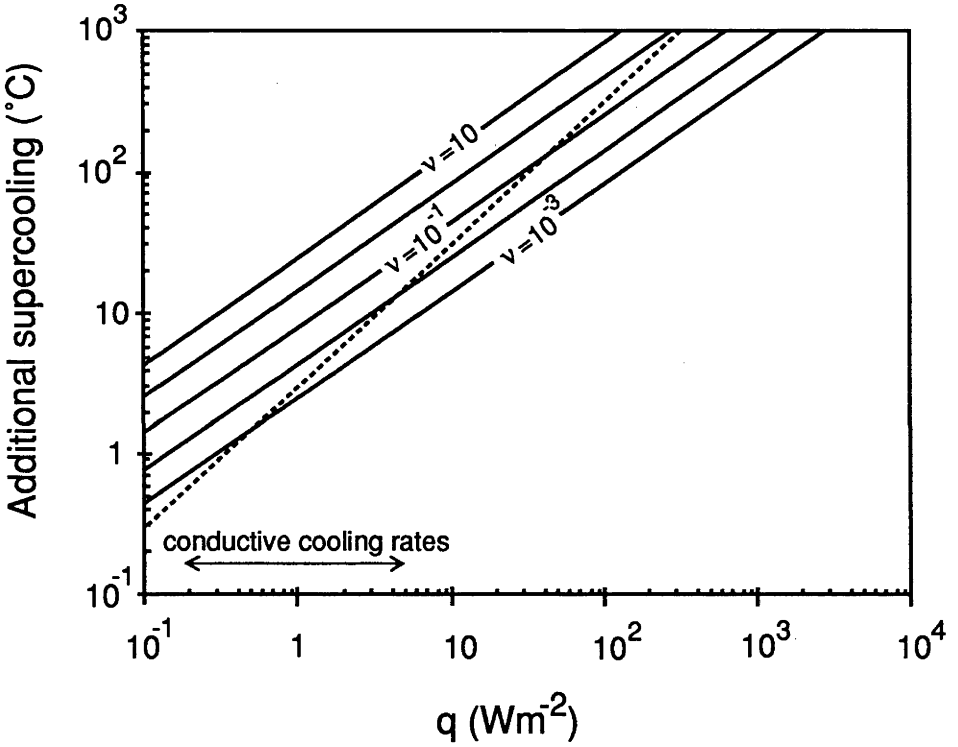

Figure 7.6. The excess amount of supercooling of fluid in the thermal boundary-layer at the top of a magma chamber plotted as a function of cooling rate for different viscosities (in $m^2 s^{-1}$). The calculation assumes (i) that all growth is taking place *in situ* on the floor of a high-aspect-ratio magma chamber and (ii) that the surface of the crystal pile is relatively smooth. This latter assumption probably holds for the region to the left of the dotted line in the diagram, which is the line corresponding to a compositional boundary-layer thickness of 2mm.

For conductively-cooled basaltic magma chambers crystallizing olivine *in situ* on the floor, the excess amount of supercooling in the fluid at the roof of the chamber ranges from about 1°C to about 20°C. If crystallization takes place exclusively by *in situ* crystallization these are the additional supercoolings required to be sustainable in the

magma without homogeneous nucleation occurring. Unfortunately, there is insufficient data at present to determine whether this is possible.

Very tentatively, I shall use the data obtained for KNO_3 in water as a guide for olivine in basalt. It was found in the experiments above that a supercooling of between 1.9°C and 2.9°C could be maintained in the fluid without homogeneous nucleation occurring. If olivine in magma behaves similarly, figure 7.6 shows that olivine-saturated basaltic magmas are able to crystallize exclusively by the *in situ* mechanism only at the lowest cooling rates. For cooling rates greater than about 1 Wm^{-2} *in situ* crystallization is expected to be accompanied by some crystal settling which will become more important as cooling rates are increased.

TABLE 7.3

Values of parameter used in calculations

Symbol	Units	Value
c_p	$J\,kg^{-1}\,{}^oC^{-1}$	1.1×10^3
C	-	0.2
g	$m\,s^{-2}$	9.81
L	$J\,kg^{-1}$	8.4×10^5
$\left(\frac{\partial T}{\partial S}\right)_{liq}$	°C (weight fraction)$^{-1}$	7.0×10^2
κ_T	$m^2\,s^{-1}$	8×10^{-7}
κ_S	$m^2\,s^{-1}$	1×10^{-10}
α	$^oC^{-1}$	5×10^{-5}
β	(weight fraction)$^{-1}$	7.0×10^{-2}
ρ	$kg\,m^{-3}$	2.5×10^3

At this point it is worth reproducing the diagram giving the temperature drop across the thermal boundary-layer (see chapter three). Figure 7.7 reveals that the drop across the thermal boundary-layer for conductively cooled basaltic magmas is always less than 1°C. Although the thermal boundary-layer is the coldest part of the chamber, it need not be the most supersaturated part. The effect of pressure on the liquidus ensures that the liquidus temperature of an olivine-saturated magma increase by some 1.2°C per kilometre (Campbell and Turner, 1989). For a conductively-cooled chamber greater than

about 1000m deep, the drop across the thermal boundary-layer is always outweighed by the effect of pressure on the liquidus.

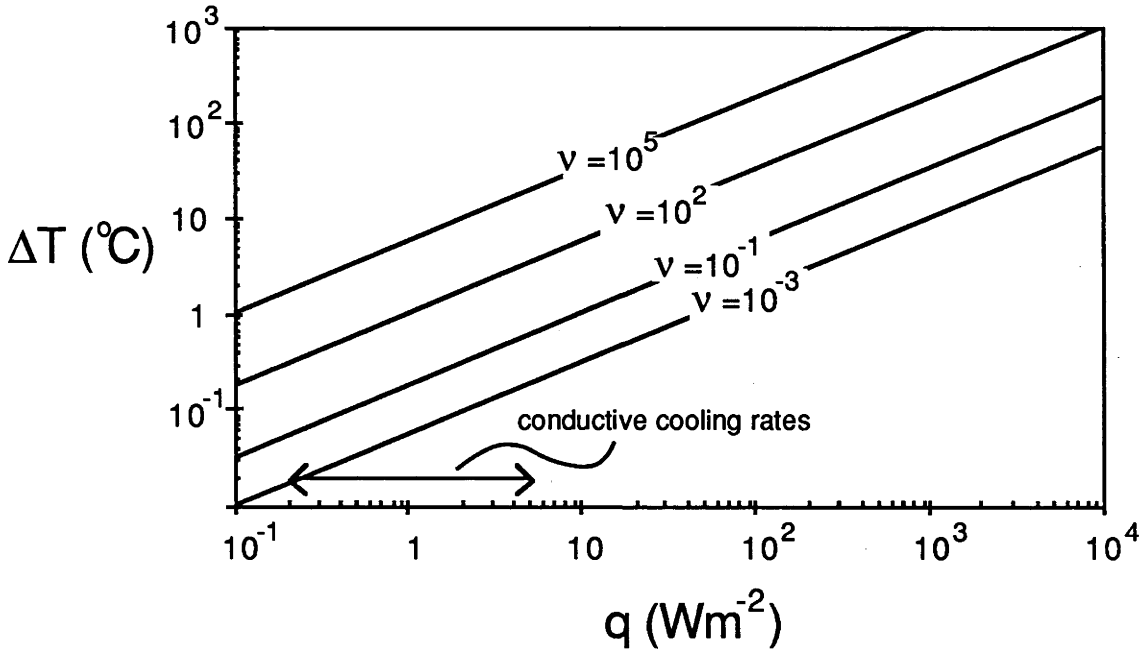

Figure 7.7. The temperature drop across the thermal boundary-layer as a function of cooling rate for different viscosities (in $m^2 s^{-1}$). (Reproduction of figure 3.4b).

Three scenarios can therefore be envisaged for the crystallization of olivine in basaltic magma chambers.

(i) For the lowest cooling rates crystallization may take place exclusively by *in situ* crystallization

(ii) As cooling rates are increased, *in situ* crystallization will be accompanied by crystal settling with crystals nucleating within the main body of the magma below a certain depth in the chamber.

(iii) As cooling rates are increased still further, *in situ* crystallization will be accompanied by crystal settling with crystals nucleating both in the thermal boundary-layer at the top of the chamber and in the main body of the magma.

Schematic temperature profiles through a chamber corresponding to these three scenarios are illustrated in figure 7.8

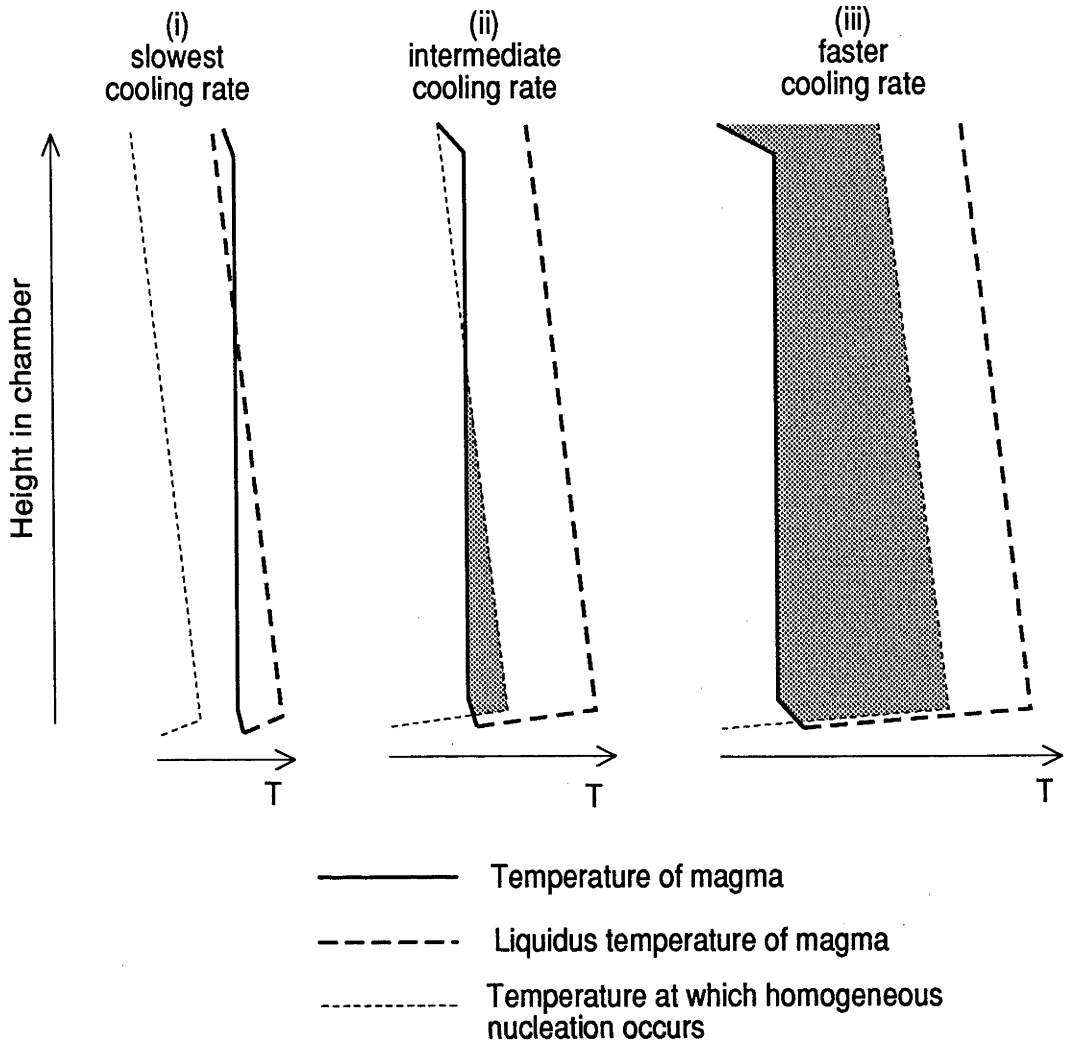

Figure 7.8. Schematic diagrams illustrating the three likely possibilities for crystallization in magma chambers. At the lowest cooling rate the magma temperature is always above the critical temperature for homogeneous nucleation and crystallization occurs by *in situ* crystallization only. At intermediate cooling rates the effect of pressure on the liquidus temperature causes the magma temperature to fall below the critical temperature for homogeneous nucleation in the bottom half of the chamber. In this situation crystals nucleate in the bottom half of the chamber (shaded) and crystal settling occurs in addition to *in situ* crystallization. At faster cooling rates the magma is everywhere below the critical temperature and nucleation of crystals occurs throughout the chamber. The diagram is not drawn to scale: the thicknesses of the thermal boundary-layer at the roof and the latent-heat and compositional boundary-layers at the floor have all been greatly exaggerated.

Finally, it was observed in the experiments described above that very porous crystal piles were produced when crystal settling is dominant. When crystallization takes place more by *in situ* crystallization, the crystal pile is less porous. It is suggested, similar (I think) to Morse's (1986b) model, that this may be part of the explanation for the range in cumulate textures from adcumulate to orthocumulate.

SUMMARY AND CONCLUSION

I have described laboratory experiments involving cooling and crystallizing aqueous solutions which display a range of crystallization mechanisms between the two end-members of *in situ* crystallization and crystal settling.

Although the quantitative application of this work to magma chambers is limited by the fact that the relevant parameters which describe the kinetics of crystallization are unknown, a definite qualitative result is indicated. The nucleation of crystals within the crystallizing magma, and hence crystal settling, is promoted by fast cooling rates and, to a lesser extent, by high viscosities.

It is suggested that the most slowly cooled magma chambers are able to crystallize purely by the *in situ* mechanism, whilst more rapidly cooled magma chambers solidify by a combination of *in situ* crystallization and crystal settling. When crystal settling is dominant, orthocumulate textures may result. Alternatively, if *in situ* crystallization is most important, adcumulate textures can be expected.

APPENDIX

The KNO_3 liquidus in KNO_3-C.M.C. aqueous solutions

Fluid and excess solid KNO_3 were placed in a stirred bucket which was cooled by means of a coil of copper tubing connected to a bath of cooled alcohol. The densities (at 20°C) of fluid saturated, at various temperatures, in KNO_3 were determined. Two determinations of the liquidus were made, the first using pure water and the second using water with (initially) 0.39 wt.% C.M.C. dissolved in it. In practise, with this viscous solution ($\sim 10^{-4}$ m^2 s^{-1}), considerable care had to be exercised to ensure that the sample of the fluid taken was as free from suspended crystals as possible. Measurements were taken as the fluid was cooled from 20°C to 6°C and then heated from 6°C to 20°C, both in steps of two degrees centigrade. The results are illustrated in figure 7.4.

The "pure" fluid and the fluid doped with C.M.C. can be fitted by least-squares regression with the following straight lines

$$T = 151.58S - 15.821; \quad r^2 = 0.996$$

and

$$T = 155.05S - 17.119;\ r^2 = 0.994$$

respectively, where S is the weight fraction of dissolved potassium nitrate.

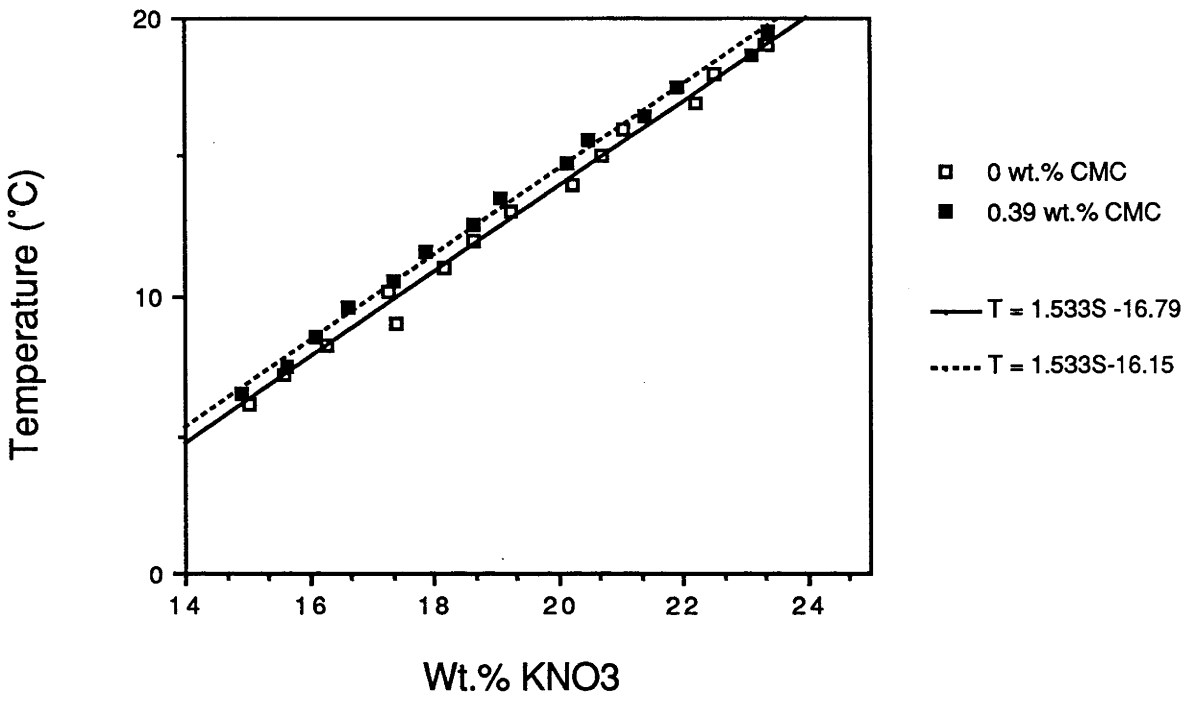

Figure A7.1. Results of the experimental determination of the KNO_3 liquidus for KNO_3 dissolved in: pure water (solid squares, dashed line), and 0.39wt.% C.M.C. solution (open squares, solid line).

Averaging the gradients of these two lines and adjusting the constants to give a best fit, the empirical equation

$$T = 153.3S - 16.15 - 165.8S_{C.M.C.} \qquad (A7.1)$$

is found, where $S_{C.M.C.}$ is the weight fraction of dissolved sodium carboxymethyl cellulose in the initial solution. The dependence of the liquidus temperature on the C.M.C. content of the fluid is thereby assumed to be linear. Shown on figure 7.4 are the lines given by (A7.1) for the two fluids used in the determination of the liquidus.

CHAPTER EIGHT

CONCLUSION

Thermal convection in magma chambers is expected to be nearly always within the turbulent régime, even at the slowest possible cooling rates. Convective velocities in basaltic chambers are of the order of metres to kilometres per day; in granitic chambers the range is from centimetres to kilometres per day. The temperature drop across the thermal boundary-layer, ΔT, however, may be very small. For conductively cooled basaltic chambers ΔT ranges from 0.02 to 1°C, for example. Because ΔT is so small, it is suggested that the temperature-dependence of magmatic viscosity and the effects of crystallization within the thermal boundary-layer can often be neglected.

When magmas crystallize, depleted fluid is generated adjacent to the growing crystals. Often this residual magma will be less dense than the original magma. When a magma chamber is undergoing *in situ* crystallization at the floor of a chamber, therefore, compositional convection may occur in addition to thermal convection . Because thermal convection and compositional convection are both ultimately driven by the same heat flux, the ratio of the compositional Rayleigh number, Rs, to the thermal Rayleigh number, Ra, is fixed for a given magma. In the case of a mafic magma undergoing olivine crystallization, Rs is a factor of about 10^6 greater than Ra, although the compositional and thermal buoyancy fluxes are roughly equal.

In addition to the generation of compositionally buoyant fluid at the floor of the chamber, *in situ* crystallization also generates thermally buoyant magma due to the release of latent heat. There are therefore two superimposed boundary-layers above the growing crystals: the compositional boundary-layer and the latent-heat boundary-layer. The parameters describing both boundary-layers have been determined for olivine-saturated magmas. The latent-heat thermal boundary-layer is of the order of 1m thick for conductive cooling rates, with very low thermal gradients. The compositional boundary-layer is about 1cm thick with large compositional gradients. As a consequence, the variation in the degree of supercooling in front of the crystal-liquid interface is dominated

by compositional effects. The habit and composition of the growing crystals may also be controlled by the nature of the compositional boundary-layer. Elongate crystals are suggested to form when the thickness of the compositional boundary-layer is small compared with the crystal-size (as in laboratory experiments with aqueous solutions). In contrast, equant crystals may form when the boundary-layer is thicker than the crystals (as in most magma chambers). Instability of the boundary-layer in the latter case may be the origin of oscillatory zoning in crystals. The incorporation of components within the growing crystals is limited by diffusion across the compositional boundary-layer. In the case of highly incompatible, or highly compatible, trace elements, the effective distribution coefficient may be significantly different from the equilibrium distribution coefficient. This effect can explain an inverse correlation, observed in layered intrusions, between Ni concentration in olivine and the proportion of Ni-bearing phases in the crystallizing assemblage.

The generation of buoyant fluid by crystallization against sloping floors, under the conditions that are likely to prevail in magma chambers, is very similar to the process that occurs at horizontal floors. Buoyant fluid builds up within a boundary-layer until its thickness reaches a critical value, at which time the fluid breaks away from the boundary to form a plume. The major difference with the sloping-floor case is that the fluid within the boundary-layer moves up the slope while the boundary-layer grows. For compositional convection driven from sloping floors the thickness of the compositional boundary-layer and the compositional drop across it are expected to be similar to the horizontal-floor case, and these parameters depend only weakly on the slope of the floor.

When *in situ* crystallization is taking place against a sloping floor, the plumes generated at the boundary by the release of buoyant fluid will combine to form a broad upslope current. This phenomenon has been modelled in the laboratory using thermal convection from a smooth, sloping heat exchanger. In tanks with an unheated horizontal floor the upslope current stratifies the fluid by means of a filling-box process. However, in tanks in which there is no horizontal floor, or when the horizontal floor is heated, the filling-box does not operate and instead there is a simple overturning circulation. This

latter situation is believed to be closest to the situation in magma chambers, a conclusion that is supported by the homogeneity of magma such as the Columbia River Basalts. Models describing the crystallization of layered intrusions which involve the interaction of crystallization against an inclined floor with compositionally stratified magma require an external cause for the stratification when crystallization releases a light magma. For example, replenishment of the chamber by a hot, dense magma may lead to persistent compositional zoning.

An alternative to the *in situ* crystallization model for magmatic differentiation is the model of crystal settling. However, predicted convective velocities in magma chambers are commonly orders of magnitude larger than settling velocities for typical crystals calculated from Stokes' Law. The ratio, s, of the Stokes' Law settling velocity, v_S, to the r.m.s. vertical component of convective velocity, W, at mid-depth in the fluid is almost always less than unity. Nevertheless, although $v_S<W$, settling is still possible because convective velocities are height- dependent and must decrease to zero at the boundaries of the fluid. Particles immediately adjacent to the bottom boundary settle out with their full Stokes' settling velocities. At the same time convection is vigorous enough to ensure that the distribution of particles in the fluid is uniform. It follows that the number of particles in suspension decays with time according to an exponential law, and the decay constant is simply the ratio of v_S to h, the depth of the fluid. This relationship has been confirmed experimentally, at least for low particle concentrations, providing $s<0.5$ and there is no re-entrainment of particles from the floor of the tank.

This result has been applied to crystals in magma chambers, and residence times for typical crystals have been calculated. It was found that for basaltic magmas the predicted residence times are small compared with the many thousands of years that a chamber takes to solidify if cooling is by conduction through the country rock. Crystal settling may therefore be an efficient differentiation mechanism. Significant magmatic evolution can, however, take place on timescales that are competitive with these residence times. Application of this work to chromitite and P.G.E. deposits in layered intrusions supports a model in which the settling of crystals and/or sulphide droplets is envisaged to

occur following precipitation in a turbulent plume during magma mixing. The data of Hiemstra (1986) on the variation of P.G.E. content with height in the UG-2 chromitite of the Bushveld Complex can be interpreted in terms of this model.

If the settling of crystals is the rate-limiting step during the crystallization of a magma chamber it is expected that a steady-state will be achieved at which the rate of supply of crystals into the convecting magma due to crystallization balances the rate at which crystals settle out. This idea can explain both the lack of hydraulic equivalence in cumulate rocks and the commonly observed discrepancy between the relative proportions of phenocrysts of various phases in fractionated basaltic lavas and the calculated relative proportions of these mineral phases in the fractionating assemblage. A comparison of the calculated steady-state crystal content of convecting magma chambers with the observed phenocryst content of typical basaltic lavas suggests that magma chambers may often cool more rapidly than would be expected for conduction through the country rock alone.

Experiments designed to simulate crystallizing magma chambers have been conducted. Aqueous solutions of potassium nitrate have been cooled from above. It is found that crystals grow on the floor of the tank and that, for low cooling rates, compositional and thermal convection are able to keep the supercooling away from the crystals low enough so that crystals do not nucleate in suspension in the fluid. In other words: at low cooling rates these experimental magma chambers solidify by the *in situ* crystallization mechanism. However, if the cooling rate or the viscosity of the solution is increased, some crystals are observed to form in suspension and settle out. In this case crystal settling occurs in addition to *in situ* crystallization.

In magma chambers undergoing *in situ* crystallization, the increase in supersaturation away from the growing crystals depends on cooling rate to the three-quarters power and viscosity to the one-quarter power. It is suggested that, in slowly cooled ultramafic chambers, crystallization may occur exclusively by the *in situ* mechanism. Elsewhere, *in situ* crystallization will be accompanied by crystal settling, which may become dominant in some situations. The range in cumulate textures may reflect, in part, the crystallization mechanism by which the cumulates were formed.

Orthocumulates may form when crystal settling is dominant. Alternatively, if crystallization occurs by *in situ* crystallization alone, adcumulate textures may result.

REFERENCES

Arndt, N.T., 1977. The partitioning of nickel between olivine and ultrabasic and basic komatiitic liquids. *Carnegie Inst. Washing. Yearb.* **76**, 553-556.

Baines, W.D. & Turner, J.S., 1969. Turbulent buoyant convection from a source in a confined region. *J. Fluid Mech.* **37**, 51-80.

Barnea, E. & Mizrahi, J., 1973. A generalized approach to the fluid dynamics of particulate systems. Pt. I. General correlation for fluidization and sedimentation in solid multiparticle systems. *Chem. Eng.* **5**, 171-89.

Bartlett, R.W., 1969. Magma convection, temperature distribution and differentiation. *Am. J. Sci.* **269**, 169-182.

Becker, G.F., 1897. Fractional crystallization of rocks. *Am. J. Sci.* 4th Ser. **4**, 257-61.

Bhattacharji, S., 1967. Mechanics of flow differentiation in ultramafic and mafic sills. *J. Geol.* **75**, 101-12.

Blake, S., 1986. Sediment entrainment in viscous fluids: can crystals be erupted from magma chamber floors? *J. Geol.* **95**, 397-406.

Blake, S. & Campbell, I.H., 1986. The dynamics of magma-mixing during flow in volcanic conduits. *Contrib. Mineral. Petrol.* **94**, 72-81.

Blake, S. & Ivey, G.N., 1986. Magma-mixing and the dynamics of withdrawal from stratified reservoirs. *J. Volcanol. Geotherm. Res.* **27**, 153-78.

Bottinga, Y. & Weill, D.F., 1970. Density of liquid silicate systems calculated from partial molar volumes of oxide components. *Am. J. Sci.* **269**, 169-182.

Bowen, N.L., 1915. Crystallization differentiation in silicate liquids. *Am. J. Sci.* **39**, 175-91.

Bowen, N.L., 1928. *The evolution of the igneous rocks.* Dover reprint, 1956.

Bowen, N.L. & Anderson, O., 1914. The binary system MgO-SiO_2. *Am. J. Sci.* 4th Ser. **37**, 487-500.

Brandeis, G. & Jaupart, C., 1986. On the interaction between convection and crystallization in cooling magma chambers. *Earth Planet. Sci. Lett.* **77**, 345-61.

Brandeis, G., Jaupart, C. & Allègre, C.J., 1984. Nucleation, crystal growth and the thermal regime of cooling magmas. *J. Geophys. Res.* **89**, 10161-77.

Campbell, I.H., 1973. Aspects of the petrology of the Jimberlana Layered Intrusion of Western Australia. Unpubl. Ph.D. Thesis, London University.

Campbell, I.H., 1978. Some problems with the cumulus theory. *Lithos* **11**, 311-23.

Campbell, I.H., 1985. The difference between continental and oceanic tholeiites: a fluid dynamic explanation. *Contrib. Mineral. Petrol.* **91**, 37-43.

Campbell, I.H., 1987. Distribution of orthocumulate textures in the Jimberlana intrusion. *J. Geol.* **95**, 35-54.

Campbell, I.H. & Turner, J.S., 1986a. The influence of viscosity on fountains in magma chambers. *J. Petrol.* **27**, 1-30.

Campbell, I.H. & Turner, J.S., 1986b. The role of convection in the formation of platinum and chromitite deposits in layered intrusions. In *Mineral Association of Canada short course in silicate melts* (ed. Scarfe, C.M.).

Campbell, I.H. & Turner, J.S., 1987. A laboratory investigation of assimilation at the top of a basaltic magma chamber. *J. Geol.* **95**, 155-72.

Campbell, I.H. & Turner, J.S., 1989. Fountains in magma chambers. *J. Petrology*, submitted.

Campbell, I.H., Roeder, P.L. & Dixon, J.E., 1977. Plagioclase buoyancy in basaltic liquids as determined with a centrifuge furnace. *Contrib. Mineral. Petrol.* **67**, 369-77.

Campbell, I.H., Naldrett, A.J. & Barnes, S.J., 1983. A model for the origin of the platinum-rich sulfide horizons in the Bushveld and Stillwater complexes. *J. Petrol.* **24**, 133-65.

Carmichael, I.S.E., Turner, F.J. & Verhoogen, J., 1974. *Igneous Petrology*. McGraw Hill, New York.

Carrigan, C.R., 1987. The magmatic Rayleigh number and time-dependent convection in cooling lava lakes. *Geophys. Res. Lett.* **14**, 915-18.

Chu, T.Y. & Goldstein, R.J., 1973. Turbulent convection in a horizontal layer of water. *J. Fluid Mech.* **60**, 141-59.

Cox, K.G. & Mitchell, C., 1988. Importance of crystal settling in the differentiation of Deccan Trap basaltic magmas. *Nature*, **333**, 447-49.

Deardorff, J.W. & Willis, G.E., 1967. Investigation of turbulent thermal convection between horizontal plates. *J. Fluid Mech.* **28**, 675-704.

DePaolo, D.J., 1981. Trace element and isotopic effects of combined wallrock assimilation and fractional crystallization. *Earth Planet. Sci. Lett.* **52**, 189-202.

Dick, H.J.B. & Bryan, W.B., 1978. Variation of basalt phenocryst mineralogy and rock composition in D.S.D.P. hole 396B. In *Initial reports of the Deep Sea Drilling Project*, Volume XLVI (eds. Dmitriev, L., Heirtzler, J. *et al.*). U.S. Government Printing Office, Washington.

Dungan, M.A. & Rhodes, J.M., 1978. Residual glasses and melt inclusions in basalts from D.S.D.P. legs 45-46: evidence for magma mixing. *Contrib. Mineral. Petrol.* **67**, 413-31.

Eichelberger, J.C., 1978. Andesitic volcanism and crustal evolution. *Nature* **228**, 446-50.

Elder, J.W., 1968. The unstable thermal interface. *J. Fluid Mech.* **32**, 29-48.

Elthon, D., 1979. High magnesia liquids as the parental magma for ocean floor basalts. *Nature* **278**, 514-517

Fitzgerald, D.E., 1976. An experimental study of turbulent thermal convection in air. *J. Fluid Mech.* **73**, 693-719.

Garon, A.M. & Goldstein, R.J., 1973. Velocity and heat transfer measurements in thermal convection. *Phys. Fluids* **16**, 1818-25.

Gibb, F.G.F, 1986. Flow differentiation in the xenolithic ultrabasic dykes of the Cuillins and the Strathaird Peninsula, Isle of Skye, Scotland. *J. Petrology* **9**, 411-43.

Griffiths, R.W., 1987. Effects of Earth's rotation on convection in magma chambers. *Earth Planet. Sci. Lett.* **85**, 525-36.

Grout, F.F., 1918. Two-phase convection in igneous magmas. *J. Geol.* **26**, 481-99.

Hart, J.E., 1971. Stability of the flow in a differentially heated inclined box. *J. Fluid Mech.* **47**, 547-76.

Herring, J.R., 1964. Investigation of problems in thermal convection: rigid boundaries. *J. Atmos. Sci.* **21**, 277-290.

Hiemstra, S.A., 1985. The distribution of some platinum-group elements in the UG-2 chromitite layer of the Bushveld Complex. *Econ. Geol.* **80**, 944-55.

Hiemstra, S.A., 1986. The distribution of chalcophile and platinum-group elements in the UG-2 chromitite layer of the Bushveld Complex. *Econ. Geol.* **81**, 1080-86.

Hildreth, W., 1981. Gradients in silicic magma chambers: implications for lithospheric magmatism. *J. Geophys. Res.* **86**, 10153-92.

Howard, L.N., 1963. Convection at high Rayleigh number. In *Proceedings of the eleventh congress of applied mechanics* (ed. Görtler, H.), pp.1109-15. Springer-Verlag.

Huppert, H.E. & Sparks, R.S.J., 1980. The fluid dynamics of a basaltic magma chamber replenished by influx of hot, dense ultrabasic magma. *Contrib. Miner. Petrol.* **75**, 279-89.

Huppert, H.E. & Sparks, R.S.J., 1985. Cooling and contamination of mafic and ultramafic magmas during ascent through continental crust. *Earth Planet. Sci. Lett.* **74**, 371-86.

Huppert, H.E. & Sparks, R.S.J., 1988a. Melting the roof of a chamber containing a hot, turbulently convecting fluid. *J. Fluid Mech.* **188**, 107-33.

Huppert, H.E. & Sparks, R.S.J., 1988b. The generation of granitic magmas by intrusion of basaltic magma into the crust. *J. Petrology* **29**, 599-624.

Huppert, H.E. & Turner, J.S., 1981. A laboratory model of a replenished magma chamber. *Earth Planet. Sci. Lett.* **74**, 144-52.

Huppert, H.E., Sparks, R.S.J. & Turner, J.S., 1982. Replenished magma chambers: effects of compositional zonation and input rates. *Earth Planet. Sci. Lett.* **57**, 345-57.

Huppert, H.E., Sparks, R.S.J. & Turner, J.S., 1983. Laboratory investigation of viscous effects in replenished magma chambers. *Earth Planet. Sci. Lett.* **65**, 377-81

Huppert, H.E., Sparks, R.S.J., Whitehead, J.A. & Hallworth, M.A., 1986a. Replenishment of magma chambers by light inputs. *J. Geophys. Res.* **91**, 6113-6122.

Huppert, H.E., Sparks, R.S.J., Wilson, J.R. & Hallworth, M.A., 1986b. Cooling and crystallization at an inclined plane. *Earth Planet. Sci. Lett.* **79**, 319-328.

Huppert, H.E., Sparks, R.S.J., Wilson, J.R., Hallworth, M.A. & Leitch, A.M., 1987. Laboratory experiments with aqueous solutions modelling magma chamber processes. II. Cooling and crystallization along inclined planes. In *Origins of Igneous Layering* (ed. Parsons, I.), Riedel, Dordecht.

Irvine, T.N., 1970. Heat transfer during solidification of layered intrusions. I. Sheets and sills. *Can. J. Earth. Sci.* **7**, 1031-61.

Irvine, T.N., 1974. Petrology of the Duke Island ultramafic complex, southeastern Alaska. *Mem. Geol. Soc. Am.* **138**.

Irvine, T.N., 1977. Origin of chromitite layers in the Muskox intrusion and other layered intrusions: a new interpretation. *Geology* **5**, 273-77.

Irvine, T.N. & Smith, C.H., 1967. The ultramafic rocks of the Muskox Intrusion, Northwest Territories, Canada. In *Ultramafic and related rocks* (ed. Wyllie, P.J.). Wiley, New York.

Irvine, T.N., Keith, D.W. & Todd, S.G., 1983. The J-M platinum-palladium reef of the Stillwater complex Montana II: origin by double-diffusive convective magma mixing and implications for the Bushveld Complex. *Econ. Geol.* **78**, 1287-1334.

Jackson, E.D., 1961. Primary textures and mineral associations in the ultramafic zone of the Stillwater Complex, Montana. *Prof. Paper U.S. Geol. Surv.* **358.**

Jarvis, G.T., 1984. Time-dependent convection in the Earth's mantle. *Phys. Earth Planet. Inter.* **36**, 305-27.

Jaupart, C. & Brandeis, G., 1986. The stagnant bottom layer of convecting magma chambers. *Earth Planet. Sci. Lett.* **80**, 183-99.

Jaupart, C., Brandeis, G. & Allègre, C.J., 1984. Stagnant layers at the bottom of convecting magma chambers. *Nature* **308**, 535-8.

Katsaros, K.B., Liu, W.J., Businger, J.A. & Tillman, J.E., 1977. Heat transfer and thermal structure in the interfacial boundary-layer measured in an open tank of water in turbulent free convection. *J. Fluid Mech.* **83**, 311-35.

Komar, P.D., 1972. Mechanical interactions of phenocrysts and flow differentiation of igneous dikes and sills. *Geol. Soc. Am. Bull.* **83**, 973-88.

Koyaguchi, T., 1985. Magma mixing in a conduit. *J. Volcanol. Geotherm. Res.* **25**, 365-69.

Koyaguchi, T., 1987. Magma mixing in a squeezed conduit. *Earth Planet. Sci. Lett.* **84**, 339-44.

Kraichnan, R.H., 1962. Mixing-length analysis of turbulent thermal convection at arbitrary Prandtl numbers. *Phys. Fluids* **5**, 1374-89.

Krishnamurthi, R., 1970. On the transition to turbulent convection. *J. Fluid Mech.* **42**, 295-320.

Krishnamurthi, R. & Howard, L.N., 1981. Large-scale flow generation in turbulent convection. *Proc. Natl. Acad. Sci.* **78**, 1981-85.

Krishnamurthy, P. & Cox, K.G., 1980. A potassium-rich alkalic suite from the Deccan Traps, Rajpiplas, India. *Contrib. Miner. Petrol.* **73**, 275-310.

Lloyd, J.R. & Sparrow, E.M., 1970. On the instability of natural convection flow on inclined plates. *J. Fluid Mech.* **42**, 465-70.

Malkus, W.V.R., 1954. Discrete transitions in turbulent convection. *Proc. Roy. Soc. Lond.* **A225**, 185-95.

Marsh, B.D. & Maxey, M.R., 1985. On the distribution and separation of crystals in convecting magma. *J. Volcanol. Geotherm. Res.* **24**, 95-150.

Martin, D. & Campbell, I.H., 1988. Laboratory modelling of convection in magma chambers: crystallization against sloping floors. *J. Geophys. Res.* **93**, 7974-88.

Martin, D. & Nokes, R.I., 1988. Crystal settling in a vigorously convecting magma chamber. *Nature* **332**, 534-36.

Martin, D. & Nokes, R.I., 1989. A fluid-dynamical study of crystal settling in convecting magmas. *J. Petrology* submitted.

Martin, D., Griffiths, R.W. & Campbell, I.H., 1987. Compositional and thermal convection in magma chambers. *Contrib. Mineral. Petrol.* **96**, 465-75.

McBirney, A.R., 1980. Mixing and unmixing of magmas. *J. Volcanol. Geotherm. Res.* **7**, 357-71.

McBirney, A.R. & Noyes, R.M., 1979. Crystallization and layering of the Skaergaard Intrusion. *J. Petrol.* **20**, 487-554.

McBirney, A.R., Baker, B.H. & Nilson, R.H., 1985. Liquid fractionation, part I: basic principles and experimental simulations. *J. Volcanol. Geotherm. Res.* **24**, 1-24.

McKenzie, D.P., 1984. The generation and compaction of partially molten rock. *J. Petrology* **25**, 723-65.

Mo, X., Carmichael, I.S.E., Rivers, M. & Stebbins, J., 1982. Partial molar volume of FeO in multicomponent silicate liquids and the pressure dependence of oxygen fugacity in magmas. *Mineral. Mag.* **45**, 237-245.

Moorbath, S. & Thompson, R.N., 1980. Strontium isotope geochemistry and petrogenesis of the early Tertiary lava pile of the Isle of Skye, Scotland, and other basic rocks of the British Tertiary Province: and example of magma-crust interaction. *J. Petrology* **21**, 295-321.

Morse, S.A., 1986a. Thermal structure of crystallizing magma with two-phase convection. *Geol. Mag.* **123**, 205-14.

Morse, S.A., 1986b. Convection in aid of adcumulus growth. *J. Petrology* **27**, 1183-1214.

Nelson, S.A. & Carmichael, I.S.E., 1979. Partial molar volumes of oxide components in silicate liquids. *Contrib. Mineral. Petrol.* **71**, 117-124.

Nilson, R.H., McBirney, A.R. & Baker, B.H., 1985. Liquid fractionation, Part II: Fluid dynamics and quantitative implications for magmatic systems. *J. Volcanol. Geotherm. Res.* **24**, 24-54.

Palm, E., 1975. Non-linear thermal convection. *Ann. Rev. Fluid Mech.* **7**, 39-61.

Parsons, I. & Butterfield, A.W., 1981. Sedimentary features of the Nunarssuit and Klokken syenites, S. Greenland. *J. Geol. Soc. Lond.* **138**, 289-305.

Poulikakos, D. & Bejan, A., 1983. The fluid dynamics of an attic space. *J. Fluid Mech.* **131**, 251-69.

Rice, A.R., 1981. Convective fractionation: a mechanism to provide cryptic zoning (macrosegregation), layering, crescumulates, banded tuffs and explosive volcanism in igneous processes. *J. Geophys. Res.* **86**, 405-17.

Roedder, E., 1979. Silicate liquid immiscibility in magmas. In *The evolution of the igneous rocks: fiftieth anniversary perspectives* (ed. Yoder, H.S.). Princeton University Press.

Roeder, P.L., 1975. Thermodynamics of element distribution in experimental mafic silicate-liquid systems. *Fortschr. Miner.* **52**, 61-73.

Roeder, P.L. & Emslie, R.F., 1970. Olivine-liquid equilibrium. *Contrib. Mineral. Petrol.* **29**, 275-289.

Ryan, M.P. & Blevins, J.Y.K., 1987. The viscosity of synthetic and natural silicate melts and glasses at high temperatures and 1 bar (10^5 pascals) pressure and at higher pressures. *U.S. Geol. Surv. Bulletin* **1764**.

Sakuyama, M., 1981. Petrological study of the Myoko and Kurohime volcanoes, Japan: crystallization sequence and evidence of magma mixing. *J. Petrology* **22**, 553-83.

Sclater, J.G., Jaupart, C. & Golson, D., 1980. The heat flow through the oceanic and continental crust and the heat loss of the earth. *Rev. Geophys. Space Physics* **18**, 269-311.

Scott, D.R. & Stevenson, D.J., 1986. Magma ascent by porous flow. *J. Geophys. Res.* **91**, 9283-96.

Segur, J.B., 1953. Physical properties of glycerol and its solutions. In *Glycerol* (eds. Miner, C.S. and Dalton, N.N.). American Chemical Society Monograph Series.

Shaw, H.R., 1965. Comments on viscosity, crystal settling and convection in granitic magmas. *Am. J. Sci.* **263**, 120-52.

Shaw, H.R., 1972. Viscosities of magmatic silicate liquids: an empirical method of prediction. *Am. J. Sci.* **272**, 870-93.

Shibata, T., Delong, S.E. & Walker, D., 1979. Abyssal tholeiites from the Oceanographer Fracture Zone. *Contrib. Miner. Petrol.* **70**, 89-102.

Sparks, R.S.J., Huppert, H.E., Kerr, R.C., McKenzie, D.P. & Tait, S.R., 1985. Postcumulus processes in layered intrusions. *Geol. Mag.* **122**, 555-68.

Sparks, R.S.J., Huppert, H.E. & Turner, J.S., 1984. The fluid dynamics of evolving magma chambers. *Phil. Trans. Roy. Soc. Lond.* **A310**, 511-34.

Sparrow, E.M. & Husar, R.B., 1969. Longitudinal vortices in natural convection flow on inclined plates. *J. Fluid Mech.* **37**, 251-56.

Tait, S.R., Huppert, H.E. & Sparks, R.S.J., 1984. The rôle of compositional convection in the formation of adcumulate rocks. *Lithos* **17**, 139-46.

Taylor, H.P., 1980. The effects of assimilating country rock by magmas on $^{18}O/^{16}O$ and $^{87}Sr/^{86}Sr$ systematics of igneous rocks. *Earth Planet. Sci. Lett.* **47**, 243-54.

Townsend, A.A., 1959. Temperature fluctuations over a heated horizontal surface. *J. Fluid Mech.* **5**, 209-41.

Tritton, D.J., 1963. Transition to turbulence in free convection boundary layers on an inclined heated plate. *J. Fluid Mech.* **16**, 417-35.

Tritton, D.J., 1985a. Experiments on turbulence in geophysical fluid dynamics. I. - Turbulence in rotating fluids. In *Turbulence and predictability in geophysical fluid dynamics and climate dynamics*, pp. 172-92, Soc. Italiana di Fisica, Bologna.

Tritton, D.J., 1985b. Experiments on turbulence in geophysical fluid dynamics. II. - Convection of a very viscous fluid. *Ibid*, pp. 193-99.

Tritton, D.J., Rayburn, D.M. & Forrest, M.A., 1980. Convection of a very viscous fluid heated from below. In *Mechanisms of Continental Drift and Plate Tectonics* (eds. Davies, P.A. & Runcorn, S.K.). Academic Press.

Turner, J.S., 1973. *Buoyancy effects in fluids*. Cambridge University Press.

Turner, J.S., 1980. A fluid-dynamic model of differentiation and layering in magma chambers. *Nature* **285**, 213-15.

Turner, J.S. & Campbell, I.H., 1986. Convection and mixing in magma chambers. *Earth Sci. Rev.* **23**, 255-352.

Turner, J.S. & Gustafson, L.B., 1981. Fluid motions and compositional gradients produced by crystallization or melting at vertical boundaries. *J. Volcanol. Geotherm. Res.* **11**, 93-125.

Turner, J.S., Huppert, H.E. & Sparks, R.S.J., 1983. Experimental investigations of volatile exsolution in evolving magma chambers. *J. Volcanol. Geotherm. Res.* **16**, 263-77.

Turner, J.S., Huppert, H.E. & Sparks, R.S.J., 1986. Komatiites, II. Experimental and theoretical investigations of post-emplacement cooling and crystallization. *J. Petrology* **27**, 397-437.

Wager, L.R. & Brown, G.M., 1968. *Layered igneous rocks.* Oliver and Boyd, Edinburgh.

Wager, L.R. & Deer, W.A., 1939. Geological investigations in East Greenland, Pt. III. The petrology of the Skaergaard Intrusion, Kangerdlugssuaq, East Greenland. *Medd. om Grønland* **105**, 1-352.

Walker, G.P.L. & Skelhorn, R.R., 1966. Some associations of acid and basic igneous rocks. Earth Sci. Rev. **2**, 93-109.

Weinstein, S.A., Yuen, D.A. & Olson, P.L., 1988. Evolution of crystal-settling in magma-chamber convection. *Earth Planet. Sci. Lett.* **87**, 237-48.

Wilson, A.H., 1982. The geology of the Great 'Dyke', Zimbabwe: the ultramafic rocks. *J. Petrol.* **23**, 240-92.

Wilson, J.R. & Larsen, S.B., 1985. Two dimensional study of a layered intrusion: the Hyllingen Series, Norway. *Geol. Mag.* **122**, 97-124.

Worster, M.G. & Leitch, A.M., 1985. Laminar free convection in confined regions. *J. Fluid Mech.* **156**, 310-20.